NANOPARTICLES AND NANOFIBERS PRODUCTION

USING SUPERCRITICAL CARBON DIOXIDE

Except where references are made to the work of others, the work described in this dissertation is my own and has been conducted with the consent of my advisor in collaboration with my advisory committee. This dissertation does not include proprietary or classified information.

_____

Ranjit Thakur

Certificate of Approval:

_____   _____
Gopal A. Krishnagopalan   Ram B. Gupta, Chair
Professor   Alumni Professor
Chemical Engineering   Chemical Engineering

_____   _____
Christopher B. Roberts   Daniel L. Parsons
Department Chair & Professor   Professor
Chemical Engineering   Pharmacal Sciences

_____
Stephen L. McFarland
Acting Dean
Graduate School

NANOPARTICLES AND NANOFIBERS PRODUCTION

USING SUPERCRITICAL CARBON DIOXIDE

Ranjit Thakur

A

Dissertation

Submitted to the

Graduate Faculty of

Auburn University in

Partial Fulfillment of the

Requirements for the

Degree of

Doctor of Philosophy

Auburn, Alabama
December 16, 2005

NANOPARTICLES AND NANOFIBERS PRODUCTION

USING SUPERCRITICAL CARBON DIOXIDE

Ranjit Thakur

Permission is granted to Auburn University to make copies of this dissertation at
its discretion, upon request of individuals or institutions and at their
expense. The author reserves all publication rights.

Signature of Author

Date of Graduation

VITA

Ranjit Thakur, son of G. Thakur, was born on October 18, 1977, in Samastipur, India. He completed his primary and secondary education at Haryana High School, Panchkula and senior secondary school at DAV Senior Secondary School, Chandigarh. After competing in common entrance exam, he joined Department of chemical engineering at Panjab University in 1994. He completed his Bachelors degree in Chemical Engineering from Panjab University in the year 1998. After completing BE, he joined Chambal Fertilizers and Chemicals Ltd. as Process Engineer and worked in commissioning of 2700 MTPD urea manufacturing plant. Later on, in 2001 he resigned and moved to USA to obtain higher education and planned to accomplish a Doctor of Philosophy in Chemical Engineering at Auburn University.

DISSERTATION ABSTRACT

NANOPARTICLES AND NANOFIBRES PRODUCTION

USING SUPERCRITICAL CARBON DIOXIDE

Ranjit Thakur

Doctor of Philosophy, December 16, 2005
(B.E., Panjab University, 1998)

217 typed pages

Directed by Dr. Ram B. Gupta

This dissertation deals with the production of nanostructured organic, inorganic and biopolymer materials using supercritical carbon dioxide. Over the past decade, supercritical fluids (SCFs) have emerged for particle formation due to SCFs adjustable solubility and significantly high diffusivity. Various methods have been developed, which can be classified into two basic processes: (a) rapid expansion of supercritical solutions (RESS) for processing CO_2-soluble materials, (b) and supercritical antisolvent (SAS) for processing CO_2-insoluble materials. In this work, further developments in both the methods have been made to overcome the existing challenges and to achieve new nanostructures.

Chitin nanofibers are potentially of use in many biomedical and pharmaceutical applications. But, due to highly crystalline nature, it is very difficult to convert into a

nanofibrous form. In this work, a SAS method is used to produce chitin nanofibers of average diameter 84 nm using hexafluoroisopropanol as solvent while preserving the molecular structure of the processed chitin.

Using SAS with enhanced mass transfer, hydrocortisone nanoparticles were produced. A sonicating horn at 20 kHz frequency was used to enhance the mass transfer between solvent-antisolvent and to avoid agglomeration of nanoparticles. Particles as small as 180 nm are obtained using this method and the size was easily controlled using the ultrasound intensity.

The SAS process was further extended by including a chemical reaction. A new supercritical fluid based method, SAS-R was developed to form silica coating onto gold nanoparticles. Here supercritical CO_2 is utilized both as an antisolvent and as a reactant. Silica-coated gold particles of 30-300 nm size were obtained with the coating thickness of as low as 20 nm. Pressure can be used to control coating thickness. Such particles are of interest in producing optical switches and biosensors.

In the conventional RESS process, a supercritical solution is rapidly expanded through a nozzle to precipitate the solute as microparticles. The modeling of RESS has shown that the precipitated particles at the nozzle tip are of the order of 5-25 nm in size. However, for most solutes, the final particles experimentally obtained are in the order of 800-3000 nm in size, due to growth by coagulation in the expansion chamber. Another difficulty is that most pharmaceutical compounds have poor solubility in supercritical carbon dioxide. In this work, both challenges are addressed by utilizing a cosolvent that is solid at the nozzle exit conditions. The solid cosolvent (SC) enhances the solubility and provides barrier for coagulation in the expansion chamber. The solid cosolvent is later

remove from the solute particles by lyophilization (sublimation). The new process is termed as RESS-SC. A suitable solid cosolvent is menthol which is solid below 35 ^{o}C (typical nozzle exit temperature is 5-30 ^{o}C) and can be easily sublimed. RESS-SC concept is demonstrated by producing nanoparticles of griseofulvin, 2-aminobenzoic acid, phenytoin, and acetazolamide. A significant increase in the solubility and reduction in the particle size is observed in all four cases.

ACKNOWLEDGEMENTS

In this social world it is difficult to achieve anything without taking help from anybody else. This is also true for my PhD and I would like to acknowledge all of them. Special mention is needed of Dr. Ram B Gupta for his suggestions and advice in research problems. I also appreciate his direction, patience, and ready availability for consultation. I would also like to extend my gratitude to Dr. Christopher B Roberts, Dr. Gopal A Krishnagopalan and Dr. Daniel L Parsons for enthusiastically agreeing to serve on my dissertation committee and giving valuable inputs to my research.

I cannot forget my parents, sister and brother for encouragement and continuous support throughout my life. I would not have achieved anything without their help and support.

Friends and colleagues are also important parameter of my life who contributed a lot in my research and stay in auburn. I like to thank Bhavin Vadgama, Hiral Vadgama, Gracy Bell and Sherin Padinjaremury to make my life enjoyable at Auburn. I would also like to thank my colleagues Dr. Amol Thote, Philip Bell, Dan Obrzut, Mukund Karanjaikar, Kyoko Uno, Dr. Pardeep Parsad, Dr. Parag Garhyan, Raghu Vishwanathan, Dr. Chandler Mcleod, Dr. Nimir Elbashir, Dr. B K Chang, Dr. Chris Kitchens, Madhu Anand, Debbie Boroughs and others who helped me in day to day research activities some way or other. I cannot forget Haley Brooks, Auburn Hudgins, Sheena Lewis,

Suheila, Dan, and Adam for their help. And I also like to thank Mr. Joe Alderholt and

Sue Ellen Abner for their help.

TABLE OF CONTENTS

xi

LIST OF FIGURES

xvi

LIST OF TABLES

CHAPTER 1

INTRODUCTION

In 1960, several years before the word "chip" became a lexicon in electronics, Richard Feynman, a physicist at Cal Tech, gave a ground breaking lecture titled "There is Plenty of Room at the Bottom". In that lecture, he not only talked about extreme miniaturization but also talked about manipulating matters at nanoscale and physical laws feasibility at that level. In 21st century, significant research is being done on finding new methods of particle synthesis or their application at nano scale. Nanotechnology can be defined as any functional device or material which is of 1-100 nm (nanometer) size.

Because of the unique properties offered by nanoparticles, their application can be found in every aspect of life from biological medicines to day to day use sunscreen lotions. This is attributed to the high surface area to volume ratio of nanoparticles. Going to the nano level not only enhances surface to volume ratio but also change their chemical or biological activity, optical, magnetic, and other physical properties. Classical laws can not be applied to these particles or fibers and quantum physics is needed to explain the entire phenomenon at this level.

Many methods have been employed till date for synthesis of nanomaterials such as chemical vapor deposition, plasma spraying, methods based on supercritical fluids, and also some chemical methods. Spray drying (Nass, 1988), fluid energy grinding (Nass,

1988), lypophilization (Briggs and Maxwell, 1975) and milling (Hixon et. Al., 1990; Van Cleef, 1991) were some other methods employed for dry particulate formation. But every method has some drawbacks like thermal degradation, excessive use of organic solvent, toxicity, broad size distribution, and chemical degradation for incomplete solvent removal. In recent years supercritical fluids (SCFs) are finding wide application in nano materials systemization.

1.1   Supercritical Fluid (SCF)

In 1980s SCFs emerged as an important tool for nanotechnology although dissolving power of SCFs was known as early as 1879. Any fluid above its critical point is called supercritical fluid. SCFs have solubility comparable to liquids and diffusivity much higher than gases. Figure 1 shows the typical pressure-temperature phase diagram. Two phases are in equilibrium along the lines. At the triple point, all the three phases (solid-liquid-gas) coexist. Critical point is the last point where liquid and gas coexist and above the two phases are non-distinguishable. Properties of fluids significantly vary right after that critical point.

Density of SCFs can be controlled by varying pressure. Solubility in a fluid depends on its density; hence by changing pressure we can change density which in turn changes the solubility. In SCF based processes, this property of changing solubility with pressure are utilized to obtain uniform particles. Many SCFs have been tested till date for particle formation including ethylene (Krukonis, 1984), water (Matson et. al. , 1986; Petersen et. al., 1986)and carbon dioxide (Matson et. al., 1987; Debendetti et. al., 1993). Out of these CO_2 is widely used because of its mild critical point of $31.1^{\circ}C$ and 73.8 bar.

Other than solubility power of SCF, supersaturation (Bristow et. al., 2001), volumetric expansion of solute in the solvent, and intermolecular force of attractions between solute-solute, solute-solvent and solvent-solvent are also important (McHugh and Krukonis, 1994). Figure 2 shows the phase-diagram for CO_2 at three different temperatures (based on NIST data), one close to critical temperature, one below and one above the critical temperature. It is clear from this figure that density changes rapidly at critical pressure and continue to increase with pressure.

1.2 SCF Based Particle Formation Processes:

There is growing interest of technologies which can be operated at mild conditions with controlled uniform size distribution and high product quality. Debendetti (1994) discussed two routes for particle formation using SCF: rapid expansion of supercritical solution (RESS) for substances which are soluble in supercritical solvent and Supercritical antisolvent (SAS) for sparingly soluble materials. Knez and Weidner (2003) also discussed the particle formation using supercritical fluids. There are many modifications in the SAS process to achieve monodisperse micron or nano sized particles. SCF technologies offer following processes which can be use for desired need of industries.

1.2.1 Rapid Expansion of Supercritical Solutions (RESS):

RESS processes are based on the principle that low vapor pressure solids can dissolve quite comfortably in fluids at temperature and pressure slightly above their critical points. In RESS, SCF dissolves solid at pre-expansion condition and then expanded through micro-nozzle in atmospheric zone. Because of rapid expansion of

3

solution solvent looses its solvating power, leading to supersaturation and precipitation of solute. Inorganic/ceramic, organics/pharmaceuticals, polymers and two solute systems material have been made so far by using this technique. Figure-3 shows the schematic diagram for RESS process.

After more than a century, when Hannay and Hogarth (1879) observed change in particle size and morphology upon expansion of supercritical solutions, Krukonis (1984) described this method for particle formation (Tom et. al., 1990). Krukonis made inorganic particle aluminum iso-propoxide using ethylene as supercritical fluid. Petersen et. al. (1986) discussed about using solvent above their critical point for dissolving low vapor pressure solids (GeO_2, Polyvinyl chloride/KI and SiO2/KI) and precipitating them after rapid expansion. They used pentane, propane, and ethanol in supercritical region as solvent. Later Turner et. al. (1987) studied the effect of gas and aerosol dynamics and optimized the design of nozzle to get monodisperse particles. Organic polymer fibers cellulose acetate of typical diameter 1-5 μm was obtained by RESS method (Petersen et. al., 1987). Reverchon et. al. (1995) used trifloromethane (CHF_3) as SCF for griseofulvin micronization using RESS process. Carbon-di-oxide (CO_2) is preferred SCF for RESS process because of its properties like non-toxicity, mild critical condition, non-flammable and also it is benign for the environment.

Most of the organic compounds are highly soluble in supercritical CO_2. Benzoic acid (Schmitt et. al. 1986) and cholestrol (Singh et. al. , 1993) were precipitated using SC carbon-di-oxide. Several researchers tried the RESS technique for precipitation of PLA using co-solvents for controlled drug delivery system (Tom et. al., 1994). Chernyak et. al. (2001) did perfluoropolyether coating using RESS process. Some researchers have

4

modified RESS process and expanded supercritical solution with a non-solvent for formation of microcapsules of medicine and named it as RESS-N process (Matsuyama et. al. 2002). Pharmaceutical drugs like griseofulvin, digoxin, and 2-aminobenzoic acid have very little solubility in SC CO_2 and also difficult to make nano-sized particles, though at tip of the nozzles particle size is only 5 nm.

To better understand the particle formation and growth mechanism and the factors which affect those mechanism process modeling is important. Mathematical modeling of compressible flow dynamics started in 1992 by Lele and Shine assuming dilute solutions with steady, one–dimensional, inviscid flow with adiabatic expansion. They used the Altumin equation of state (EOS) (1987) for their thermodynamic calculations. Kwauk et. al. (1993) mathematically modeled the aerosol formation in RESS. They have the same assumption as Lele and Shine but they used Peng and Robinson's EOS (1976). Also they did not account for any heat effects associated with evaporation and condensation, but they modeled nucleation, condensation, and growth mechanism. Berends et. al. (1993) verified some factors which affect the nucleation and growth by their theoretical calculations. One of the methods which is widely accepted and utilized to solve non-linear aerosol dynamic equation is population balance. General dynamic equation for aerosols was theoretically described by Gelbard and Sinfeld way back in 1979. Kumar and Ramkrishna (1997) solve population balance equations by discretization for nucleation, growth, and aggregation processes. Reverchon et. al. (1996) looked into the hydrodynamic modeling part of RESS. Later on, Weber et. al. (2002) modeled subsonic part with same assumptions and calculated that subsonic RESS is an effective method of

forming 10-15 nm diameter range particles. Though Domingo et. al. (1996) showed that adiabatic assumption is not valid.

Several researchers incorporated a heat effect in their mathematical model. They also used more accurate EOS to define all the thermodynamic conditions inside the process. Helfgen et. al. (2001) treated capillary inlet flow as isentropic and also included heat exchange and friction in nozzle with heat exchange in supersonic free jet. They also used a more accurate Bender EOS method (Platzer and Maurer, 1989) for thermodynamic properties. To date none of the modeling works have been able to explain the practical results with one hundred percent accuracy, though they provide us good information of factors which affect the particle size, their distribution and morphology.

All solids of interest cannot be dissolved in SCF, esp. SC CO_2, and even if we are able to dissolve, then solubility is very low. This is one important bottleneck of RESS process.

1.2.2   Supercritical Anti-solvent (SAS):

The SAS technique is based on volumetric expansion of liquid after coming in contact with SCFs. In this method, particles are dissolved in suitable solvent and then that solution is sprayed inside SCF. This SCF acts as an antisolvent for the solution and dissolves solvent causing particles precipitation. Solvent has more affinity for SCF than that for solutes.   Figure-4 shows schematic diagram for this technique.

High volumetric expansion of dimethylsulfoxide (DMSO) and dimethylformamide (DMF) was produced with CO2 near the mixture's critical point (Yeo et. al., 1993). Debenedetti (1994) mentioned that significant volumetric expansion

which causes decrease in liquid's cohesive energy density results in particle formation. This is one of the fundamental concepts of the SAS process.

Though gaseous CO2 as an antisolvent has been used since 1986 in hydrocarbon industry (Davis, 1986) but use of supercritical CO2 as an antisolvent started in the late 1980s. Krukonis et. al. (1988) recrystallizes the RDX (cyclotrimethylenetrinitramine) using supercritical fluid antisolvent method. They crystallized 100-150 μm RDX crystals. Another semibatch process, gas antisolvent recrystallization (GAS) was introduced by Gallagher (1989) and in this process antisolvent is continuously introduced into a stationary bulk liquid phase. Later on Yeo et. al. (1993) introduced supercritical fluid as an antisolvent for particle formation and named the process as Supercritical Antisolvent (SAS) method. Dixon et. al. (1993) produced fibers by spraying polymeric solution into compressed CO_2 through a 100 μm nozzle and named that process as PCA (Precipitation with Compressed Antisolvent). Randolph et. al. (1993) studied the effect of pressure, temperature, concentration, and flow configuration for the control of particle size in the GAS method. They sprayed the solution into a CO_2 continuous phase. Also, a sonicating nozzle (120 kHz) was used for atomizing solution droplets for continuous system. Mawson et. al. (1996) proposed coaxial nozzle method for better control of particle morphology in compressed fluid antisolvent technique. Using a coaxial nozzle increases the particle size but decreases the flocculation. Pharmaceutical compounds (Reverchon et. al., 1999) and inorganic precursors (Reverchon et. al., 1999) were also produced using the SAS method. Dixon et. al. (1993) observed decrease in particle size with increase in pressure and relate that phenomenon with the Weber number where as

7

Randolph et. al.(1993) observed increase in size with increase in pressure above critical pressure and explains that on the basis of mass transfer between solvent and antisolvent.

After development of PCA and SAS processes which are modified methods of GAS process, Hanna and York (1994) patented another method called Solution Enhanced Dispersion by Supercritical fluids (SEDS). In the SEDS process, solution is introduced inside the precipitation chamber along with supercritical fluid through same nozzle. Later on, Palakodaty et. al. (1998) modified this SEDS process by mixing co-solvent along with SCF to form lactose particles. Particles from gas saturated solutions or the PGSS method was presented by Weidner et. al. (1994). In the PGSS process compressible gas is dissolved in a mixture of substances till saturation and then expanded to precipitate microparticles. Chattopadhyay and Gupta (2001) proposed another method of nanoparticle formation called supercritical antisolvent with enhanced mass transfer (SAS-EM). Solution is injected on the tip of the ultrasound horn vibrating at 60 kHz frequency inside a supercritical CO_2 precipitation chamber. Acoustic energy provided by vibrating surface enhances the mass transfer and also prevents particle agglomeration.

By the end of the twentieth century, researchers started working on better control of particle size and morphology in antisolvent method. Various mechanisms have been proposed for explaining the precipitation of particles with antisolvent techniques. Solubilities of pure solids in GAS process were first studied using a molecular thermodynamic model (Dixon et. al., 1991) but only till 64 bar pressure. Kikic et. al. (1997) did the thermodynamic analysis of RESS, PGSS and SAS processes. They used the Peng-Robinson equation of state (PR-EOS) and the classical mixing rule to understand phase behavior of the system. To understand the two way mass transfer both

into the droplet and into the bulk antisolvent, Werling et. al. numerically modeled the SAS process for subcritical region (1999) and miscible condition (2000). They used a time dependent conservation equation assuming spherical symmetry, stagnant droplet, and equilibrium at vapor-liquid interface. For modeling a miscible condition they assumed full miscibility of two phases. Complete simulation (thermodynamics, hydrodynamics, and mass transfer) of the SAS recrystallization process assuming isothermal condition inside the precipitation chamber was studied by Kikic group (Lora et. al., 2000). Lengsfeld et. al. (2000) explained atomization vs nucleation and growth for the PCA process. Deviating from the earlier understanding of atomization or one droplet-one particle theory, they proposed another mechanism by which gaseous shear layers cause disappearance of surface tension without discrete droplet formation. The effect of initial droplet size on particle size was also studied in the SAS process (Rantakyla et. al., 2002). Theoretically they did not observe any change of particle size with change of droplet size at the nozzle. Recently, effect of flow rate and thermodynamic states on droplet size has been studied by mass and heat transfer analysis (Mukhopadhyay et. al., 2004).

1.3   Current Thesis Work

The major thrust in this thesis work is to develop the science of supercritical fluids. Dealing with nature and natural product is a very hard task. So is the case for producing chitin (a biopolymer) nanofibers. Production of chitin nanofibers can be achieved by the SAS process after dissolving the chitin in hexafluoroisopropanol (HFIP) solvent. Because of its highly crystalline nature, dissolution of chitin in any conventional

solvents is difficult. By the SAS process a web of chitin nanofibers of 84 nm size was obtained (Chapter 2).

SAS-EM is one of the methods which can be used to change particle morphology from rod- to sphere-like. Hydrocortisone, an anti-inflammatory drug, forms rod-like particles by the conventional SAS process. But the SAS-EM method is used to produce spherical hydrocortisone particles of 150 nm size by controlling the ultrasound intensity (Chapter 3). Hydrocortisone is a very soft material having a tendency of agglomeration which was avoided by using the vibrating horn. After the process, drug purity remains constant and this was supported by HPLC (High Performance liquid Chromatography) results.

The SAS process has been used for many applications other than producing nanoparticles. Microemulsion, as other particle formation technique, is also being widely used. By combining microemulsion and the SAS method, uniform particles of nano scale range were formed for coating application. Silica coating of gold colloid is achieved using W/O microemulsion by reacting supercritical CO_2 with sodium silicate solution. Particle size of silica coated gold particles of as small as 50 nm is obtained by this method (Chapter 4). CO2 acts not only as an antisolvent but also as a reactant as described earlier by Chattopadhyay and Gupta (2003).

Keeping the limitations of RESS process in mind, a new method is developed (RESS-SC) where cosolvent that is solid at nozzle exit condition is used. As per the conventional RESS method, particles in the order of 800-3000 nm in size are obtained due to agglomeration and growth in expansion chamber. But by the new process, RESS-SC, particles in nanometer size range can be obtained and also at high yields. This

process has been demonstrated with griseofulvin (Chapter 5), 2-aminobenzoic acid (Chapter 6), phenytoin (Chapter 7), and acetazolamide (Chapter 8) compounds. Menthol is used as a solid cosolvent which can be easily sublimed and is solid below 35 $^{\circ}$C. The presence of solid cosolvent in expansion chamber decreases the chances of particle aggregation as the desired compound is mostly surrounded by cosolvent which has comparatively higher solubility in SC CO_2.

The low solubility of pharmaceutical drugs in SC CO_2 is another limitation in conventional RESS process and has been addressed in the RESS-SC process. By using menthol as cosolvent, drug solubility in supercritical CO_2 is increased multiple fold. Menthol is polar compound and increases the polarity of CO_2 which helps in increasing the solubility.

LITERATURE CITED

1. Feynman, R. There's Plenty of Room at Bottom. Engineering and Science. 1960

2. Nass, R., Pharmaceutical Suspensions. Pp. 151-199, In: H.A. Lieberman, M.Reiger, and G. Banker (editors), Pharmaceutical Dosage Forms, Marcel Dekker, New York, 1988.

3. Briggs, A.; Maxwell, T. Method of preparation of lyophilised biological products. US patent 3,928,555, 1975.

4. Hixon, L.; Prior, M.; Prem, H.; Van Cleef, J. Sizing Materials by crushing and grinding. Chem. Eng., 97, 9-103, 1990.

5. Van Cleef, J. Powder Technology. Am. Sci., 79, 304-315, 1991.

6. Krukonis, V. Supercritical Fluid Nucleation of difficult-to-comminute solids. AIChE Fall Meeting, San Fransisco, CA paper 140f, 1984.

7. Matson, D.W.; Petersen, R. C.; Smith, R. D. Formation of silics powders from the rapid expansion of supercritical solutions. Advanced Ceramic Materials, 1(3), 242-6, 1986.

8. Petersen, R.C.; Matson, D. W.; Smith, R.D. Rapid precipitation of low vapor pressure solids from supercritical fluid solutions: formation of thin films and powders. Journal of American Chemical Society, 108(8), 2100-2, 1986.

9. Matson, D.J.; Fulton, J. L.; Petersen, R. C.; Smith, R. D. Rapid expansions of supercritical fluid solutions: solute formation of powders, thin films and fibers. Ind. Eng. Chem. Res., 26(11), 2298-306, 1987.

10. Debenedetti, P.G.; Lim, G. B.; Prud'homme, R. K. Formation of protein microparticles by antisolvent precipitation. Eur. Patent Appl., 1993.

11. McHugh, M.A.; Krukonis, V.J.; Pratt, J. A. Supercritical Fractionation of polymers and copolymers. Trends in Polymer science. 2(9), 301-7, 1994.

12. Bristow, S.; Shekunov, T.; Shekunov, B.Y.; York, P. Analysis of supersaturation precipitation process with supercritical CO_2. Journal of supercritical fluids. 21(3), 257-271, 2001.

13. Debenedetti, P.G. Supercritical fluids as particle formation media. J. Supercritical Fluids. 719-729, 1994.

14. Knez, Z.; Weidner, E. Particle formation and particle design using supercritical fluids. Cureent opinion in solid state and material science, 7(4-5), 341-351, 2003.

15. Hannay, J.B.; Hogarth, J. Proc. R. Soc.London 29, 324, 1879.

16. Tom, J.W.; Debenedetti, P.G. Particle formation with supercritical fluids- A review. J. Aerosol Sci., 22(5), 555-584, 1991.

17. Turner, J. R.; Kodas, T.T.; Friedlander, S. K. Monodisperse particle production by vapor condensation in nozzles. Journal of Chemical Physics, 88(1), 457-65, 1988.

18. Petersen, R. C.; Matson, D. W.; Smith, R. D. The formation of polymer fibers from the Rapid expansion of supercritical fluid solutions. Polymer Engg. Sci., 27(22), 1693-97, 1987.

19. Reverchon. E.; Della Porta, G.; Taddeo, R.; Pallado, P.; Stassi, A. Solubility and micronization of griseofulvin in supercritical CHF_3. Ind. Eng. Chem. Res., 34(11), 4087-91, 1995.

20. Schmitt, W.J.; Reid, R.C. Solubility of monofunctional organic solids in chemically diverse supercritical fluids. J. Chem. Eng. Data, 31(2), 204-12, 1986.

21. Tom, J.W.; Debenedetti, P.G.; Jerome, R. Precipitation of PLA and composite PLA-Pyrene particles by Rapid Expansions of supercritical solutions. J. Supercritical Fluids, 7, 9-29, 1994.

22. Chernyak, Y.; Henon, F.; Harris, R.B.; Gould, R.D.; Franklin, R.K.; Edwards, J.R.; DeSimone, J.M.; Carbonell, R.G. Formation of Perfluoropolyether coatings by the Rapid expansion of Supercritical Solutions (RESS) process. Part 1: Experimental Results. Ind. Eng. Chem. Res., 40, 6118-6126, 2001.

23. Matsuyama, K.; Mishima, K.; Hayashi, K.; Ishikawa, H.;Matsuyama, H.; Harada, T. Formation of microcapsules of Medicines by Rapid Expansion of Supercritical Solution with a Nonsolvent. J. Appl. Poly. Sci., 89, 742-752, 2003.

24. Lele, A.K.; Shine, A.D. Morphology of Polymers Precipitated from a Supercritical Solvent. AIChE Journal, 38(5), 742-752, 1992.

25. Kwauk, X.; Debenedetti, P.G. Mathematical Modeling of Aerosol Formation by Rapid Expansion of Supercritical Solutions in a converging nozzle. J. Aerosol Sci., 24(4), 445-469, 1993.

26. Berends, E.M.; Bruinsma, O.S.L.; van Rosmalen, G.M. Nucleation and Growth of fine crystals from supercritical carbon dioxide. J. Crystal Growth, 128, 50-56, 1993.

27. Gelbard, F.; Seinfeld, J.H. The General dynamic equation for aerosols. J. Colloid Interface Sci., 68(2), 363-382, 1979.

28. Kumar, S.; Ramkrishna, D. On the solution of population balance equations by discretization − III. Nucleation, growth and aggregation of particles. Chem. Eng. Sci., 52(24), 4659-4679, 1997.

29. Reverchon, E.; Pallado, P. Hydrodynamic Modeling of the RESS Process. J. Supercritical Fluids, 9, 216-21, 1996.

30. Weber, M.; Russell, L.M.; Debenedetti, P.G. Mathematical Modeling of nucleation and growth of particles formed by the rapid expansion of a supercritical solution udner subsonic conditions. J. Supercritical Fluids, 23, 65-80, 2002.

31. Domingo, C.; Berends, E.; van Rosmalen, G. M. Precipitation of ultra fine benzoic acid by expansion of a supercritical carbon dioxide solution through a porous plate nozzle. J. Crystal Growth, 166, 989-995, 1996.

32. Helfgen, B.; Hils, P.; Holzknecht, Ch.; Turk, M.; Schaber, K. Simulation of particle formation during the rapid expansion of supercritical solutions. Aerosol Science, 32, 295-319, 2001.

33. Yeo, S.D.; Debenedetti, P.G.; Radosz, M.; Schmidt, H.W. Supercritical antisolvent process for substituted para-linked aromatic polyamides: phase equilibrium and morphology study. Macromolecules, 26(23), 6207-10, 1993.

34. Davis, T.A. Deashphalting heavy oils using a miscible solvent at a low treat ratio and a carbon dioxide antisolvent. US Patent 84-642502, 1986.

35. Krukonis, V.J.; Coffey, M.P.; Gallagher, P.M. Exploratory development on a new process to produce improved RDX (cyclotrimethylenetrinitramine) crystals: supercritical fluid anti-solvent recrystallization. Report (BRL-CR-606; order no. AD-A207760), 1988.

36. Gallagher, P.M.; Coffey, M.P.; Krukonis, V.J.; Klaustis, N. Gas antisolvent recrystallization : new process to recrystallize compounds insoluble in

supercritical fluids. ACS Symposium Series, 406 (Supercrit. Fluid Sci. Technol.), 334-54, 1989.

37. Yeo, S.D.; Lim, G.B.; Debenedetti, P.G.; Bernstein, H. Formation of microparticulate protein powders using a supercrtitical fluid antisolvent. Biotechnology and Bioengineering, 41(3), 341-6, 1993.

38. Dixon, D.J.; Johnston, K.P.; Bodmeier, R.A. Polymeric materials formed by precipitation with a compressed fluid antisolvent. AIChE Journal, 39(1), 127-39, 1993.

39. Randolph, T.W.; Randolph, A.D.; Mebes, M.; Yeung, S. Sub-micrometer sized biodegradable particles of Poly (L-lactic acid) via the GAS antisolvent spray precipitation process. Biotechnol. Prog., 9, 429-435, 1993.

40. Mawson, S.; Johnston, K.P. Precipitation with a compressed fluid antisolvent: Advanced concepts. Polymeric Material Sci. and Engg., 74, 180-1, 1996.

41. Reverchon, E.; Della Porta, G. Production of antibiotic micro- and nano-particles by supercritical antisolvent precipitation. Powder Tech., 106(1-2), 23-29, 1999.

42. Reverchon, E.; Della Porta, G.; Sannino, D.; Ciambelli, P. Supercritical antisolvent precipitation of nanoparticles of a zinc oxide precursor. Powder Tech., 102(2), 127-134, 1999.

43. Hanna, M.; York, P. Patent Application PCT/GB94/01426, 1994.

44. Palakodaty, S.; York, P.; Pritchard, J. Supercritical fluid Processing of Materials from Aqueous Solutions: The application of SEDS to Lactose as a model substance. Pharmaceutical Research, 15(12), 1835-43, 1998.

45. Weidner, E.; Knez, Z.; Novak, Z. PGSS (Particles from the Gas saturated Solutions) a new process for powder generation. Proceedings of the 3rd International Symposium on Supercritical Fluids, ISSF, Strasbourg, p 229, 1994.

46. Chattopadhyay, P.; Gupta, R.B. Production of antibiotic nanoparticles using Supercritical CO2 as antisolvent with Enhanced mass transfer. Ind. Engg. Chem. Res., 40(16), 3530-39, 2001.

47. Dixon, D.J.; Johnston, K.P. Molecular thermodynamics of solubilities in gas antisolvent crystallization. AIChE Journal, 37(10), 1441-9, 1991.

48. Kikic, I.; Lora, M.; Bertucco, A. A thermodynamic analysis of three-phase equilibria in Binary and ternary systems for applications in Rapid expansion of a supercritical solutions (RESS), particles from gas saturated solutions (PGSS), and Supercritical antisolvent (SAS). Ind. Eng. Chem. Res., 36, 5507-15, 1997.

49. Werling, J.O.; Debenedetti, P.G. Numerical Modeling of mass transfer in the supercritical antisolvent process. J. Supercr. Fluids, 16, 167-181, 1999.

50. Werling, J.O.; Debenedetti, P.G. Numerical modeling of mass transfer in the supercriticla antisolvent process: miscible conditions. Journal of Supercritical fluids, 18(1), 11-24, 2000.

51. Lora, M.; Bertucco, A.; Kikic, I. Simulation of the semicontinuous supercritical antisolvent recrystallization process. Ind. Eng. Chem. Res., 39, 1487-96, 2000.

52. Lengsfeld, C.S.; Delplanque, J.P.; Barocas, V.H.; Randolph, T.W. Mechanism governing microparticle morphology during precipitation by a compressed antisolvent: atomization vs nucleation and growth. J. Phys. Chem. B, 104, 2725-2735, 2000.

17

53. Rantakyla, M.; Jantti, M.; Aaltonen, O.; Hurme, M. The effect of initial drop size on particle size in the supercritical antisolvent precipitation (SAS) technique. J. Supercrirical Fluids, 24, 251-263, 2002.

54. Mukhopadhyay, M.; Dalvi, S.V. Mass and heat transfer analysis of SAS: effects of thermodynamic states and flow rates on droplet size. J. Supercritical Fluids, 30(3), 333-348, 2004.

55. ChattoPadhyay, P.; Gupta, R.B. Supercritical CO_2 based formation of silica nanoparticles using water-in-oil microemulsions. Ind. Eng. Chem. Res., 42(3), 465-472, 2003.
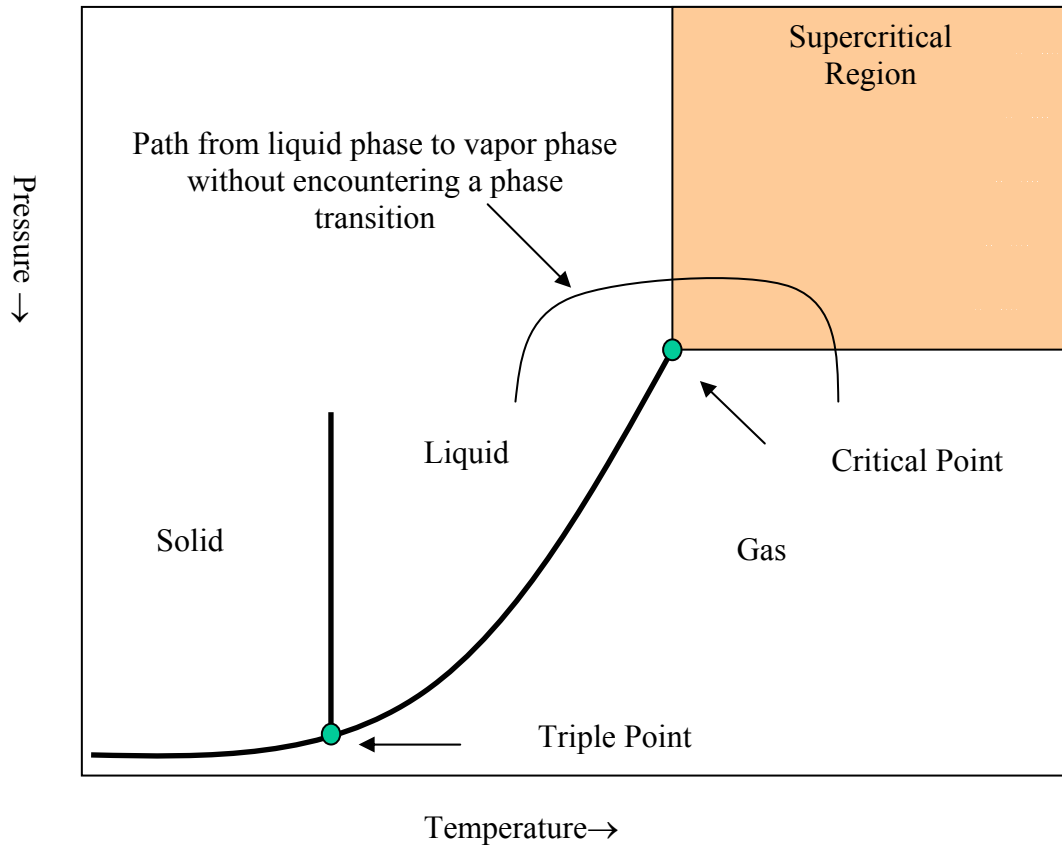
Figure 1.1 P-T phase diagram
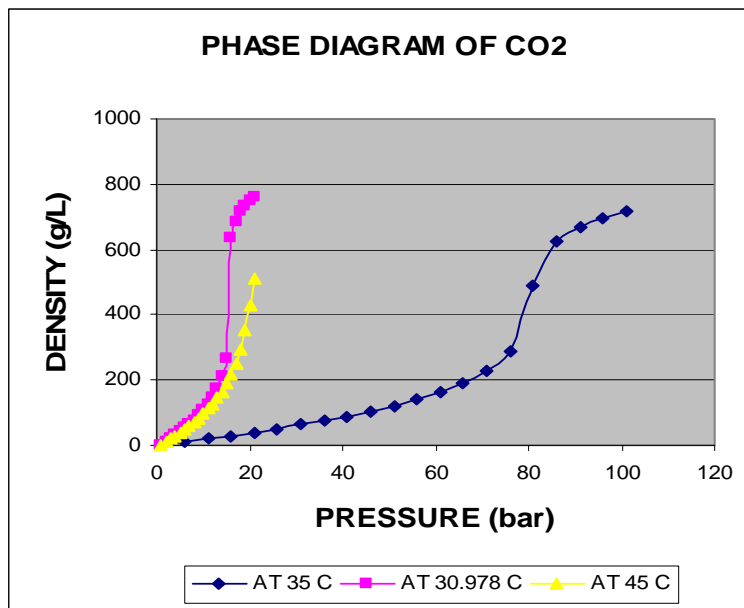
Figure 1.2 Phase diagram for CO$_2$
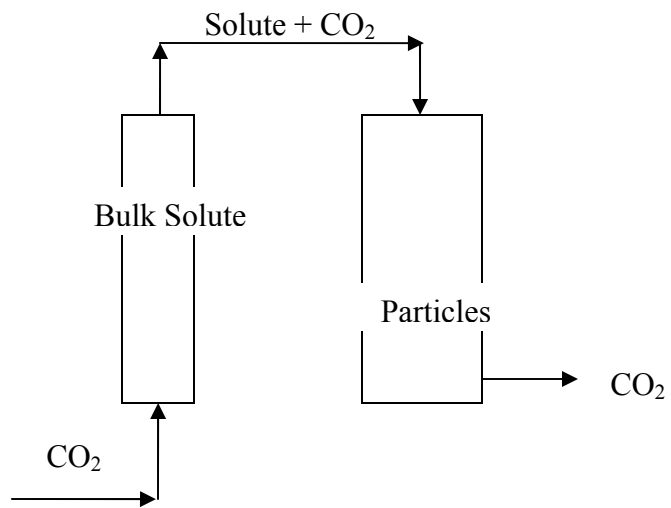
Figure 1.3 RESS schematic diagram
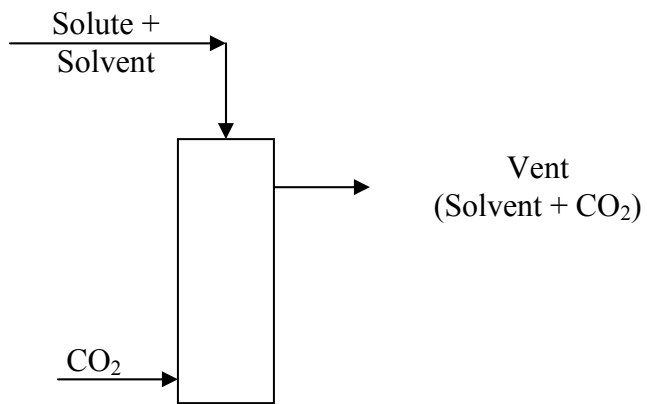
Figure 1.4 SAS Process schematic diagram

CHAPTER 2

FORMATION OF CHITIN NANO-FIBERS BY SUPERCRITICAL ANTISOLVENT

2.1 Abstract

Chitin is emerging as a biopolymer of choice due to its potential uses in the numerous biomedical and pharmaceutical applications (e.g., wound dressing, tissue engineering, drug delivery, anti-allergic agent, etc.). Nanofibers can provide enhanced properties in many of these applications. Unfortunately, due to highly crystalline nature, chitin is not soluble in conventional solvents, and it is very difficult to produce it in the fine particulate fibrous forms. In this work, chitin is dissolved in hexafluoroisopropanol solvent. This solution is then sprayed into supercritical carbon dioxide, which rapidly removes the solvent precipitating chitin as nano-fibers. Based on scanning electron microscopy, precipitated chitin is observed as a web made of nano-fibers of about 84 nanometer in diameter. According to the Fourier-transform infrared spectroscopy, chitin molecular structure is preserved during the processing.

2.2 Introduction

Chitin is the second most abundant natural polymer in nature, commonly found in the exoskeletons or cuticles of many invertebrates and in the cell walls of most fungi and some algae. It is usually obtained from the shells of shellfish, crab, lobster, or shrimp. Chitin is a cationic amino polysaccharide, and its molecular structure

(shown in Figure 2.1) is idealized as a linear polysaccharide of β-(1-4)-2-acetamido-2-deoxy-D-glucopyranose where all residues are comprised entirely of N-acetyl-D-glucosamine residues. Chitosan is the deacetylated form of chitin, and its molecular structure is idealized as a linear polysaccharide of β-(1-4)-2-amino-deoxy-D-glucopyranose where all residues are comprised entirely of D-glucosamine residues. However in most natural forms, this biopolymer exists as a random co-polymer of D-glucosamine and N-acetyl-D-glucosamine units. When the number of acetamido groups is more than 50% (more commonly 70-90%) the biopolymer is termed chitin (Tharanathan and Kittur, 2003; Khor, 2001).
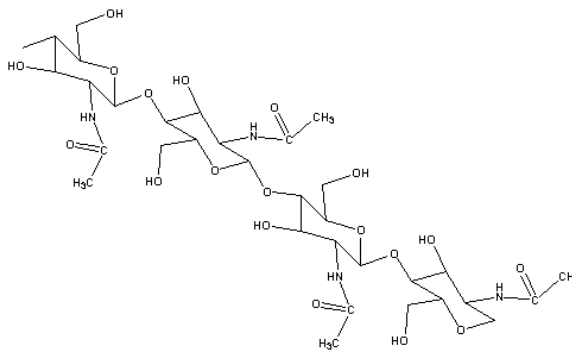
Figure 2.1. Molecular structure of the repeat unit in chitin polymer

Chitin exists in three polymorphic solid-state forms: $\alpha–$, $\beta–$ and $\gamma–$chitin. Out of these, α-chitin is the most stable and abundant form in which the chains are organized in anti-parallel configuration. The highly ordered crystalline structure is attributed to the extensive hydrogen bonding (Khor, 2001).

Chitin is emerging as a biopolymer of choice due to its potential uses in the numerous biomedical and pharmaceutical applications (e.g., wound dressing, tissue engineering, drug delivery, anti-allergic agent, etc.). For example, chitin-based wound

dressings promote and accelerate wound healing, due to the formation of fibrous networks for protein attachment which is attributed to the presence of N-acetylglucosamine (Yusof et al., 2001). Nanofibers and nanoparticles can provide enhanced properties in many of these applications (Hermann et al., 2001).

De-acetylated form of chitin, termed as chitosan, has been more utilized because of its easier solubilization. In contrast, chitin is not soluble in the most conventional solvents; hence it has been termed as "intractable" which has been the main reason for lack of studies on chitin (Khor, 2002). There are only a few "exotic" solvents that can solubilize chitin, including dimethylacetamide with 5 w/v % LiCl (Tokura et al, 1983), methanol saturated with calcium chloride dihydrate (Tokura et al, 1996), hexafluoroisopropanol (HFIP), and hexafluoroacetone sesquihydrate. These solvents appear to provide solubilization without alteration of the chitin molecular structure. For example, preparation of chitin films and fibers using HFIP as solvent were reported by Capozza (1976a; 1976b). In that report, there was no indication of polymer degradation and the solution was transparent and quite viscous even at 1.5 wt % concentration.

Once chitin is dissolved in a suitable solvent, it can be precipitated as particles or fibers using an antisolvent. So far liquid antisolvents have been utilized that give chitin precipitate of large or macro size, mainly because of the strong inter- and intra-molecular H-bonding in chitin molecules resulting in strong agglomeration during the precipitation process. It would be possible to obtain micro- or nano-size precipitate if a faster precipitation process is used. Diffusivity of supercritical fluids is about 100 fold that of liquids, hence a supercritical antisolvent can provide faster precipitation leading to a decrease in size of the precipitated polymer.

2.2.1 Supercritical Antisolvent (SAS)

In SAS, solution (e.g., solute + solvent) is sprayed through a fine nozzle into supercritical fluid which acts as an antisolvent. Supercritical carbon dioxide is most widely used antisolvent for SAS process. The process is operated at conditions in which the solvent and antisolvent are miscible, and solvent has more liking for antisolvent than solute, forming a homogeneous phase. Due to the rapid extraction of the solvent from the solution, super-saturation occurs, causing homogeneous nucleation and the solute to precipitate. After the solute is precipitated, it is further washed with the supercritical antisolvent to remove any residual solvent, and then the system is depressurized for product collection.

Supercritical carbon dioxide has been widely used for pharmaceutical processing for the last fifteen years, and several reviews have been published where the benefits of using supercritical CO_2 are highlighted, including: (a) reduced usage of conventional liquid solvents; (b) production of relatively contaminant-free products; (c) micron and submicron-size particles production with controlled particle size and purity (Gupta and Chattopadhyay 2003; Chattopadhyay and Gupta, 2001, 2002; Subramaniam et al., 1997, Kompella and Koushik, 2001); (d) control of porosity by choosing the appropriate process path (Palakodaty and York, 1999); (e) extraction and fractionation of pharmaceutical compounds; (g) drug encapsulation, impregnation and coating; and (h) sterilization of pharmaceutical products (Foster et al, 2003).

Hirokazu et al. (2003) have used SAS to produce chitosan particles. However, so far, chitin has not been precipitated by supercritical solvent, again mainly because of the chitin insolubility issues. Recently, HFIP solvent was found to be suitable for SAS

process by Snavely et al. (2002) while processing insulin. Fortunately this HFIP solvent can dissolve chitin to some extent.   Hence, chitin/HFIP solution can be used in SAS process. The main focus of this work is to produce chitin nano-fibers using supercritical carbon dioxide antisolvent.

2.3   Experimental section

2.3.1   Materials

Chitin from crab shells was purchased from Sigma (Practical grade, Batch # 033K1181) with 20 mesh size and a 96% degree of acetylation as reported by the manufacturer. Hexafluoroisopropanol (HFIP) was purchased from SynQuest Labs (99% min, Lot # Q 88-106) and was filtered through a PTFE syringe filter (0.2 micron pore size) prior to use. Liquid carbon dioxide was purchased from BOC gases (SFC/SFE grade 5.5) and was used as received.

2.3.2   Chitin purification

Chitin purification requires removal of proteins and minerals. To remove minerals, 90 gram chitin was soaked for 24 hours with 0.5 liter HCl (2 N) at 10 ºC. This mixture was then rinsed with tap water until neutral pH was obtained. Now to remove proteins, the rinsed chitin from previous step was added to 1 liter NaOH (2.5 N) and stirred at 90 ºC for 2 hours. This mixture was then rinsed with tap water until neutral pH was obtained and then dried in a vacuum oven. Ash tests were performed on raw chitin, demineralized chitin, and demineralized-deproteinized chitin with the following purities:

96.7%, 99.2%, and >99.2%, respectively. Purified chitin was stored at room temperature for further use in SAS.

2.3.3 Chitin dissolution

Chitin was dissolved in HFIP to obtain a 2 mg/mL solution, and then stirred for 48 h. The solution was filtered through a 0.2 micron PTFE syringe filter before using in SAS.

2.3.4 Apparatus and procedure

A schematic of the SAS apparatus used to produce the chitin fibers is shown in Figure 2.2. Using ISCO pump, the vessel is filled with CO_2 from the tank and pressurized to the desired pressure, which is measured using a Heise ST-2H pressure transducer connected directly to the vessel. The vessel is heated by means of a heating tape and temperature is controlled with a Barnant R/S temperature controller using a type K thermocouple inserted into the vessel. Once the system is in equilibrium, the TESCOM 44100 backpressure regulator is opened to allow CO_2 to flow through the system while the flow rate of CO_2 is being maintained by the ISCO pump.

Once the system is equilibrated and CO_2 is flowing, the chitin/HFIP solution is injected by means of an injection device. The injection device is a small piston-cylinder assembly from HIP with neoprene O-rings. The solution is taken in one side of the device, and then water is pumped to the other side using a hand pump. The solution is injected into the vessel using a 50-cm long silica-capillary tubing of 150-μm inner diameter.
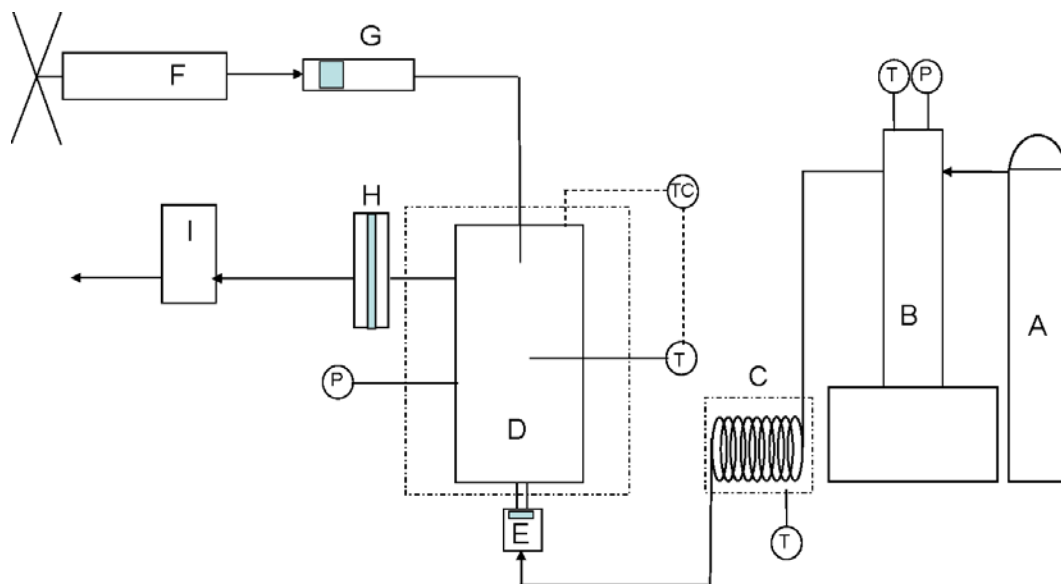
Figure 2.2. SAS apparatus showing (A) CO$_2$ tank, (B) ISCO pump, (C) preheating coil, (D) precipitation vessel, (E) 0.5 micron stainless steel frit, (F) HIP hand pump, (G) injection device, (H) high pressure filter holder, and (I) backpressure regulator.

When the solution injection is complete, the solution line is closed and CO$_2$ is kept flowing for the purging step. A 0.5-μm stainless steel frit situated in the CO$_2$ inlet line and a 0.2-μm PTFE filter in the CO$_2$ outlet line are used to collect the particles/fibers formed during the process. The PTFE filter is kept inside of a high pressure filter holder from Millipore. After the vessel is purged with a sufficient quantity of CO$_2$, the CO$_2$ feed is closed and the vessel is allowed to depressurize slowly. Finally, vessel is open to collect the product.

The critical point of the binary mixture CO$_2$ containing 0.012 mol fraction HFIP is 33-34 °C and 80.0 bar (Snavely et al., 2002). In our SAS experiments, temperature was set to 40 °C and pressure to 103.4 bar. Enough CO$_2$ flow was used so that all times, HFIP mole fraction remains below 0.012 in the vessel, to make sure that the fluid phase is supercritical.

2.3.5   Analyses

Size and morphology of the obtained fibers was examined by scanning electron microscopy (SEM: Zeiss, model DSM 940). Samples were sputter-coated with gold prior to SEM analysis and the operating voltage in SEM was 10kV.

Chemical analysis of the fibers was performed Fourier-transform infra-red spectroscopy, using a Nicolet instrument. The spectra were collected in the transmission mode at room temperature in 4000-400 cm^{-1} range at a resolution of 4 cm^{-1}. Each spectrum was an average of 32 scans.

2.4   Results and discussion

The size of purified chitin flakes prior to solution preparation is about $0.2 - 1.3$ mm (Figure 2.3). These flakes are light brown and very difficult to grind.
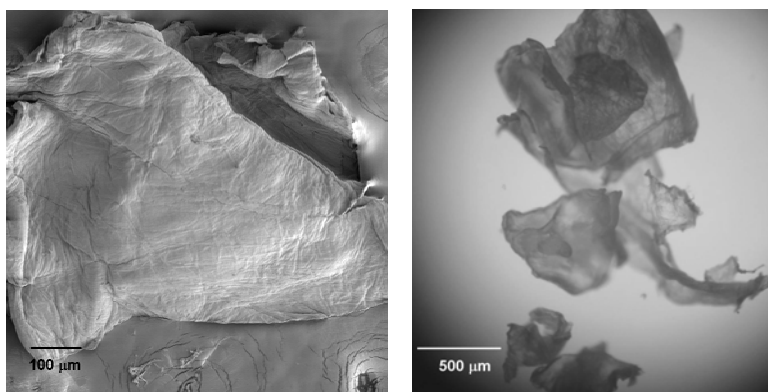
Figure 2.3. SEM micrograph and optical picture of purified chitin flake

When the chitin/HFIP solution is injected into supercritical carbon dioxide, a fast precipitation of chitin in fiber form occurs. However in the present case, due to strong intra-molecular H-bonding in chitin, fibers were obtained. The obtained material is of

cream color (Figure 2.4), and is extremely fluffy with an estimated bulk density of about

0.012-0.004 g cm^{-3}. When handling with tweezers, the fibers appear to be sticky.
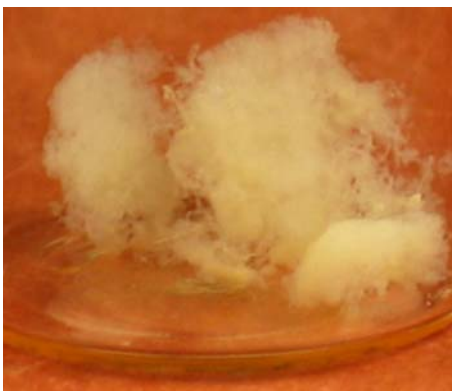
Figure 2.4. Chitin fibers obtain from SAS process

Figure 2.5 shows scanning electron micrographs of the fibers at varying

magnifications. At 50x magnification (Figure 2.5a) macro-structure of the material can be

seen. The diameter is around 50-80 μm which is of the order of the 100 μm nozzle

diameter used for injection of the solution. To look at the actual structure, higher

magnifications are needed. Figures 2.5b and 2.5c show that each macro-fiber is

composed of many small fibers. Figures 2.5d and 2.5e are 20,000x magnifications which

clearly show the presence of nano-fibers. Figure 2.5f is at 30,000x magnification, which

again confirms that nanostructure of the resultant chitin fibers. The diameters of around

200 particles in Figures 2.5e and 2.5f were measured. The average diameter was found to

be 84 nm with standard deviation of 26 nm.

The fine nanostructure of the obtained chitin fibers can be attributed to the strong

inter-chain and intra-chain H-bonding. The molecular structure of the chitin repeat unit

(Figure 2.1) has plenty of H-bonding sites as evident by the infra-red spectra (Figures 2.6

and 2.7). In addition, for the nano-scale materials, the van der Waals attraction also

become significant; this may be reason for very sticky nature of the obtained fibers as compared to the original chitin. To further examine if the SAS processing resulted in any chemical alteration, infrared spectra were taken from the nano-fibers and compared to the original (purified) unprocessed chitin.

a   b

c   d

30
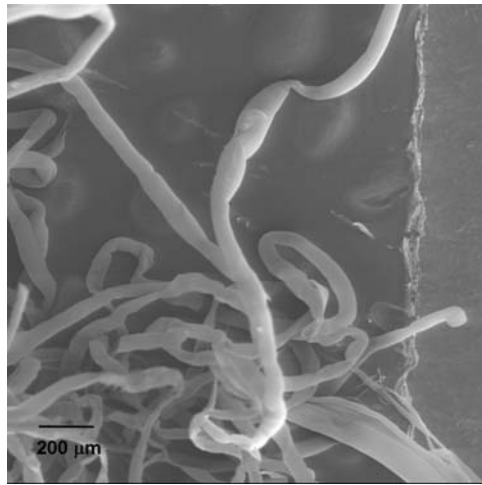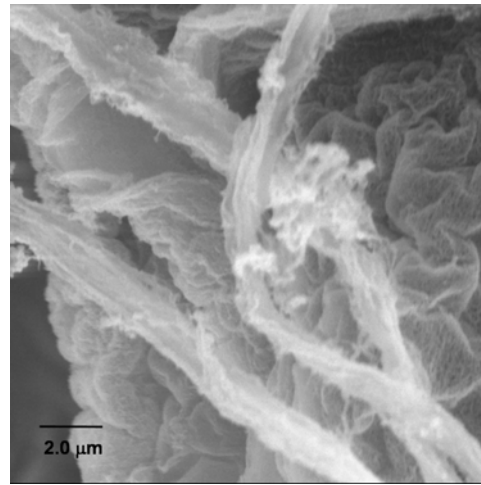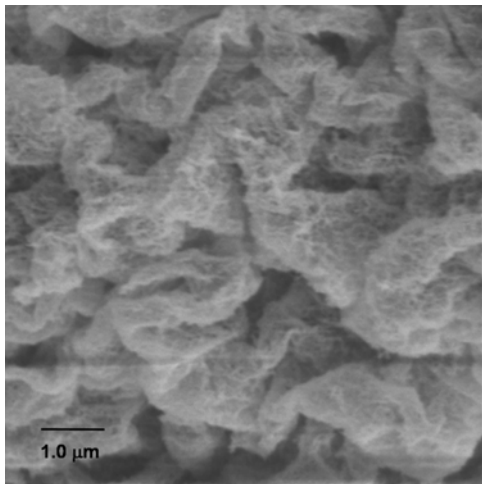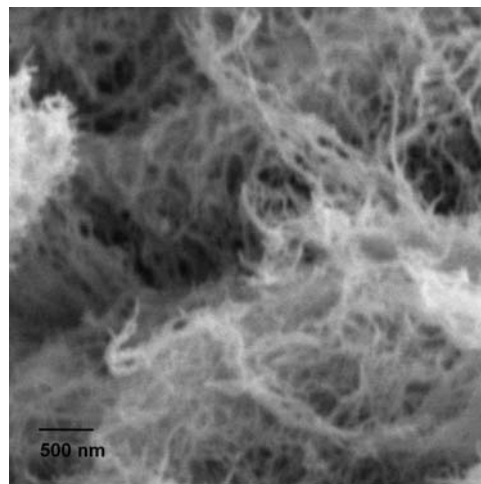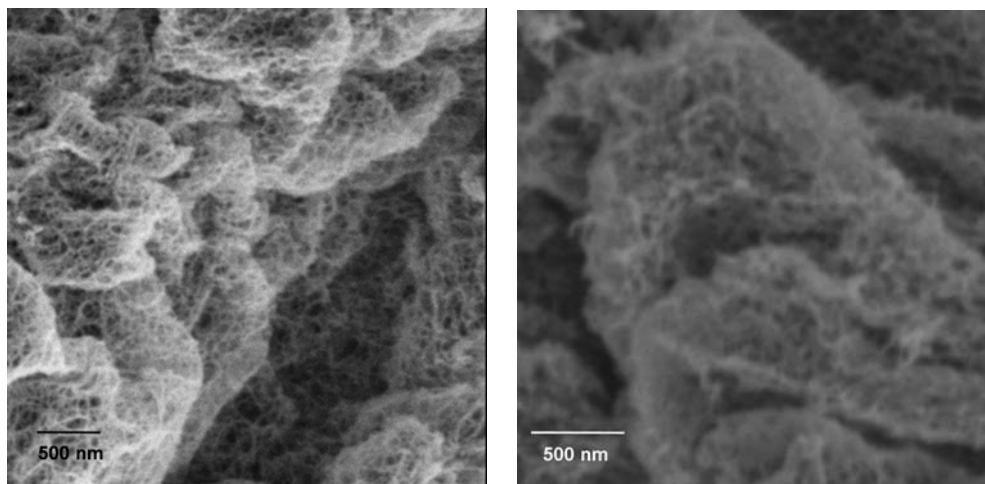
<center>e   f</center>

Figure 2.5. SEM micrographs of obtained chitin nano-fibers

A infra-red spectrum of purified chitin is shown in Figure 2.6 which shows typical peaks of α-chitin at 894, 951, 1028, 1072, 1113, 1156, 1202, 1259, 1310, 1377, 1415, 1556, 1625, 1658, 3102, 3265, and 3450 cm^{-1} as also reported by Gow and Gooday (1987).

In the –NH and –OH stretching regions there are two strongly absorbing bands centered one at 3441 cm^{-1} (with two more peaks at 3484 and 3414 cm^{-1}, probably due to noise) and the other at 3267 cm^{-1}. The bands around 3441 cm^{-1} is attributed to –OH stretching, while the band at 3267 cm^{-1} is attributed to a strongly hydrogen bonded –NH stretch and is related to the inter-chain –C=O···H-N hydrogen bonded –NH stretches.
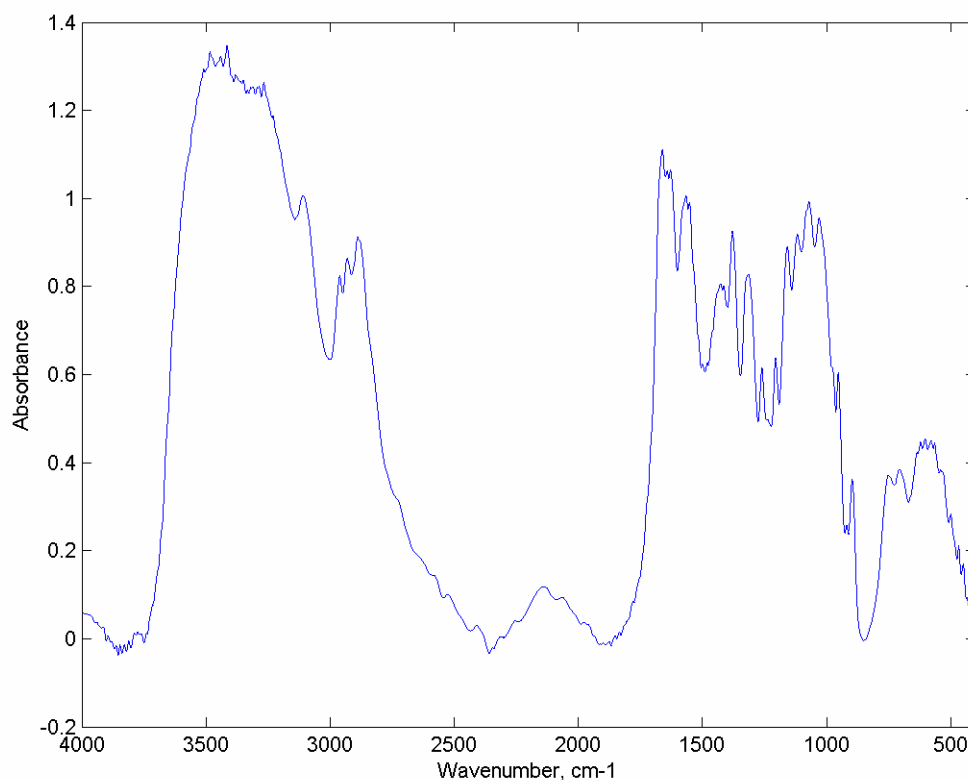
Figure 2.6. Infrared spectrum of purified chitin

The band at 3108 cm^{-1} is characteristic of secondary amides. Three resolved bands in the –CH stretching region correspond to the asymmetric –CH$_3$ stretching at 2961 cm^{-1}, to the –CH$_3$ symmetric and –CH$_2$ asymmetric stretching at 2932 cm^{-1}, and finally, to the –CH stretching at 2890 cm^{-1}. Focher et al. (1992) also observed similar five well resolved bands in the deconvoluted spectrum.

The amide I band is very complex with three main peaks at 1661, 1642, and 1629 cm^{-1}. Mikkelsen et al. (1997) note these three well resolved peaks but only explain two of them as well as other authors. These bands are the result of the two types of hydrogen bonds formed by amide groups in the anti-parallel alignment present in α-chitin crystalline regions (Brugnerotto et al, 2001). The band at 1661 cm^{-1} is related to the

32

ordinary hydrogen bonded carbonyl group (C=O···H-N). Darmon and Rudall (1950) assigned the frequency 1660 cm^{-1} to the stretching of –C=O hydrogen bonded to –NH group, while Focher et al (1992) explained that this band corresponds to the stretching of –C=O groups hydrogen bonded to –NH groups of a neighboring chain, an inter-chain hydrogen bond. The band at 1629 cm^{-1} is related to the bifurcated hydrogen bonded carbonyl group. Darmon and Rudall (1950) assigned the frequency of 1625 cm^{-1} to –C=O stretching when –C=O is bonded to an –OH group, however, Focher et al. (1992) related this band to the stretching of the –C=O groups hydrogen bonded to both the –NH group and to the –OH of the same chain. The amide II band is resolved into two peaks at 1568 and 1552 cm^{-1}, and the amide III band appears at 1310 cm^{-1}.

Figure 2.7 shows the spectra for original (purified) chitin (a) and chitin nano-fibers obtained from different runs of SAS process (b, c, and d). The spectra of the processed chitin are similar to that of the original chitin. Hence, the molecular structure is preserved after SAS processing. The high stickiness of the nano-fibers can be attributed mainly to the size reduction. Due to the increased surface area, there are more surface molecules with –OH and –NH groups which possibly remain non-H-bonded.   The presence of these H-bondable groups may be giving rise to high adhesiveness of the nano-fibers.
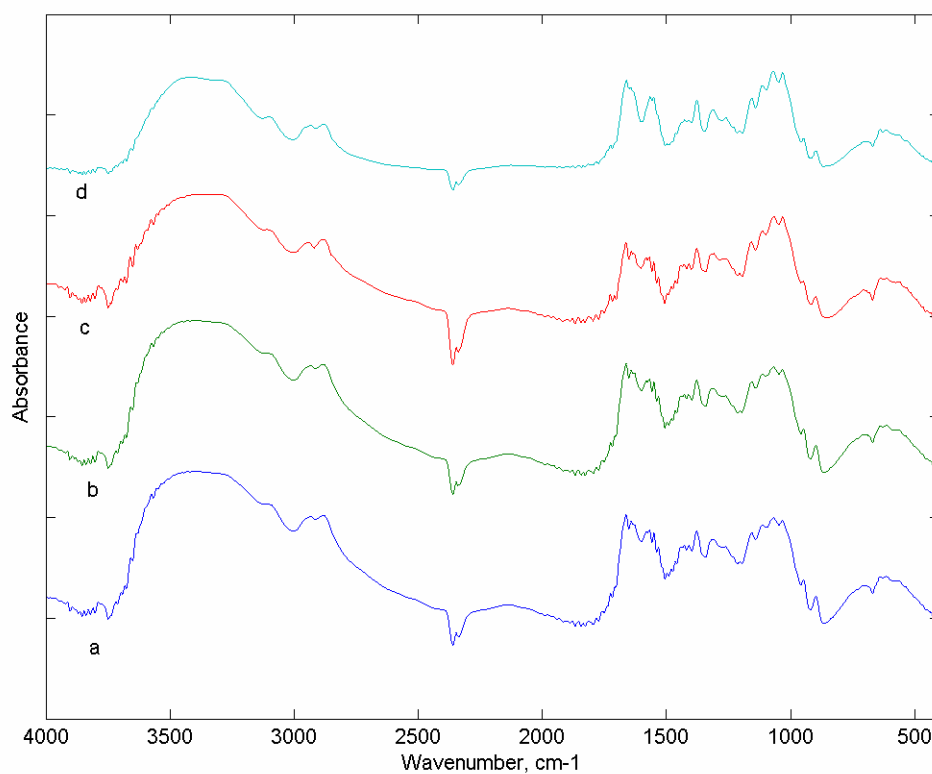
Figure 2.7. Infrared spectra of original chitin (a)SAS process chitins nano-fibers (b, c, d)

2.5   Conclusion

Nano-fibrous chitin can be successfully produced using supercritical antisolvent process. The obtained nano-fibrous chitin is very porous and sticky, and has very low bulk density. The average diameter of the nano-fibers is 54 nm with standard deviation of 16 nm.   Infra-red analyses show that the molecular structure is not altered during the supercritical antisolvent processing.

2.6 Acknowledgment

REFERENCES

1. J. Brugnerotto, J. Lizardi, F. M. Goycoolea, W. Argüelles-Monal, J. Desbrières, and M. Rinaudo, An infrared investigation in relation with chitin and chitosan characterization, Polymer, 42, 2001, 3569-3580.

2. R. C. Capozza, Spinning and shaping poy-(N-acetyl-D-glucosamine), 1976a, US Patent 3,988,411

3. R. C. Capozza, Solution of poy-(N-acetyl-D-glucosamine), 1976b, US Patent 3,989,535.

4. P. Chattopadhyay; Gupta, Ram B. Protein nanoparticles formation by supercritical antisolvent with enhanced mass transfer. AIChE J. (2002), 48, 235-244.

5. P. Chattopadhyay; Gupta, R. B. Production of griseofulvin nanoparticles using supercritical CO2 antisolvent with enhanced mass transfer. Int. J. Pharm. (2001), 228(1-2), 19-31.

6. P. Chattopadhyay; Gupta, Ram B. Production of Antibiotic Nanoparticles Using Supercritical CO_2 as Antisolvent with Enhanced Mass Transfer. Ind. Eng. Chem. Res. (2001), 40(16), 3530-3539

7. S. E. Darmond and K. M. Rudall, Discus. Faraday. Soc., 9. 1950, 251.

8. B. Focher, A. Naggi, G. Torri, A. Cosani, and M. Terbojevich, Structural differences between chitin polymorphs and their precipitates from solutions --- evidence from CP-MAS ^{13}C-NMR, FT-IR and FT-Raman spectroscopy, Carbohydrate Polymers, 17, 1992, 97-102.

9. N. Foster, R. Mammucari, F. Dehghani, A. Barret, K. Benzanehtak, E. Coen, G. Combes, L. Meure, A. Ng, H. L. Regtop, and A. Tandya, Processing

Pharmaceutical Compounds Using Dense Gas Technology, Ind. Eng. Chem. Res., 42, 2003, 6476-6493.

10. N. A. R. Gow and G. W. Gooday, Infrared and X-ray diffraction data on chitins of variable structure, Carbohydr. Res., 165, 1987, 105-110.

11. Gupta, R.B.; Chattopadhyay, P. Method of forming nanoparticles and microparticles of controllable size using supercritical fluids with enhanced mass transfer, US Patent 6,620,351; September 16, 2003.

12. H. Hermann, E. Anke, K. Joerg, B. Axel, Preparation and use of nanoscale cationic compounds for cosmetic and pharmaceutical compositions, 2001, WO 2001045666 A1.

13. O. Hirokazu, N. Seiko, T. Hiroaki, S. Yuki, I. Kotaro, D. Kazumi, Pulmonary gene delivery by chitosan-pDNA complex powder prepared by a supercritical carbon dioxide process, J. Pharm. Sci., 92(2), 2003, 371-380.

14. E. Khor, Chitin: Fulfilling a Biomaterials Promise, Elsevier, 2001, Oxford, UK.

15. U. B. Kompella and K. Koushik, Preparation of Drug Delivery Systems Using Supercritical Fluid Technology, Critical Reviews in Therapeutic Drug Carrier Systems, 18(2), 2001, 173-199.

16. Mikkelsen, S. B. Engelsen, H. C. B. Hansen, O. Larsen, and L. H. Skibsted, Calcium carbonate crystallization in the α-chitin matrix of the shell of pink shrimp, Pandalus borealis, during frozen storage, Journal of Crystal Growth, 177, 1997, 125-134.

17. S. Palakodaty and P. York, Phase Behavioral Effects on Particle Formation Processes Using Supercritical Fluids, Pharm. Res., 16(7), 1999, 976-985

37

18. W. K. Snavely, B. Subramaniam, R. A. Rajewski and M. R. Defelippis. Micronization of Insulin From Halogenated Alcohol Solution Using Supercritical Carbon Dioxide as an Antisolvent, J. Pharm. Sci., 91(9), 2002, 2026-2039.

19. B. Subramaniam, R. A. Rajewski and K. Snavely, Pharmaceutical Processing with Supercritical Carbon Dioxide, J. Pharm. Sci., 86(8), 1997, 885-890.

20. R. N. Tharanathan and F. S. Kittur, Chitin ---The Undisputed Biomolecule of Great Potential, Critical Reviews in Food Science and Nutrition, 43(1), 2003, 61-87.

21. S. Tokura, N. Nishi, A. Tsutsumi and O. Somorin, Studies on Chitin. VIII. Some properties of water soluble chitin derivates, Polymer J, 15(6), 1983, 485-489.

22. S. Tokura, S-I. Nishimura, N. Sakairi and N. Nishi, Biological activities of biodegradable polysaccharide, Macromol. Symp., 101, 1996, 389-396.

23. N. L. M. Yusof, L. Y. Lim, and E. Khor, Preparation and Characterization of Chitin Beads as a Wound Dressing Precursor, J. Biomed. Mater. Res., 54(1), 2001, 59-68.

CHAPTER 3

PRODUCTION OF HYDROCORTISONE MICRO- AND NANO-PARTICLES USING

SUPERCRITICAL ANTISOLVENT WITH ENHANCED MASS TRANSFER

3.1 Abstract

Supercritical antisolvent precipitation with enhanced mass transfer (SAS-EM) is used for formation of particles of hydrocortisone (HC), an anti-inflammatory drug. This technique is similar to supercritical antisolvent process, but uses a reflecting horn surface that vibrates at 20 kHz frequency, which enhances the mass transfer of the solvent to supercritical fluid anti-solvent, reducing the growth of the particles. Controllable sizes and morphologies of HC particles are obtained using SAS-EM process. At 0 watt of power supply (to ultrasonic transducer), HC fibers of average length ~81 μm and average diameter of ~6 μm are obtained. Upon increasing the power supply to 120 watts, which enhances mass transfer, particles of average size as low as 180 nm are obtained. Intermediate particle size and morphology are easily obtained by adjusting the power supply to the desired intermediate value. The obtained powder is free of impurities and is mostly amorphous.

3.2 Introduction

Hydrocortisone is an anti-inflammatory corticosteroid. To cross Peyer's patches and mesentery on the surface of gastrointestinal mucosa for effective drug delivery,

particles smaller than 500 nm in size are needed (Tomlinson, 1983; Kreuter, 1991). In addition, the solubility of hydrocortisone in water is only 0.28 g/liter, providing a low bioavailability, which causes a problem in providing accurate dosage formulations. Going from micro- to nano-size particles, rate of dissolution increases, due to the increased surface area. Also, nanoparticles can be delivered by oral, subcutaneous, intravenous, and/or intra-peritoneal routes. Hence a decrease in the particle size can improve its release and uptake efficacies.

Supercritical fluids are emerging as excellent media for particle formation, mainly because the solvating power of supercritical fluids can be adjusted by changing the pressure. Two major processes are: RESS (rapid expansion of supercritical solutions), and SAS (supercritical antisolvent). Out of several supercritical fluids, including ethylene (Krukonis, 1984) and water (Matson et. al., 1986; Petersen et. al., 1986), CO_2 is being utilized in pharmaceutical particle formation because of its mild critical point (31.1˚C, and 73.8 bar) and environmentally benign nature.

In RESS, first the solute is dissolved in supercritical CO_2 and then the solution is abruptly expanded using a nozzle (Debendetti et al., 1993; Matson et al. 1987). The sudden loss of solvating power results in the precipitation of small size particles. Unfortunately, most pharmaceutical compounds have very low solubility ($\leq$0.01 wt %) in CO_2 at moderate pressures and temperatures, hence RESS is not suitable. For such materials, SAS process can be used, in which material dissolved in a solvent is injected into supercritical CO_2 antisolvent. Supercritical CO_2 removes solvent from the solution causing solute precipitation. In fact, SAS works well when solvent has a high solubility in CO_2 and solute has negligible solubility (Reverechon and Della, 1999).

40

Several researchers have used supercritical antisolvent to produce micro-particles of hydrocortisone (Velaga et. al., 2002; Ghadheri et. al., 2000). For example, budesonide (a hydrocortisone steroid) particles of size 1-10 μm were obtained using precipitation technique with a stabilizing agent and compared with evaporation technique (Frederic and Matijevic, 2000). Recently, hydrocortisone particles of 600 nm were obtained using SAS process with ultrasound nozzle by Subramaniam et al. (2001).

In this work, we examine SAS-EM process (Chattopadhyay and Gupta, 2001, 2002), for the formation of hydrocortisone nanoparticles. This process utilizes a vibrating surface to enhance mass transfer rate between supercritical CO_2 and solvent. The effect of mass transfer is studied on the particle size and morphology. The goal is to obtain particles of controllable size and morphology.

3.3   Experimental Section

3.3.1   Materials

CO_2 and N_2 (both 99.9% pure) were received from Airco. Hydrocortisone (11β, 17α, 21-trihydroxypregn-4-ene-3, 20-dione) (98% pure) was purchased from Sigma-Aldrich (lot no. 81K1132). Methanol (HPLC grade, 99.9% pure) was purchased from Fischer Scientific. All materials were used as received.

3.3.2   Apparatus

Figure 3.1 shows the schematic of the apparatus used in this work. In this diagram, R is the precipitation cell of 80 cc volume and H is the titanium horn (Sonics and Materials, Inc.) with a 1.25 cm diameter tip. The titanium horn vibrates at 20 kHz by

vibrations generated by an ultrasonic processor, which can deliver maximum power up to 600 watts, through a piezoelectric transducer. The ultrasonic processor delivers vibrations of constant frequency, but the amplitude can be varied by changing the power supplied. Process is carried out at a constant temperature by keeping the vessel R in water bath. CO_2 is filled in reactor using valves V1 and V2 with a high pressure ISCO syringe pump (model 500D). Valve V4 is used for venting while purging the system with CO_2. Drug solution is supplied to the vessel R through valve V3 using solution injection device S, to the tip of the horn H with a 100 μm capillary tube. Solution injection device is divided into two chambers separated by a piston; in the front chamber drug solution is filled and in the back chamber N_2 is supplied as a pressurizing fluid. While injecting, a pressure difference of ~ 500 psi between solution injection device S to reactor R, is maintained.

3.3.3 Procedure

Batch experiments were conducted by first pressurizing the vessel with CO_2 at 1400 psi using ISCO syringe pump. The vessel temperature is stabilized at 37°C for an hour to equilibrate temperature inside the vessel. Experiments were carried out at the same process conditions to analyze the effect of ultrasound on particle morphology and size. About 4 ml of hydrocortisone solution in methanol (concentration ~ 5 mg/ml) was loaded in front chamber of solution injection device. Then the titanium horn is tuned and ultrasound horn was switched on at desired power level. Now by opening valve V5 to supply nitrogen in back chamber of solution injection device, solution is pressurized. The solution is injected into the vessel R using 100 μm diameter nozzle. The nozzle was

placed touching the horn at about 45° angle. The whole injection process takes only 30 – 60 seconds. Because of the short time, the amount of heat dissipated due to ultrasonic horn is not significant enough to alter the system temperature. On the other hand, the vigorous mixing causes equalization of the temperature to a greater degree. After injection of fluid, whole system is left for half an hour to allow the particle to fully harden and settle. Continuous operation of large reactor vessel is required for carrying out experiments for longer injection time or large amount of solute. Inside the vessel, jet coming out from the nozzle breaks up into small droplets after reflecting from vibrating surface. When injection is complete, the ultrasound is switched off. Supercritical CO_2 antisolvent, assisted by enhanced mass transfer removes the solvent from the droplets, causing precipitation of solute particles. To remove the solvent from the system, the vessel is purged with 200 ml of fresh CO_2 over a period of 1.5 hrs. Then the vessel is slowly depressurized. Particles are collected and analyzed.

3.3.4   Analysis and Characterization

Analysis of particle size and morphology was done using a scanning electron microscope (SEM) (Zeiss, model DSM 940). The particles are placed on top of a carbon tape on the aluminum stub. These particles were coated twice with gold using a sputter coater (Pelco, model Sc-7), and then analyzed in SEM. From these micrographs, average size was calculated by measuring 150-200 particles. Attempt was made to represent an overall size distribution when selecting the particles for size analysis.

Rigaku X-Ray Diffraction (XRD) equipment was used for analyzing the crystallinity of the particles. This vertical diffractometer was equipped with Cu Kα_1 radiation source and D/MAX-B data acquisition system.

HPLC analysis was also done to compare the purity of processed sample with un-processed one.   The HPLC was equipped with a 7725i six-port injection valve (Rheodyne), model 600 HPLC pump, model 2410 refractometer and model 2487 Dual λ UV spectrometer with the wavelengths set to 248 nm.   A Spectronic Genesys2 UV spectrophotometer was used to initially select the wavelength at which hydrocortisone absorbs the maximum of UV light which was found to be 248 nm. The mobile phase used for HPLC was a mixture of methanol (3 vol.%), water (57%), and acetonitrile (40%) flowing at 1 ml/min through a 3.9 mm x 150 mm Novapak C-18 column.

3.4   Results and Discussion

The observed morphology and size of hydrocortisone particles obtained from different experiments are summarized in Table 3.1. All the experiments were carried out at ~1400 psi and 37˚C with 5 mg/ml hydrocortisone solution in methanol. Horn surface vibrates at constant ultrasonic frequency of 20 kHz but varying amplitudes which is controlled by the power supplied to the piezoelectric transducer. SEM micrographs of particles obtained are shown in Figure 3.2. XRD pattern of processed hydrocortisone are shown in Figure 3.3. Figure 3.3a shows XRD pattern for SAS processed hydrocortisone while Figure 3.3b shows pattern for 90 watts of ultrasound (SAS-EM) processed particles. To compare our processed hydrocortisone particles with unprocessed particles, XRD of unprocessed HC is shown in Figure 3.3c.

44

At 0 watt of power supply which is basically SAS process, needle shaped particles with average length of 81 μm and average diameter of 5.8 μm were obtained. Similar results were obtained by Velaga et. al. (2002) using SEDS process. By increasing the power supply to 30 watts, a reduction in length and diameter of hydrocortisone needles, to an average length of 13 μm and an average diameter of 1 μm is seen.

As the ultrasound power was increased to 60 watts, morphology changes from needles to particles of average diameter 1.6 μm. Earlier Subramaniam et al. (2001) observed hydrocortisone particles of size range ~500 nm using SAS process with ultrasonic nozzle.

Smallest particles of 180 nm diameter were obtained at 120 watts of power supply. When the power supply was further increased, particles started agglomerating; for example, at 150 watts, average size increased to 510 nm. Similar trend was also observed by Chattopadhyay and Gupta (2001) for lysozyme particles using SAS-EM process. Particles size starts reducing as we increase the ultrasound power, due to increase in mass transfer between droplets and the antisolvent. The increase is mainly due to the finer atomization of the drug/solvent droplets into the supercritical carbon dioxide antisolvent. In addition, the ultrasonic waves provide a vigorous mixing effect further enhancing the mixing or the solvent removal from the droplets. This effect is further discussed by Chattopadhyay and Gupta (2001) for the production of antibiotic nanoparticles.

XRD pattern of hydrocortisone particles obtained from SAS-EM is similar to those from SAS as shown in Figures 3.3a-b. Both show a small sharp peak, due to a small fraction of crystalline particles and, a large broad peak at 2-theta value of 23.7° due

to the amorphous particles. Unprocessed hydrocortisone particles are mostly crystalline as evident from XRD pattern in Figure 3.3c. The mostly amorphous particles obtained from SAS-EM are expected to provide a faster dissolution behavior. The amounts of the particles taken for the XRD shown in Figures 3.3a-c are not the same, and hence the differences in the absolute intensities arose. Table 3.2 shows the inter-planar spacing (d) for processed and unprocessed hydrocortisone derived from XRD peaks. Velaga et. al. (2002) also observed the peaks at same inter-planar spacing for processed (with methanol) and unprocessed HC samples.

HPLC analysis was performed to test purity of processed HC. Figure 3.4 shows the HPLC peaks for unprocessed (a) and processed (b) HC. Figure 3.4a shows two peaks for unprocessed HC; the first one is due to an impurity, whereas the second one at 1.85 min is due to HC. In SAS-EM processed sample only one peak is present which is due to HC. Supercritical CO_2 was able to remove the impurity from the feed HC. The peak position is unaltered, indicating no alteration in the molecular structure of HC. No quantitative attempt was made to determine the type or extent of the impurity removal; especially due to the fact that impurity peak was negligible in the HPLC analysis of the process HC. The impurity removal is expected to be proportional to the amount of purge CO_2 used in the process.

Number average diameters are shown in Figure 3.5 and standard deviation in Figure 3.6. With particle size, standard deviation also decreases to minimum value of 68 nm at 120 watts of power supply. Standard deviations for needle-shaped particles are not plotted in the figure. At 5% ultrasound standard deviation in length is 5 μm whereas for

no ultrasound (normal SAS process) system it is 47 μm. Volume average diameter also follows a similar trend (Figure 3.7).

3.5   Conclusions

Hydrocortisone particles of controllable size and morphology can be easily produced using SAS-EM process due to adjustable mass transfer. Size can be reduced down to 180 nm for 120 watts of power supply. After SAS-EM processing, a purified HC is obtained which is mostly amorphous.

3.6   Acknowledgement

REFERENCES

1. Chattopadhyay, Pratibhash; Gupta, Ram B. Supercritical CO_2 Based Production of Magnetically Responsive Micro- and Nanoparticles for Drug Targeting. Ind. Eng. Chem. Res. 2002, 41(24), 6049-6058.

2. Chattopadhyay, Pratibhash; Gupta, Ram B. Protein nanoparticles formation by supercritical antisolvent with enhanced mass transfer. AIChE J. 2002, 48(2), 235-244.

3. Gupta, Ram B.; Chattopadhyay, Pratibhash. Method of forming nanoparticles and microparticles of controllable size using supercritical fluids and ultrasound. U.S. Pat. Appl. Publ. 09/858,301 2002.

4. Chattopadhyay, Pratibhash; Gupta, Ram B. Production of Antibiotic Nanoparticles Using Supercritical CO2 as Antisolvent with Enhanced Mass Transfer. Ind. Eng. Chem. Res. 2001, 40(16), 3530-3539.

5. Debenedetti, P.G.; Tom, J. M.; Kwauk, X.; Yeo, S. D. Rapid Expansion of Supercritical Solutions (RESS): fundamentals and applications. Fluid Phase Equilib. 1993, 82, 311-321.

6. Frederic, Ruch; Egon, Matijevic. Preparation of Micrometer Size Budesonide Particles by Precipitation. J. Colloid Interface Sci. 2000, 229, 207-211.

7. Ghaderi, R.; Artursson, P.; Carlfors, J. A new method for preparing biodegradable microparticles and entrapment of hydrocortisone in DL-PLG microparticles using supercritical fluids. Eur. J. Pharm. Sci. 2000, 10, 1-9.

8. Kreuter, J. Nanoparticle-based drug delivery systems J. Control. Release. 1991, 16(1-2), 169-176.

9. Krukonis, V. Supercritical Fluid Nucleation of Difficult-to-comminute solids. paper 140f, AIChE meeting. 1984, San Francisco, Nov.

10. Matson, D. W.; Petersen, R.C.; Smith, R. D. Formation of silica powders from the rapid expansion of supercritical solutions. Adv. Cer. Mat. 1986, 1(3), 242-6.

11. Matson, D. W.; Fulton, J. L.; Petersen, R.C.; Smith, R.D. Rapid Expansion of Supercritical Fluid solutions: solute formation of powders, thin films, and fibres. Ind. Eng. Chem. Res. 1987, 26, 2298-2306.

12. Nass, R. Pharmaceutical Suspensions. In: H.A. Lieberman; M. Rieger; G. Banker (editors), Pharmaceutical Dosage forms. 1988, Marcel Dekker, New York, 151.

13. Petersen, R.C.; Matson, D. W.; Smith, R.D. Rapid precipitation of low vapor pressure solids from supercritical fluid solutions: the formation of thin films and powders. J. Am. Chem. Soc. 1986, 108(8), 2100-2.

14. Reverchon, E.; Della Porta, G. Production of antibiotic micro- and nanoparticles by supercritical antisolvent precipitation. Powder Technol. 1999, 106, 23-29.

15. Sharpe, H.M.; Tomich, E.G. Studies on the toxicology of griseofulvin. Toxicol. and Applied Pharmaco. 1960, 2 44-53.

16. Subramaniam, B.; Saim, S.; Rajewski, R.; Stella, V.J. Green Process Concepts for the Pharmaceutical Industry. Am. Chem. Soc. 2001, 96-110.

17. Subramaniam, B.; Saim, S.; Rajewski, R.; Stella, V.J. Method for Particle Precipitation and Coating Using Near-Critical and Supercritical Antisolvents. U.S. Patent 5,833,891, 1997.

18. Tomlinson, E. Microsphere delivery systems for drug targeting and controlled release. Int. J. Pharm. Prod. Manf. 1983, 4, 49-57.

19. Velaga, S.P.; Ghadheri, R.; Carlfors, J. Preparation and Characterization of hydrocortisone particles using a Supercritical Fluids extraction process. Intl. J. Pharm. 2002, 231, 155-166.

Table 3.1 Results of the experiments carried out at different power supplied to ultrasound horn.

Power Supply (Watts)	Pressure (psi)	Temperature (˚C)	Average Size and Morphology
0	1418	37	81.2 μm long 5.9 μm diameter Needle shaped
30	1418	37	13 μm long 1 μm diameter Needle shaped
60	1420	37	1.6 μm diameter particles
90	1415	37	1 μm diameter particles
120	1413	37	180 nm diameter particles
150	1410	37	500 nm diameter particles

Table 3.2 Inter-planar spacing and XRD intensity

Unprocessed		SAS Processed		SAS-EM Processed	
Intensity	d (Å)	Intensity	d (Å)	Intensity	d (Å)
8486	6.003375	1276	6.085442	988	6.064714
4128	5.022984	356	5.051379	451	5.051379
1441	4.482149	416	3.744891	512	3.83241
927	3.768353	422	2.821534	443	2.821534
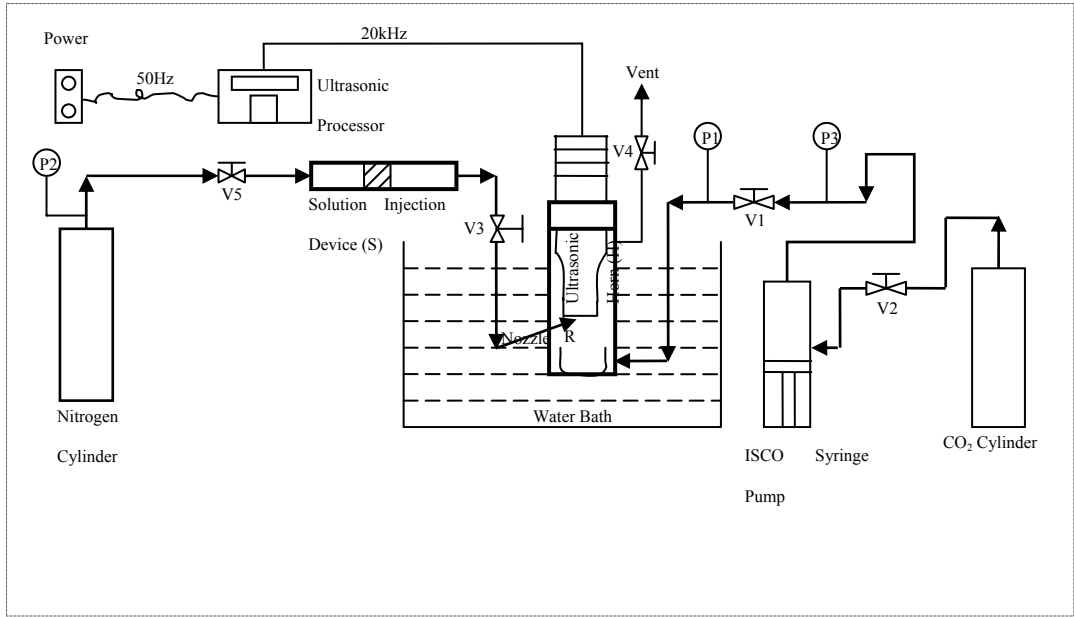
Figure 3.1 Schematic of SAS-EM apparatus
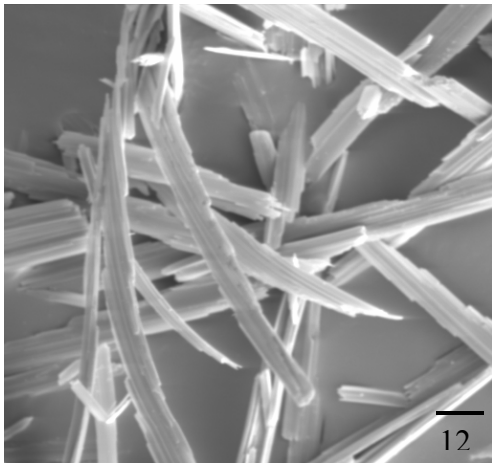
(a) 0 watts; magnification x1000
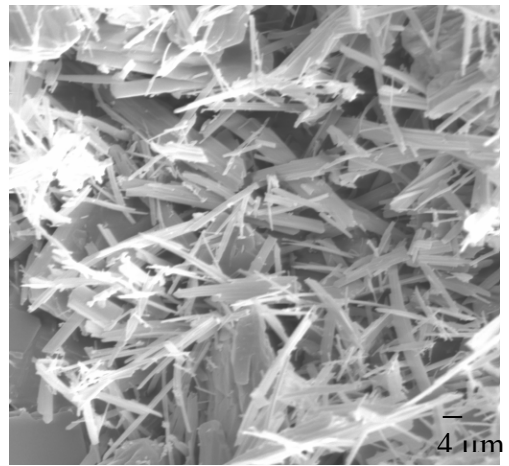
(b) 30 watts; magnification x1500
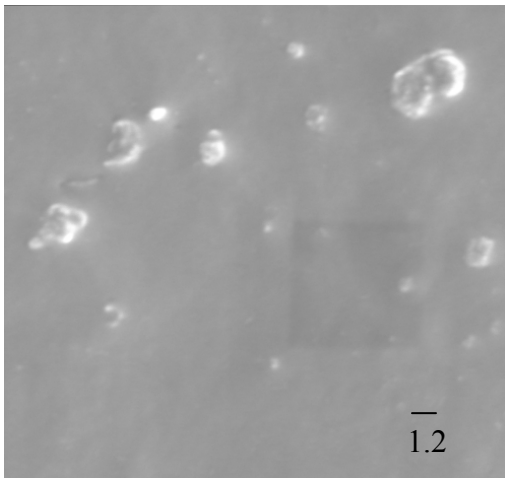
(c) 60 watts; magnification x5000
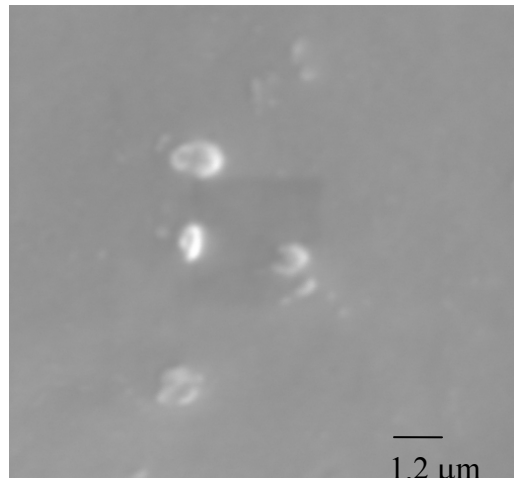
(d) 60 watts; magnification x10000
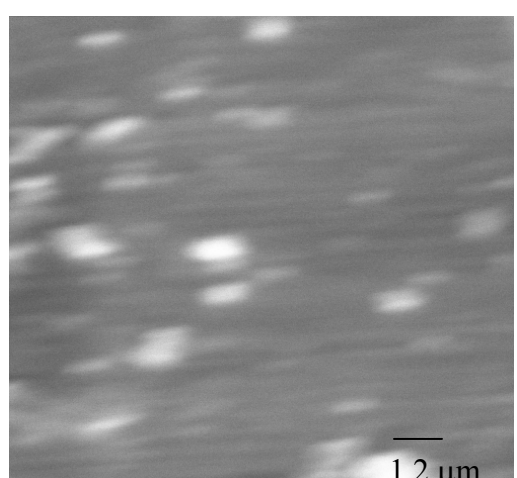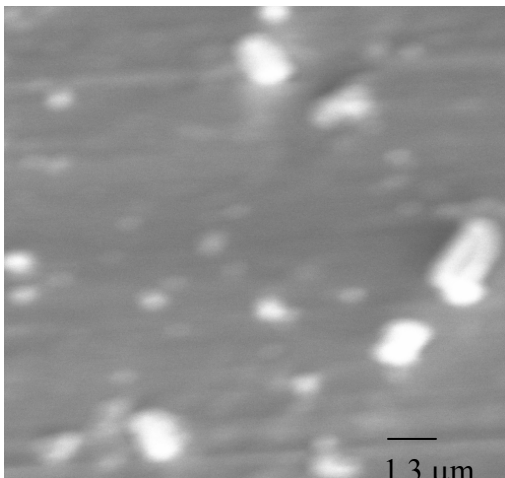
(e) 90 watts; magnification x10000
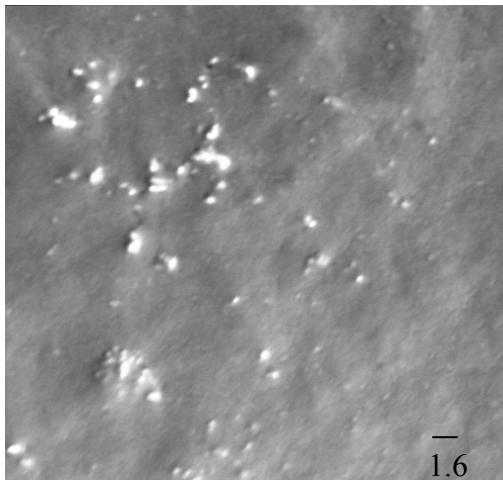
(f) 90 watts; magnification x13500

1.6

650 nm
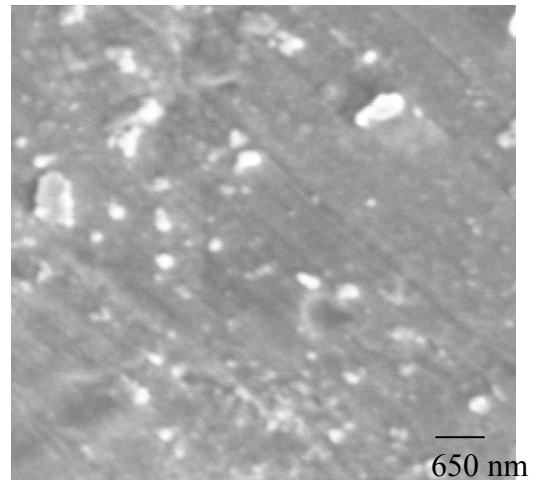
(g) 120 watts; magnification x5000
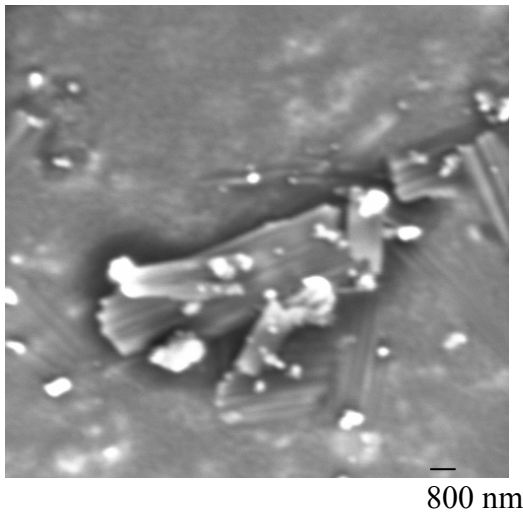
(h) 120 watts; magnification x22000

800 nm

700 nm
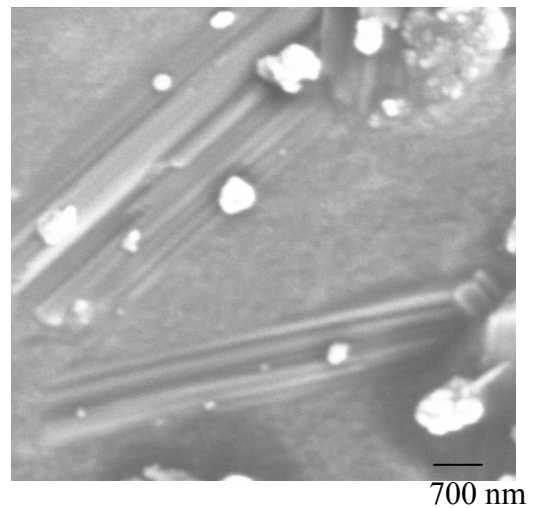
(i) 150 watts; magnification x10000

(j) 150 watts; magnification x20000

Figure 3.2 SEM micrographs of hydrocortisone particles obtained at varying ultrasound power
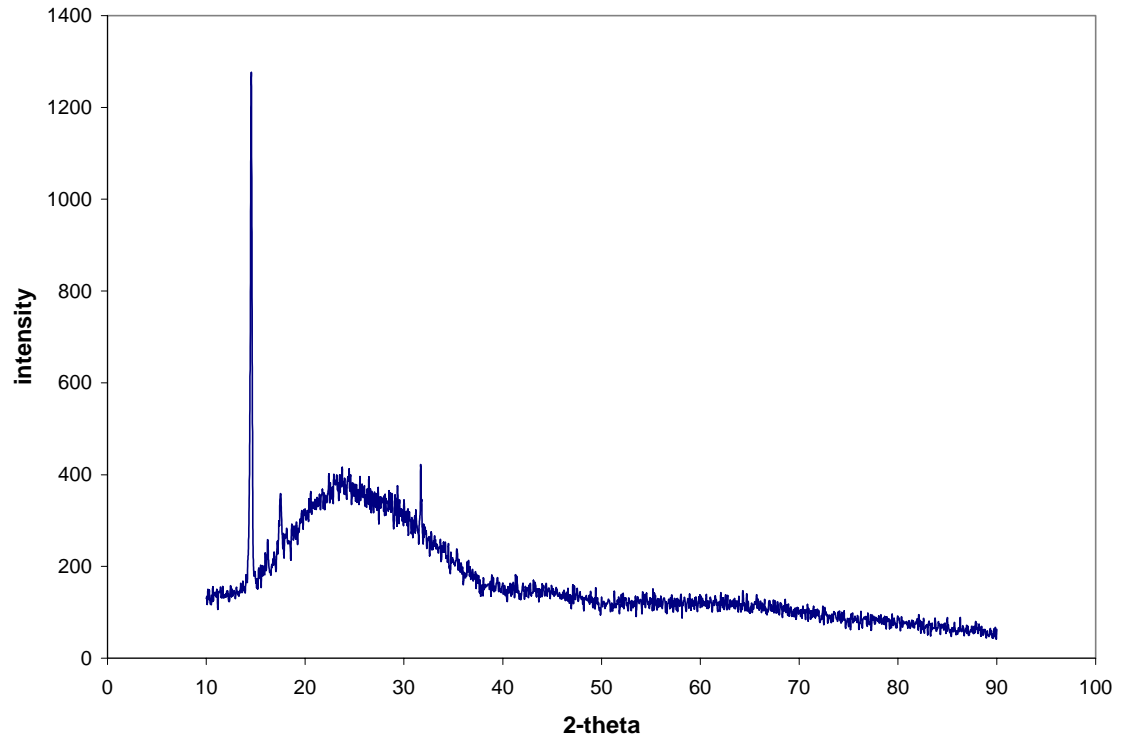
(a) 0% ultrasound (SAS process)
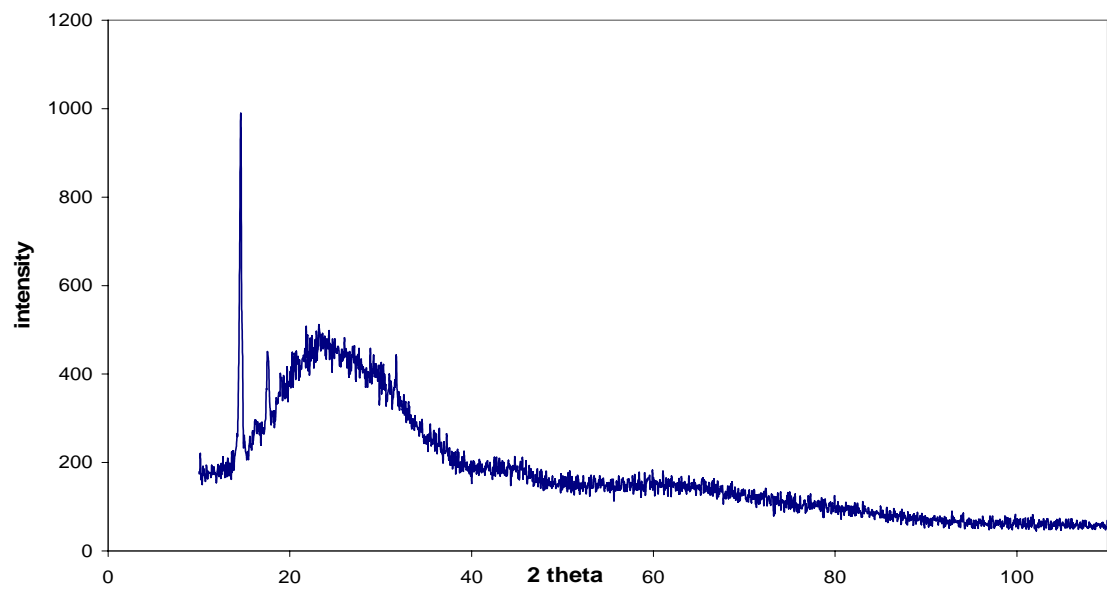
(b) 15% Ultrasound (SAS-EM process)

56
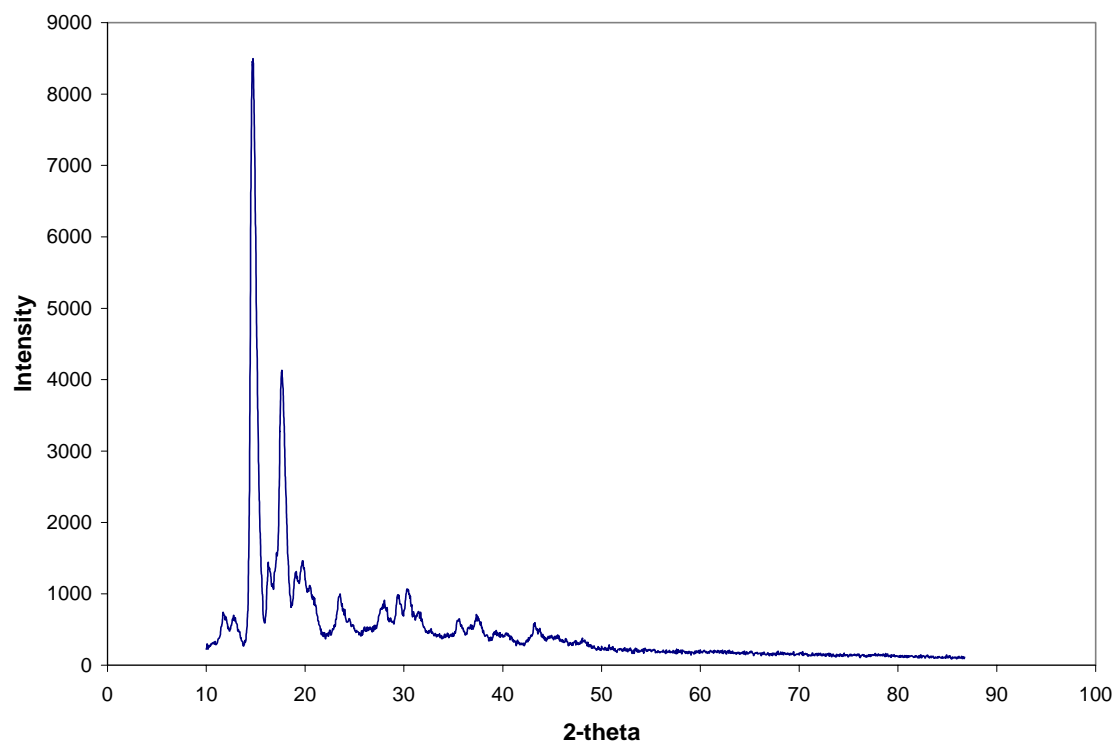
(c) Unprocessed hydrocortisone

Figure 3.3 XRD patterns for processed and unprocessed hydrocortisone particles
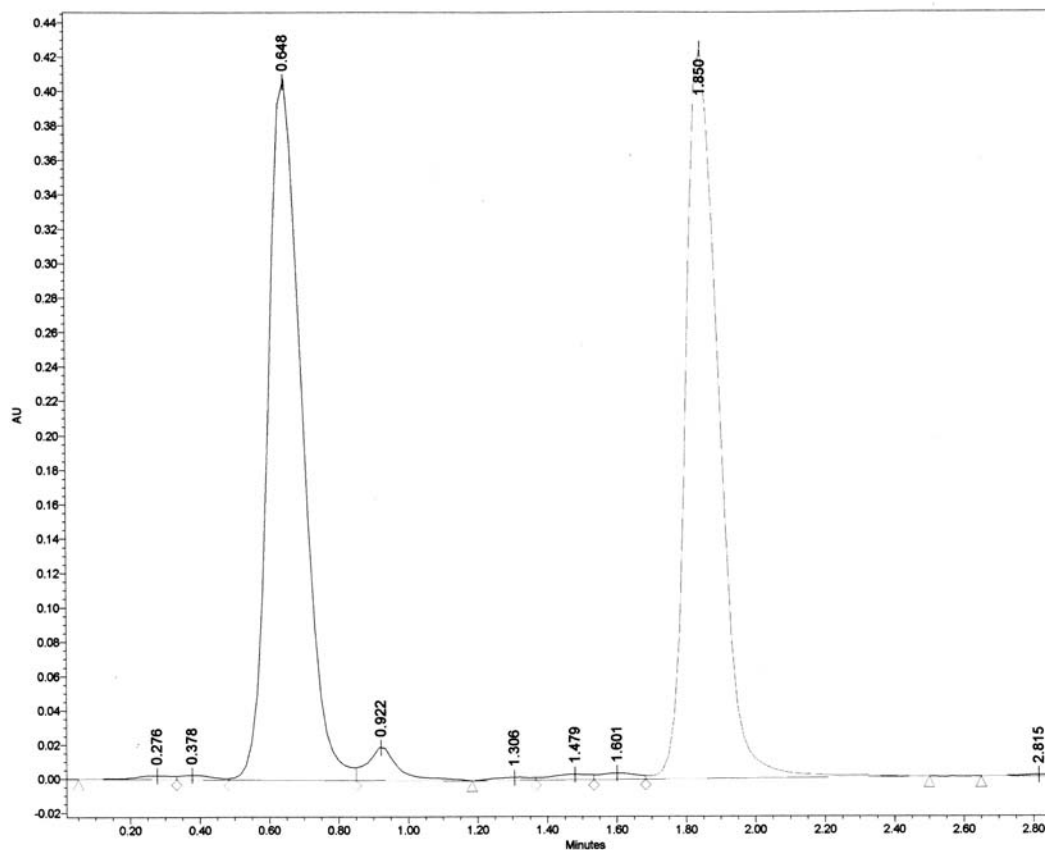
(a) Unprocessed HC sample

58
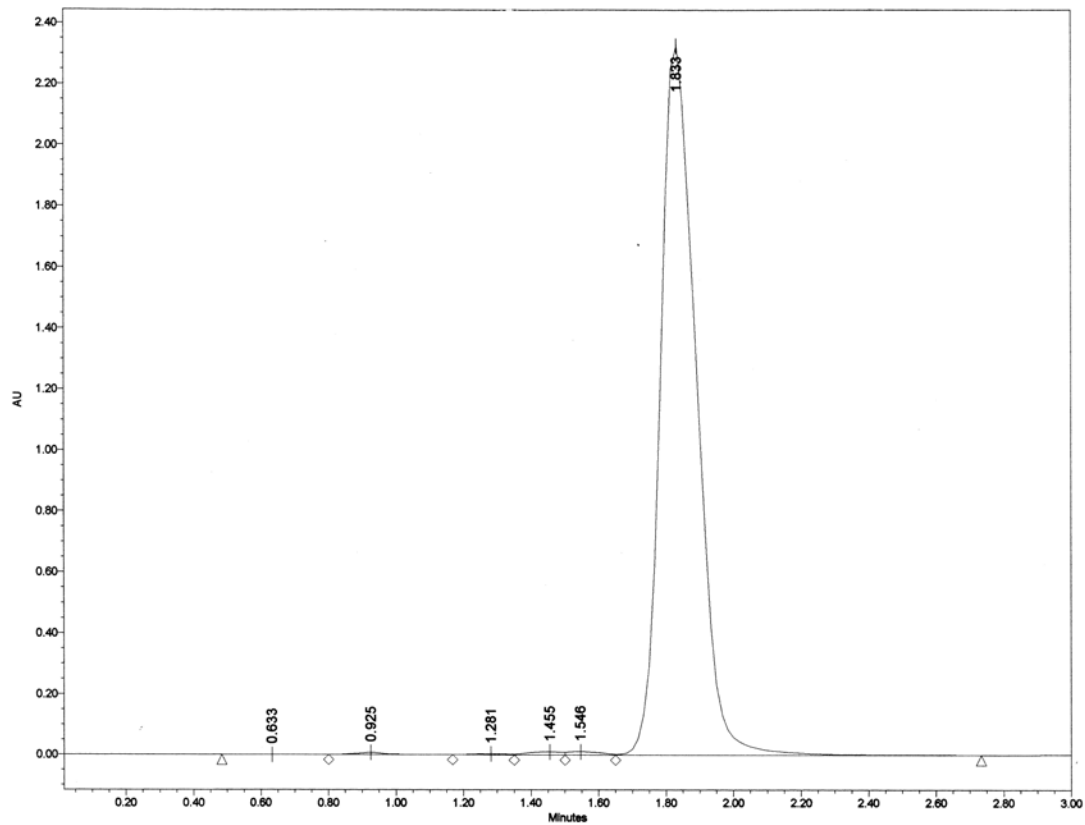
(b) SAS-EM Processed HC sample

Figure 3.4 HPLC analysis of processed and unprocessed HC samples
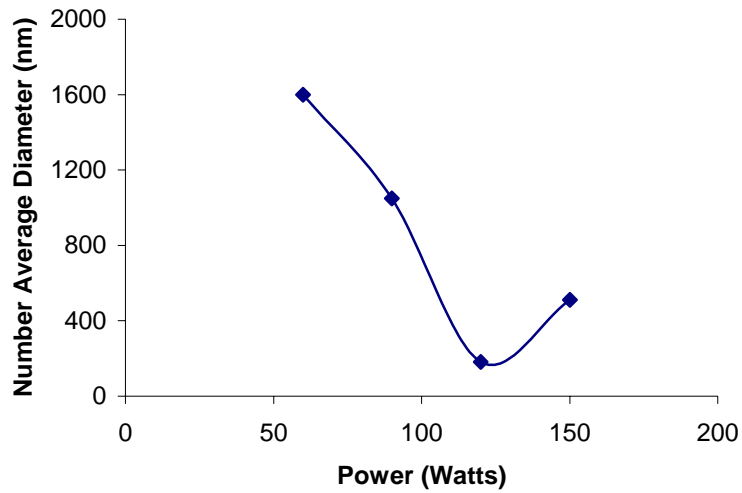
Figure 3.5 Number average diameter versus power supplied to ultrasonic
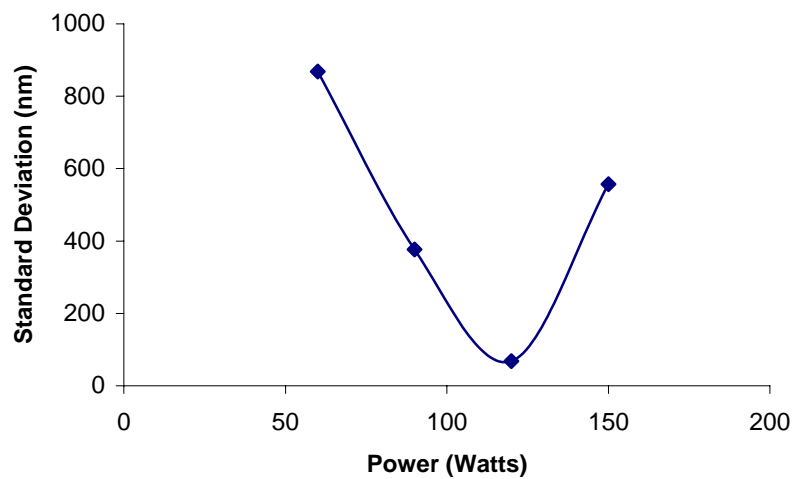
transducer

Figure 3.6 Standard deviation versus power supplied to ultrasonic transducer
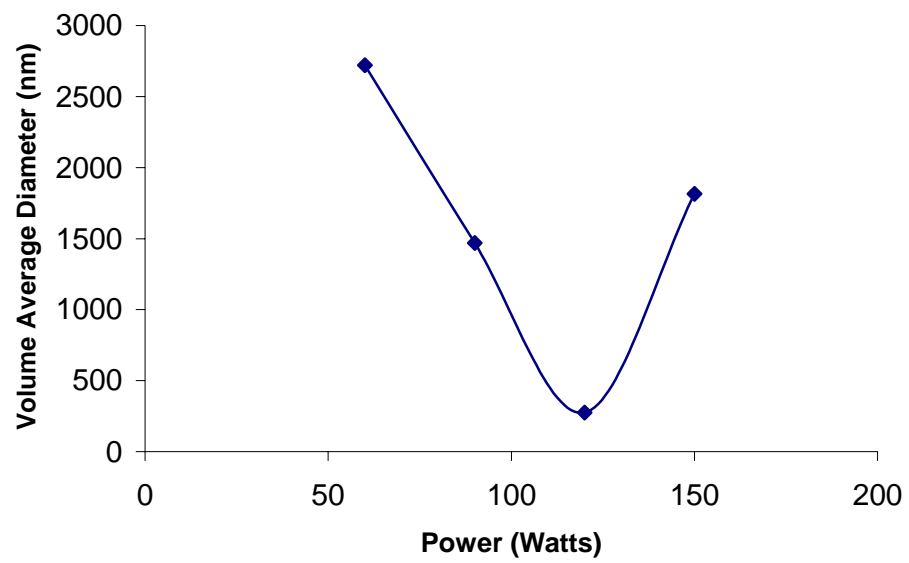
Figure 3.7 Volume average diameter versus power supplied to ultrasonic transducer

CHAPTER 4

SUPERCRITICAL CO_2 BASED SILICA COATING OF GOLD NANOPARTICLES

USING WATER-IN-OIL MICROEMULSIONS

4.1   Abstract

A method is developed for the formation of silica coating on nanoparticles using supercritical CO_2, in which supercritical CO_2 acts both as the antisolvent and as a reactant.   A water-in-oil microemulsion of aqueous sodium silicate solution in an organic solvent is injected into supercritical CO_2 by means of a micro-nozzle, forming small droplets.   Supercritical CO_2 rapidly extracts the solvent out from the droplet and reacts with the exposed surfactant-supported aqueous sodium silicate, forming silica.   When gold nanoparticles are suspended in the sodium silicate solution, silica coating on those nanoparticles is obtained.   The particle size is controlled by controlling the coagulation process, i.e. how fast the "sticky" sodium silicate is reacted into "hard" silica. The reaction rate is simply controlled by adjusting CO_2 concentration. Particles in the size range 30-300 nm were obtained by changing CO_2 pressure from sub-critical to supercritical with coating thickness of as low as 20 nm. The particle size increases linearly with the CO_2 molar volume. Water to surfactant mole ratio in the microemulsion also influences silica coating.

4.2 Introduction

Physical, chemical and biological properties of the particles change significantly from macro- to nano-grain size. Also with decrease in the size, the surface area per unit volume increases which enhances the properties due to available surface area. Various techniques have been developed for the formation of metal nano-particles using water-in-oil microemulsion.[1] Many of these nanoparticles are difficult to utilize due to aggregation, biocompatibility, stability, and inertness issues. To meet these challenges, heterogeneous nanoparticles of the core-shell or onion like forms can be utilized. For example, band edge luminescence can be enhanced from the photo-excited core particles by trapping excited-state charge carriers for semiconductor applications [2] and interesting acoustic breathing modes have been observed for core-shell nanoparticles.[3]

Coating is one of the methods which can be used for the formation of core-shell nanoparticles. For some applications, silica can be a good coating material because of its excellent optical, electrical, mechanical and thermal properties. So far, several techniques have been developed for silica particle formation including sol-gel and thermal methods. [4] In an early sol-gel technique proposed by Patrick [5], acid gelation of sodium silicate solution causes silica formation. Later, Strober et al. [6] formed silica by hydrolysis of tetraethylorthosilicate (TEOS) in basic solution containing ethanol and ammonium hydroxide. Particles produced by Strober's method were 200 to 1500 nm in diameter. Osseo-Asare et al. [7, 8] carried out Strober's reaction in water-in-oil microemulsion to form smaller silica particles of 25 to 70 nm in diameter. The major challenges of this method are the high aging time needed and the broad size distribution

obtained. To accelerate the reaction and produce more monodisperse particles, Chattopadhyay and Gupta [9] developed supercritical antisolvent (SAS) method for silica formation using water-in-oil microemulsion. In this method supercritical CO_2 acts both as an antisolvent and as a reactant.

So far, there have been several efforts to produce silica-coated particles. For example, pigmented silica particles of size range 2-100 μm were prepared by acidification of water-in-oil emulsion, which were then coated with dense amorphous silica particles for use as an opacifying agent and as a filler for paints or fibrous substrates. [10] Tan developed silica coated particles as core and shell structure using water-in-oil microemulsion [11] and then attached proteins and nucleic acids on the silica shell. Santra et al. [12] produced silica coated iron oxide particles, where iron was precipitated by reaction of ferrous and ferric salts with inorganic bases, and silica by hydrolyzing TEOS. Tago et al. [13] coated rhodium particles with SiO_2 layer of 15 nm thickness by hydrolysis of TEOS. Here, use of an ionic surfactant, AOT (Sodium bis (2-ethylhexyl) sulfosuccinate), provided irregular coating, whereas a non-ionic surfactant, polyethylene cetyl ether, provided a uniform coating. Vetsal and Zhang [14] characterized silica coated magnetic particles for coercivity and magnetization. Silica coated particles can endure large variations in pH, avoid coalescing and provide photochemical stability. These properties help silica shell in protecting the encapsulated quantum dots and the metal clusters in a core. [15]

This work utilizes a technique for silica coating in which supercritical CO_2 acts both as a reactant and as an antisolvent. Chattopadhyay and Gupta [9] method is used to form silica but in the presence of pre-made gold nanoparticles to achieve silica coating.

One of the advantages of using this coating method is the low aging time. For example this process requires less than 1 minute of reaction time for the formation of silica-coated particles. The water-in-oil microemulsion (in n-heptane) of aqueous sodium silicate and gold nanoparticles is injected into supercritical CO_2. Supercritical CO_2 readily extracts the organic phase (n-heptane) and diffuses inside the water core to react with the sodium silicate to form silica as

$$2NaOH \bullet SiO_2 + CO_2 \rightarrow Na_2CO_3 + 2SiO_2 + H_2O$$
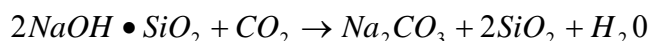
Since the gold nano-particles are suspended in sodium silicate solution, the silica starts forming on the top of the gold nanoparticles. Residual surfactant and formed sodium carbonate can be easily removed by ultrafiltration. In this work the effect of CO_2 pressure and water to surfactant molar ratio (W_o) are examined.

4.3   Experimental Section

4.3.1   Materials

CO$_2$ (99.9% pure) from BOC gases, sodium bis (2-ethylhexyl) sulfosuccinate (AOT; 99 +% pure) from Fisher Scientific, sodium silicate solution (14 wt% NaOH, 27 wt% SiO_2, and 59 wt% H_2O) from Aldrich Chemicals, n-heptane from Alfa-Aesar (HPLC grade, 99+% pure), and gold nanoparticles (10 nm) from Sigma were used as received. It was assumed that AOT molecules are hydrated with one water molecule each, as supplied.

4.3.2 Preparation of Microemulsion

A 77 mM AOT surfactant solution in n-heptane was prepared. A known amount of aqueous sodium silicate solution (27 wt% SiO_2) along with 0.5 ml gold colloid was added to the above mixture such that W_o is maintained at 20. This solution is stirred for 24 hrs to obtain clear reverse miceller solution. Similarly, microemulsion solution having W_o of 10 was also prepared using 77 mM AOT in n-heptane.

4.3.3 Apparatus

Figure 4.1 shows the schematic of the apparatus used. In this figure, R is the high pressure reactor (precipitation cell) having a volume of approximately 40 cm^3 wherein the silica formation takes place. A collection plate is placed inside the cell for collecting silica-coated particles. A syringe pump is used to pressurize the cell with CO_2. V1 and V2 are used as CO_2 injection valves. In order to maintain the constant temperature of the reactor, precipitation cell is placed in a water bath. Valve V4 is used to maintain the desired pressure inside the cell and for venting during the purging of the system with fresh CO_2. The microemulsion containing aqueous sodium silicate and gold nanoparticles is injected through valve V3 using the solution injection device, S. The solution injection device is made of stainless steel cylinder divided into two chambers by a piston having a neoprene o-ring. The front chamber has the microemulsion solution and the rear chamber has water as the pressurizing fluid. A hand pump is used to pressurize water in the rear chamber. The solution injection device is connected to the precipitation cell by a 50 cm long, 150 μm diameter capillary nozzle. The pressure difference between the injection device and the cell is maintained constant (~ 68 bars).

66

Supercritical CO_2 is injected into the system through the bottom port of the cell while W/O microemulsion is injected through the top port as countercurrent flow. Venting or purging is done from one of the two top flange ports. The pressure inside the cell is measured using a Heise ST-2H pressure transducer connected directly to the vessel through one of the side ports. There is also a pressure gauge connected just after the hand pump for the pressurizing fluid. A collection vial filled with deionized, ultra-filtered water is attached to the purge/vent line at the end to collect any particles escaping out from the cell.

4.3.4 Procedure

All the experiments were carried out in semi-batch mode in which CO_2 flows constantly while the microemulsion is injected in one shot. First the precipitation cell is pressurized with CO_2 using the syringe pump to a desired pressure and the cell is maintained at 40 ^{o}C. Approximately 7-8 ml of the microemulsion solution is loaded in the front chamber of the injection device, S. This microemulsion is injected into the reactor by opening the valve V5 which pressurizes the rear chamber with water and the piston pushes the front chamber solution inside the cell. The flow rate of the microemulsion inside the cell is controlled by maintaining a pressure difference between the pressurizing fluid and the cell pressure. The solution comes out as a jet inside the cell and fills the entire precipitation cell as a white smoke. The entire injection process takes only about 1-2 minutes. CO2 reacts with sodium silicate solution inside the core of the micelle after extracting organic bulk solvent and forms silica. In the entire process, the gold nano-particles do not take part in any reaction. Silica starts precipitating on the gold

67

surface to form coating. During the entire process, 1-2 ml/min of continuous CO_2 purge rate was maintained using a vent line to remove the solvent from the system. Some of the particles flow out with vent and are collected in vent vial while the rest of the particles settle down at the bottom of the vessel on the collection plate along with sodium carbonate as byproduct and residual surfactant.

The obtained powder was suspended in water and ultra-filtered using a 5000 Da membrane to remove surfactant and sodium carbonate.

4.3.5 Analyses

Size and morphology analysis was performed using Zeiss EM 10CR transmission electron microscope. A few drops of silica-coated gold particles suspended in water were placed on the carbon (Formvar) coated copper grid of 400 mesh size. The suspended particles were left for 24-40 hrs for drying at ambient condition. This dried grid was placed on the TEM grid holder and the particles were analyzed. TEM micrographs were taken at different locations on the grid to ensure overall distribution of the obtained particles.

Dynamic light scattering (PSS NICOMP model 380), DLS, was used to measure the approximate hydrodynamic diameter of silica-coated nanoparticles. Measurements were made using 638 nm laser light with 90° scattering angle at room temperature. The diffusion coefficients were calculated using autocorrelation function. Stokes-Einstein equation was used to calculate the particle size.

4.4 Results and Discussion

Table 4.1 shows the variation of the particle size (number weighted average by NICOMP analysis) of silica-coated gold analyzed using DLS with change in the CO_2 pressure. All the experiments were carried out at constant temperature of 40 $^{\circ}$C using 50 cm long nozzle of 150 μm diameter. From approximately 53 nm at 136 bar pressure, particle size increases to 182 nm at 34 bar pressure. This is attributed to the reactivity and rate of diffusion of supercritical CO_2 inside the water core. [9] The size of the water core controls the hydrodynamic diameter of reverse micelles which affect the particle size. After decreasing W_o from 20 to 10, the particle size decreases from about 52 nm to about 32 nm at the same conditions. The particle size appears to increase linearly with CO_2 molar volume as shown in Figure 4.2.

Figures 4.3 and 4.4 show the TEM micrographs of silica-coated gold particles obtained from experiments at Wo of 20 and 10, respectively. Both TEM and DLS show that the obtained particles from microemulsion with Wo of 10 are smaller than from Wo of 20. Increase in water concentration provides more time for "newly made" sticky silica to grow and agglomerate, before hardening. In all the TEM micrographs, the gold particles appear to be randomly oriented inside the silica shell. Also the shape of the silica shell is not always spherical. Tago et. al. [133] also observed a similar behavior for silica coating of rhodium particles by aqueous phase hydrolysis of TEOS. Some silica vesicles were also observed in this process (Figure 4.4b). Since the gold particles have a better transmission of electrons because of its electronic structure, it comes out to be darker than silica in TEM micrographs. The difference in the shades of these particles (silica and gold) is evident in all the micrographs. Figure 4.4c was taken at corner of the

metallic grid in mesh. Also, error in grid making can cause unusual shape of the particles.

The size of the individual micelles without gold in the microemulsion is 5 nm whereas with gold micelle size is approximately 20 nm. Chattopadhyay and Gupta [9] analyzed the effect of micelle size with change in water concentration and type of solvent use. If each micelle results in one particle, then all coated particles should be at about 12 nm in diameter, as gold nanoparticles are 10 nm in diameter considering one gold particle inside each micelle. However, the smallest particle obtained from the experiments is 32 nm in diameter. This implies that content from more than one micelles come together to form a larger particle. This coagulation is caused by the sticky nature of the "newly made" silica still containing some sodium silicate. Due to lower CO_2 concentration (density) at low pressures, more time is needed to complete hardening of all the silica. This results in coagulation and thicker silica coating. On the other hand, a high pressure provides high concentration (density) of CO_2 providing a high reactivity which causes silica hardening in smaller time, reducing the particle coagulation. The mechanism proposed in this process is reaction of CO_2 from outside to inside of micelle with sodium silicate to form silica particles. This reaction rate is governed by CO_2 pressure as reported earlier by Chattopadhyay and Gupta [9]. Gold particles are not controlling the particle size or quality as silica particles of 20-800 nm size range can also be produced by this process without gold particles [9]. In addition, with an increase in the pressure of CO_2, the Weber number, ratio of the inertial forces to the surface forces, increases. An increase in the Weber number, or higher diffusion coefficients, yields smaller initial droplet sizes.[16] Also, two-way mass transfer results in high supersaturation leading to

70

faster nucleation rates and ultimately formation of smaller particles.[17] Although most of the particles observed are clusters of gold particles coated with silica, a few individual gold particles coated with silica are also observed (Figure 4.3c). Coating thickness of as low as 25 nm is observed at 102 bar for individual particles (Figure 4.3c). Also, silica-coated gold particles of ~ 300 nm are observed at 34 bar pressure. These results show that pressure (density) and water concentration can be used to control the silica coating and the size of final particle. It is interesting to note that the particle size linearly increases with CO_2 molar volume (Figure 4.2).

4.5   Conclusion

Silica-coated gold particles are obtained using supercritical antisolvent method with water-in-oil microemulsion. Coated particles of size in the range 30-300 nm are formed by varying the CO_2 pressure. Particle size increases with increase in Wo or in CO_2 molar volume.

4.6   Acknowledgement

REFERENCES

1. Capek, I. Preparation of metal nanoparticles in water-in-oil microemulsions. Advances in Colloid and Interface Sci. 2004, 110, 49-74.

2. Hines, M. A.; Guyot-Sionnest, P. Synthesis and Characterization of Strongly Luminescing ZnS-Capped CdSe Nanocrystals. J. Phys. Chem. 1996, 100, 468-471.

3. Sader, J. E.; Hartland, G. V.; Mulvaney, P. Theory of Acoustic Breathing modes of Core-Shell Nanoparticles. J. Phys. Chem. B 2002, 106, 1399-1402.

4. Scherer, G. W.; Luong, J. C. Glasses from Colloids. J. Non-Cryst. Solids 1984, 63 (1-2), 163-72.

5. Patrick, W. A. Silica gel and process of making same. U. S. Patent 1,297,724, 1918.

6. Strober, W.; Fink, A.; Bohn, J. J. Colloid Interface Sci. 1968, 26, 62.

7. Osseo-Asare, K.; Arrigada, F. J. Preparation of silica nanoparticles in a nonionic reverse miceller system. Colloids Surf. 1990, 50, 321-39.

8. Arrigada, F. J.; Osseo-Asare, K. Synthesis of Nanosize silica in Nonionic water in oil Microemulsions. J. Colloid Interface Sci. 1994, 170, 8-17.

9. Chattopadhyay, P.; Gupta, R. B. Supercritical CO_2 based Formation of Silica Nanoparticles Using Water-in-Oil Microemulsions. Ind. Eng. Chem. Res. 2003, 42, 465-472.

10. Marquisee, M. J.; Sandell, L. S. Pigmented microporous silica microspheres produced by a water in oil emulsion. U. S. Patent 4090887, 1977, 37pp.

11. Tan, W.; Santra, S.; Zhang, P.; Tapec, R.; Dobson, J. Coated Nanoparticles. PCT Int. Appl. (2001), 34pp

12. Santra, S.; Tapec, R.; Theodoropoulou, N.; Dobson, J.; Hebard, A.; Tan, W. Synthesis and Characterization of Silica-Coated Iron oxide Nanoparticles in Microemulsion: The Effect of Nonionic Surfactants. Langmuir 2001, 17, 2900-2906.

13. Tago, T.; Shibata, Y.; Hatsuta, T.; Miyajima, K.; Kishida, M.; Tashiro, S.; Wakabayashi, K. Synthesis of Silica Coated Rhodium nanoparticles in reversed miceller solution. J. Matl. Sci. 2002, 37, 977-982.

14. Vestal, C.R.; Zhang, Z.J. Synthesis and Magnetic characterization of Mn and Co Spinel Ferrite-Silica Nanoparticles with Tunable Magnetic Core. Nano Letters. 2003, 3 (12), 1739-1743.

15. Mulvaney, P.; Liz-Marzan, L.M.; Giersig, M.; Ung, T. Silica encapsulation of quantum dots and metal clusters. J. Mater. Chem. 2000, 10, 1259-1270.

16. Dixon, D. J.; Johnston, K. P.; Bodmeier, R. A. Polymeric materials formed by precipitation with a compressed fluid antisolvent. AIChE Journal. 1993, 39 (1), 127-39.

17. Randolph, T. W.; Randolph, A.D.; Mebes, M.; Yeung, S. Sub-micrometer-sized biodegradable particles of poly (L-lactic acid) via the gas antisolvent spray precipitation process. Biotechnology Progress. 1993, 9 (4), 429-435.

Table 4.1 Number average particle size (NICOMP analysis) of the obtained silica-

coated gold nanoparticles

CO$_2$ Pressure (bar)	[Water] / [AOT]	Particle Size (nm)	Std. Deviation (nm)
34	20	182	20
68	20	75	9
136	20	53	7
102	10	59	7
136	10	32	12
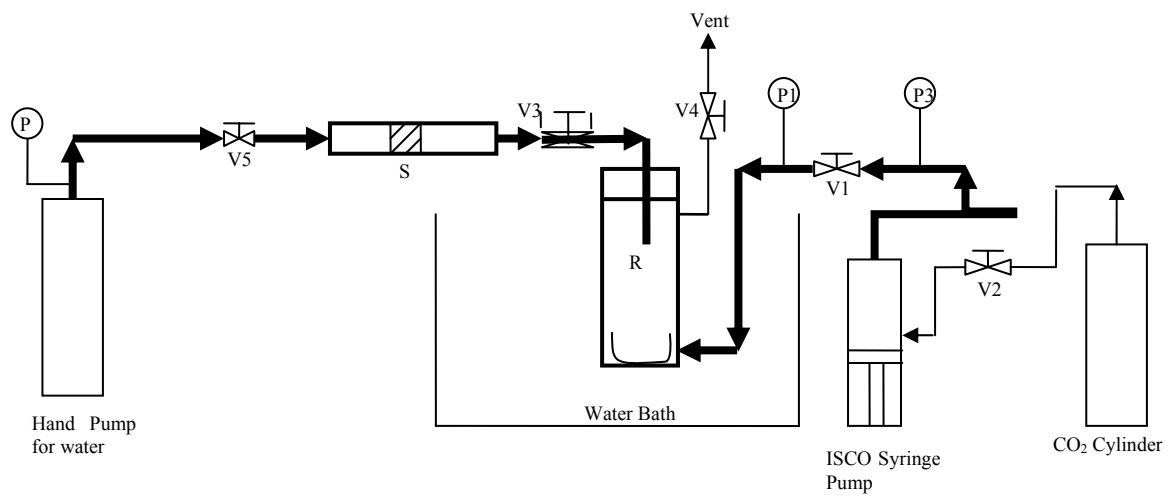
Figure 4.1 Schematic of apparatus for silica-coating using supercritical CO_2
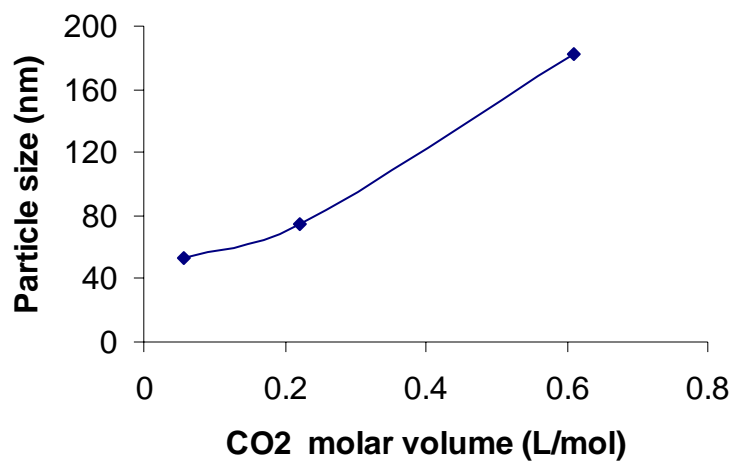
Figure 4.2 Mean hydrodynamic diameter of silica-coated particles versus CO_2 using microemulsion of $W_o = 20$.

(a) 34 bar

(b) 68 bar

77
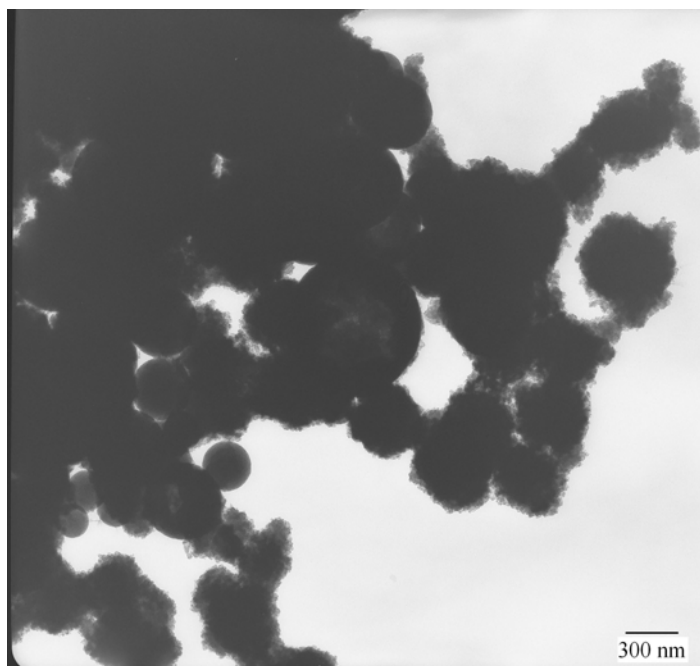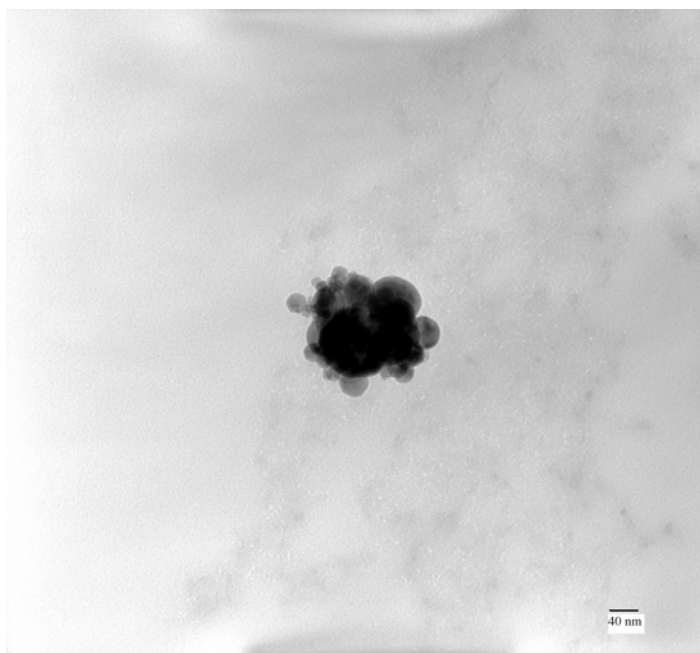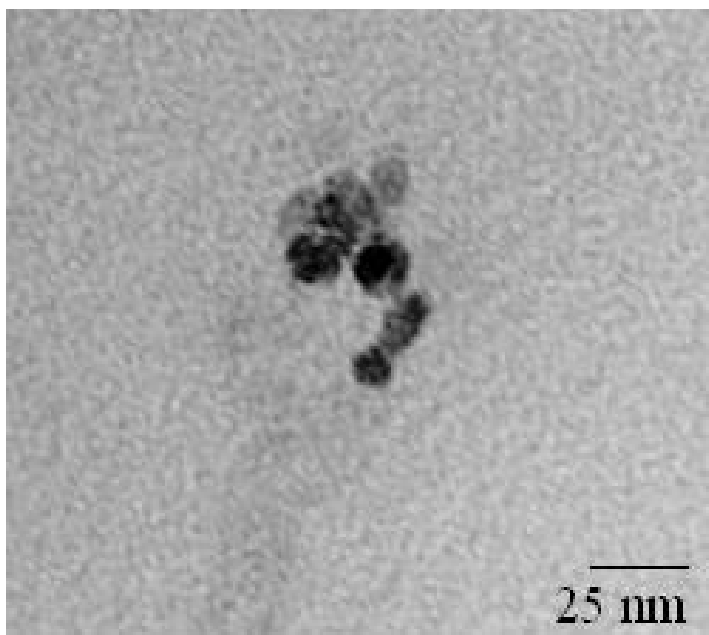
(c) 102 bar

(d) 136 bar

Figure 4.3 TEM micrographs of particles obtained at Wo = 20 and different

pressures.
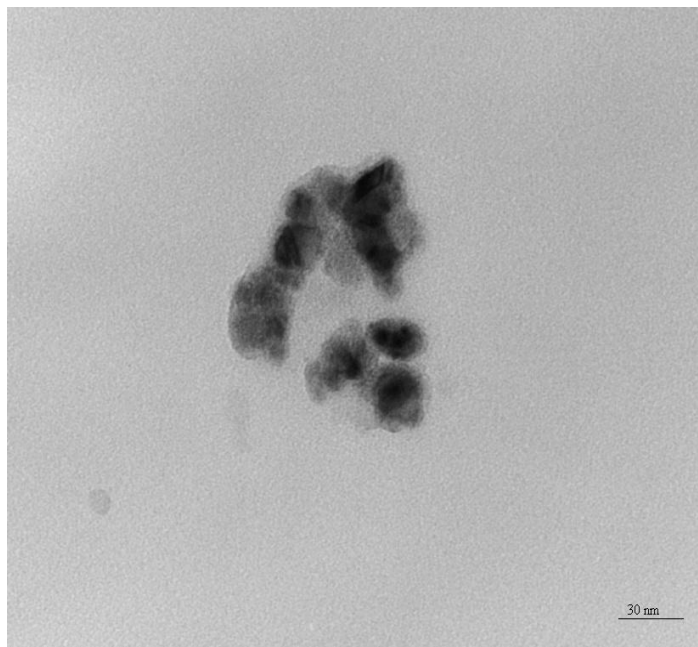
(a) 68 bar
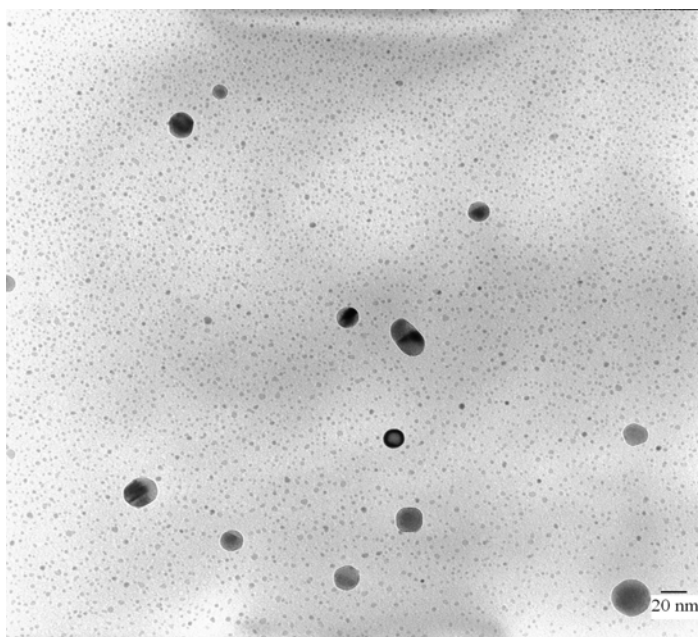
(b) 102 bar

(c) 136 bar

Figure 4.4 TEM micrographs of particles obtained at $W_o = 10$ and different pressures.

CHAPTER 5

RAPID EXPANSION OF SUPERCRITICAL SOLUTION WITH SOLID COSOLVENT

(RESS-SC) PROCESS: FORMATION OF GRISEOFULVIN NANOPARTICLES

5.1   Abstract

In conventional RESS process, a supercritical solution is rapidly expanded through a nozzle to precipitate the solute as microparticles. The modeling of RESS has shown that the precipitated particles at the nozzle tip are of the order of 5-25 nm in size. However, for most solutes, the final particles experimentally obtained are in the order of 800-3000 nm in size, due to growth by coagulation in the expansion chamber. Another difficulty is that most of the pharmaceutical compounds have poor solubility in supercritical carbon dioxide (a fluid of choice).   In this work, both challenges are addressed by utilizing a cosolvent that is solid at the nozzle exit conditions. The solid cosolvent (SC) enhances the solubility and provides barrier for coagulation in the expansion chamber. The solid cosolvent is later remove from the solute particles by lyophilization (sublimation). The new process is termed as RESS-SC. A suitable solid cosolvent is menthol which is solid below 35 ^{o}C (typical nozzle exit temperature is 5-30 ^{o}C) and can be easily sublimed.

RESS-SC concept is demonstrated by producing nanoparticles of griseofulvin, an antifungal drug which has very low solubility in supercritical CO_2. By using menthol

cosolvent, griseofulvin solubility in supercritical CO_2 is increased by about 28 fold. Using a simple capillary nozzle, griseofulvin particles in the range 50-250 nm were obtained, which is a 10 fold reduction from conventional RESS process. The final powder is pure griseofulvin, free of any stabilizing agents. Particles are characterized by SEM, XRD and DSC analyses. In addition, data and modeling of solubility enhancement are presented.

5.2   Introduction

The dissolution rate and the bioavailability of poorly-water-soluble drugs are heavily dependent on the particle size and the morphology. The bioavailability of such drugs is usually the limiting factor in deciding a dosage window for oral or systemic administration. Various methods have been used to improve the drug solubility, including micronization or comminuation into fine particulate form. Supercritical fluid technology provides opportunities for the particle size reduction where the final product is obtained in a powder form, free of organic solvent or stabilizing agents. The two major processes based on supercritical fluids are rapid expansion of supercritical solutions (RESS) and supercritical anti-solvent (SAS). In RESS, rapid expansion causes sudden reduction in the solubilization strength and hence fast precipitation, whereas in SAS the dense supercritical fluid is used to lower the solubilization strength of organic solvent. Supercritical CO_2, due to its environmentally benign nature and low cost, is a widely used in both the processes for forming particles of organic and pharmaceutical compounds [1, 2, 3].

Nucleation and growth are two important phenomena that govern particle size and morphology in RESS process (Figure 5.1). As the pressure reduces in the nozzle, supersaturation causes nucleation of the solute particles at the nozzle tip. On the Mach disk (where the speed of fluid changes from supersonic to subsonic) most of the solute starts coagulating. This coagulation leads to growth of the particles in expansion chamber [4, 5]. The mathematical model based calculation shows that the size of the particles at the tip of the nozzle is in 5-25 nm range [4, 5], but the final particles are usually in 800-3000 nm size range, as observed in the experiments conducted in this work. The large particle size is attributed to the growth by coagulation in the expansion chamber. Smaller particles can be maintained if the coagulation is reduced in the expansion chamber. Another difficulty in conventional RESS process is that most of the pharmaceutical compounds have poor solubility in supercritical carbon dioxide (a fluid of choice), which results in a low processing rate.

In this work, both challenges (low solubility and growth by coagulation) are addressed by utilizing a cosolvent that is solid at the nozzle exit conditions. The solid cosolvent (SC) enhances the solubility in supercritical carbon dioxide and provides barrier for coagulation in the expansion chamber. The solid cosolvent is later removed from the solute particles by lyophilization (sublimation). The new process is termed as RESS-SC. In RESS, all the nuclei or small particles of solute are surrounded by the same kind of particles as shown in Figure 5.1. But in RESS-SC process, nuclei or small particles of the solute are surrounded by the excess solid co-solvent particles. This reduces the probability of solute particle growth by coagulation. The RESS-SC concept is

depicted in Figure 5.2. The lyophilization process shown in the Figure 5.2 occurs after the expansion and not part of the RESS-SC set up.

RESS-SC concept is demonstrated by formation of griseofulvin (GF) nanoparticles. A model solute GF (Figure 5.3) is an antifungal drug and widely used for the treatment of mycotic diseases of the skin, hair and nails. The GF is one of the drugs which have very low solubility in water or supercritical CO_2. The solubility of the GF in water is only about 1 µmol/mol at 37 ^{o}C [6], whereas in supercritical CO_2 solubility is reported as 15 µmol/mol at 200 bar and 50 ^{o}C [7]. Therapeutic dosage limit of GF is very close to toxicity limit of the drug; because of this limitation improvement of the GF bioavailability by size reduction or by co-formulation is desired [8, 9].

GF is a highly crystalline organic compound. Due to very low polarity, CO_2 is not a good solvent for GF as reported earlier in the literature [7]. To improve the solubility, several liquid cosolvents have been examined [7, 10, 11]. Tavana et al. used dichloromethane, butyl acetate and cyclohexanone as co-solvents to enhance the GF solubility [7], with a maximum solubility enhancement of about 4 fold. Using 6 mol% acetone cosolvent, GF solubility was enhanced to 140 µmol/mol at 280 bar and 60 ^{o}C [8]. By replacing supercritical carbon dioxide with polar fluid trifloromethane, GF solubility of 252 µmol/mol was obtained at 330 bar and 333 K [12].

SAS method was used to form small GF particles because of the low GF solubility in supercritical CO_2 [12,13, 14]. But all the methods employed so far did not give promising results, as long needle shaped or quasispherical GF particles in the size range of micron to millimeter length were observed. Later, Chattopadhyay and Gupta [6] used ultrasonic energy in SAS-EM process to obtain small GF particles of size as small

as 130 nm. By changing the ultrasound intensity, particles morphology was changed from needle like to a mixture of needle and sphere. Till date, all those methods or processes which were used to increase solubility of GF and its micronization involves harmful solvents or severe operating conditions. To overcome these limitations this paper proposes enhancement of GF solubility using a solid cosolvent by utilizing RESS-SC concept for nanoparticle production.

5.3   Choice of Solid Cosolvent

The choice of a proper solid cosolvent is the key element in the RESS-SC process. Various requirements for the selection of a solid cosolvent are:

a) good solubility in supercritical CO_2,

b) should be in a solid phase at the nozzle exit temperature (typically, 5-30 ^{o}C),

c) have a sufficiently high vapor pressure so that cosolvent can be removed by sublimation,

d) non-reactive with drug or CO_2,

e) non-toxic, and

f) Inexpensive.

Menthol (Figure 5.4) is a solid compound that satisfies above requirements. It has appreciable solubility in CO_2 [15] and can easily sublime under vacuum. Menthol naturally occurs in mint-flavored plants, and is widely used in antipruritic agents, mouthwashes, nasal sprays, food, etc. Because of its wide use in food and pharmaceutics, menthol does not possess any harmful effects. The use of menthol as a cosolvent with supercritical carbon dioxide still carries environmentally benign benefit of

the technology. Menthol solubility in supercritical CO_2 is about one thousand fold that of GF at the same conditions [15].

In this work, the solubilities of pure menthol and pure GF in supercritical CO_2 are measured using gravimetric and spectroscopic analyses, respectively. Also, the enhancement of GF solubility in the presence of menthol is measured for a wide range of conditions. The solubility and its enhancement is correlated using a Mendez-Santiago and Teja model [16, 17]. The GF solution in supercritical carbon dioxide is expanded through a nozzle without menthol (as in RESS) and with menthol (as in RESS-SC). Obtained particles are analyzed to validate the RESS-SC concept.

5.4   Experimental Section

5.4.1   Materials

CO_2 (99.9% pure) from Air Gas, menthol (99% pure) with melting point of 34-36 ^{o}C and dichloromethane (99+% pure, HPLC grade) from Sigma- Aldrich were used as received. GF (95% pure, HPLC grade) from Sigma was stored below 0 ^{o}C prior to use.

5.4.2   Apparatus

Figure 5.5 shows the schematic of RESS-SC apparatus. The experimental set up is divided in to three parts – a pre-extraction chamber (section I), an extraction chamber (section II) and an expansion chamber (section III). In section I, P is a high pressure syringe pump for pressurizing CO_2 at desired pressure using CO_2 from cylinder A. Two vessels, M and G are used as extraction column for menthol and GF, respectively, in section II. Glass wool was used on the both ends of the vessels M and G to avoid carry

over of the undissolved material with the CO_2 flow. Both vessels containing solute and co-solvent were kept in a water bath to keep the constant extraction temperature ($\pm$ 0.1 ^{o}C) by a temperature controller. The pressure of the extraction section was measured using an online Heise ST-2H pressure transducer connected just before valve V1. The section III is either an expansion chamber of 3 liters capacity for RESS-SC experiments or a U-tube for solubility experiments, kept at ambient conditions. Valve V1 connects section I with section II whereas valve V3 connects section II and section III. Valve V1 and V2 are 3-way valves for CO_2 bypass connection to vessel G to perform conventional RESS experiments for comparison. Glass wool was used at the end of the expansion chamber outlet or at the end of the second leg of the U-tube to entrap the particles. The temperature in the expansion chamber was recorded to be about 5 ^{o}C using a thermocouple.

5.4.3   Solubility Measurement

A syringe pump was filled with CO_2 from a tank A and set at the desired pressure. Vessels, M and G, having 7 ml capacity each, were filled with menthol and GF, respectively. These vessels act as extraction/solubilization columns.   After filling, the extraction columns were connected as per Figure 5.5. The extraction column containing menthol was connected first in line to the GF extraction column.   Both columns were kept in a water bath at desired temperature in such a way that the inlet was at the bottom while the outlet was at the top for proper distribution of SCF. CO_2 was fed to the first extraction column and was allowed to equilibrate for 10-15 minutes by closing valve V2 at a desired pressure. After stabilizing the first column, menthol-enriched CO_2 was

87

supplied to the second extraction column containing GF using valve V2. Again, the entire system was equilibrated for 10-15 minutes before expanding the GF solution in the U-tube. The whole system was equilibrated for longer duration, 30-45 minutes, as well but there was no change in solubility values. The change in flow rate also did not affect solubility values, which suggested that the system was in equilibrium. The U-tube was kept in an ice bath with glass wool at the other end to trap the formed particles. For pure menthol or GF solubility experiments, only one column was used. The difference of initial and final masses of the U-tube gave the amount of menthol recovered for the given conditions. The weight of empty U-tube was ~84 gm, whereas each sample mass was around 0.1 mg. Considering 7 ml extraction column, the solubility experiments are conducted for 4-5 ml of CO_2 flow to avoid entrance of any fresh solvent. For measuring the GF solubility, the powder obtained in the U-tube was dissolved in methylene chloride and was analyzed by UV spectrophotometer (Spectronic Genesys2) set at 290 nm (at this wavelength menthol is transparent, but GF absorbs light due to aromatic ring). M and G are identical columns which can be used for either solute or cosolvent.

5.4.4   Particle Formation by RESS-SC

RESS experiments without solid cosolvent are conducted before starting RESS-SC experiments so there was no contamination of GF with menthol. Also, after every run both columns were cleaned with methylene chloride and then with soap solution. For RESS-SC, the expansion chamber having 3 liters capacity was used for expansion of the menthol/GF/CO_2 solution from a desired pressure to the atmospheric pressure. A polymer-coated silica nozzle (PEEKsil nozzle from Upchurch Scientific) of 25 μm

diameter and 5 cm length was used for expansion in all the experiments. Before analyzing the particles for size, crystallinity or morphology, the particles were subjected to 3-4 mbar (absolute) vacuum for 12-15 hrs to remove all the menthol by sublimation in a lyophilizer. There was no change in the weight of the particles after applying vacuum for additional 3 hrs. Also, the lyophilized powder did not give any mint smell. These were sufficient tests for ensuring menthol absence in the lyophilized GF particles. The GF particles obtained after menthol removal were analyzed by SEM, differential scanning calorimeter (DSC) and powder X-ray diffraction (XRD) methods.

5.4.5 SEM Analysis

The particle size and morphology analysis was carried out using SEM (Zeiss, model DSM940). For analysis, the particles were attached to the carbon tape on the top of SEM aluminum stubs and were coated with gold using a sputter coater (Electron Microscopy Sciences, model 550X) for 2 runs for 2 minutes each. In order to have a proper representation of the particles collected in the expansion chamber, SEM micrographs of different regions were obtained. In menthol/GF system wherein menthol was the co-solvent, processed powder was first kept in a high vacuum of 3-4 mbar (absolute) to remove all the menthol from the particle mixture. All the SEM analysis was done after 3-4 days of experiments at an accelerating voltage of 10 kv.

5.4.6 DSC Analysis

Thermal analysis was carried out using DSC (TA instruments, model DSC Q100) for the processed and unprocessed GF particles. Melting point was measured for 3 mg

GF sample at a heating rate of 5 $^{\circ}$C/min over the temperature range from -50 $^{\circ}$C to 230 $^{\circ}$C.

5.4.7 Powder X-Ray Diffraction

GF particle crystallinity was analyzed using Rigaku X-ray diffractometer which was equipped with Cu Kα_1 radiation source and Miniflex goniometer. The powder was filled to same depth inside the sample holder and also all the parameters were kept same while performing XRD.

5.4.8 Dynamic light scattering analysis

Dynamic light scattering (DLS; PSS NICOMP model 380) was used to measure the hydrodynamic diameter of GF nanosuspension. Measurements were made using 638 nm laser light with a 90° scattering angle at room temperature.

5.5 Results and Discussion

5.5.1 Solubility Enhancement

Solubility results are summarized in Table 5.1 of pure menthol and in Table 5.2 for pure GF in supercritical CO_2. Both solubility results agree well with the published values [7, 15]. For example, the GF solubility in sc CO_2 is reported as 15 μmol/mol at 200 bar and 50 $^{\circ}$C [7], which is consistent with 13 μmol/mol of GF solubility observed in this work at 195.6 bar and 50 $^{\circ}$C. The solubility of both menthol and GF increases with density as shown in Figures 5.6 and 5.7.

Table 5.3 shows the solubility of GF in supercritical CO_2 using menthol cosolvent. In this work, cosolvent mole fraction is not constant but changes with

pressure, because supercritical CO_2 is saturated with menthol before entering GF extraction column. The GF solubility is enhanced up to 28 fold by menthol cosolvent. The GF solubility increases with increase in pressure due to higher CO_2 density and the amount of menthol cosolvent. The solubility enhancement can be attributed to the high polarity of menthol/CO_2 mixture as compared to the pure CO_2. The good solvents for the GF are polar in nature such as dimethylformamide, ethanol or acetone [18] which suggests that polar CO_2 can solubilize higher amount of the GF.

5.5.2 Modeling of Solubility Enhancement

The solubility of solids in supercritical fluids can be expressed as [19]

$$y_2 = \frac{P_2^{sat} \exp(\frac{v_2^s (P - P_2^{sat})}{RT})}{\phi_2 P} \tag{1}$$

where P_2^{sat} is the vapor pressure of the solid at temperature T, v_2^s is the solute molar volume, P is the operating pressure, R is the universal gas constant, Φ_2 is the solute fugacity coefficient and y_2 is the equilibrium mole fraction of the solid in supercritical CO_2.

The solubility of heavy, non-polar solids can be calculated using semi-empirical correlation in subcritical and supercritical solvents [20]. Fugacity coefficient has been calculated from equation of state including Peng-Robinson [21], Bender and Carnahan-Starling-De Santis [12] for solubility prediction. But there is always a problem of finding accurate values of P^{sat} for the high molecular weight solutes as well as binary and ternary interaction parameters. Here, Mendez-Santiago and Teja model [16] is utilized, in which solubility is a function of temperature and CO_2 density (ρ_1):

$$T \ln(y_2 P) = A' + B' \rho_1 + C' T \qquad\qquad (2)$$

The values for the three parameters, A', B', C' were obtained by fitting the model

to our experimental data for menthol as, -1667.3, 91939, 1.63, respectively, and for GF as

-5083.38, 173011.24, 0.00, respectively. These parameters are not dimensionless; here

temperature, pressure, and density are in K, bar, and mol/ml units, respectively. In both

the cases, the solubility data of varying temperature and pressure collapse to straight lines

with a good linear fit. The comparison between experimental and model solubilities is

shown in Figures 5.6 and 5.7 for pure menthol and GF, respectively.

GF solubility enhancement by menthol cosolvent is shown in Figure 5.8.

Mendez-Santiago and Teja [17] also developed a model for solubility of solids in

supercritical CO_2 with a cosolvent by adding a new parameter and cosolvent

concentration. However this model did not yield a satisfactory fit to our data. Hence, in

this work, a further modified form of GF solubility equation is proposed as

$$T \ln(P y_2) = A' + B' \rho_1 + (D' \rho_1 + E') y_3 \qquad\qquad (3)$$

where y_2 is the GF mole fraction and y_3 is the menthol mole fraction. Here, the parameter

A' and B' are the same what they were for GF solubility without cosolvent. The

additional parameters D' and E' are obtained by fitting model to the experimental data, as

-4467345.59, 102221.97, respectively. The correlated GF solubilities with menthol

cosolvent are in good agreement with experimental data as shown in Figure 5.8.

5.5.3   Particle Size and Morphology

Once satisfactory solubility enhancement was achieved, GF particles were formed

using RESS-SC process. For comparison, the conventional RESS experiments were also

performed without menthol. The particles were characterized by SEM, DSC and XRD analyses. The melting point of unprocessed GF was 220 ^{o}C (Figure 5.9) but after RESS-SC melting point was depressed to 202.5 ^{o}C (Figure 5.10). Similar depression in melting point was observed by several researchers after processing with dense CO_2 [22, 23]. The depression in melting point can be attributed to the lowering of crystallinity [21] and/or smaller particle size.

XRD pattern for the unprocessed particles and particles obtained from the RESS-SC process are shown in Figures 5.11 and Figure 5.12, respectively. Particles from RESS-SC show a lower intensity as compared to the unprocessed particles. The lowering of intensity can be explained either by low crystallinity and/or small particle size giving low bulk density. This decrease in crystallinity can be helpful for the better dissolution of GF particles [8]. Figure 5.13 shows the XRD of pure menthol particles. The two major peaks for menthol are at 8° and 18° angles, whereas there are no peaks at these angles for GF. This further suggests that RESS-SC processed GF after lyophilization was menthol free.

The smaller particles obtained are associated with higher surface energy, and therefore undergo sintering. The depression in melting point in Figure 5.10 and XRD result in Figure 5.12 can be interpreted either due to low crystallinity or smaller particle size or both. The purpose of this work is to qualitatively examine crystallinity rather than quantitative values.

Micronization is the one of the methods to improve better dissolution rate of poorly water soluble drugs [8, 21]. The original GF particles are big agglomerates of 2-7 μm in size (Figure 5.14). In this work, RESS processed GF particles are spherical or

quasi-spherical but bigger in size as shown in Figure 5.15. Based on SEM analysis, the particles are in 2-4 μm size range. Upon closer examination of the SEM pictures, it is evident that the each particle is made up of coagulation of smaller particles. This coagulation had occurred in the expansion chamber right after the nozzle tip. Various methods have been employed to form nanoparticles after expansion in RESS process. For example, Sun and co-workers expanded supercritical solution in liquid at receiving end to form polymeric nanoparticles [24].

SEM micrographs of the particles obtained from RESS-SC experiments are shown in Figure 5.16. Particles are about 10 fold smaller than those from RESS experiment. Here particles are from 50 to 250 nm in size. The lower particle size proves the hypothesis that presence of solid menthol hinders the particle coagulation. Once particles are formed, coagulation of particles is a major growth mechanism. Colliding particles agglomerate due to their adhesiveness. By using menthol particles as the spacer, the drug particle to drug particle collision is reduced. Due to a high concentration of the solid menthol particles in expansion chamber, the probability of GF particle collision is significantly reduced. In other words, the residence time for coagulation of the GF particles is reduced. An increase in the menthol concentration will provide further reduction in the coagulation of GF particles due to increased dilution effect. This is consistent with the work of Turk et al. [25] who used additional air flow in the expansion chamber for controlling particle growth by higher dilution and shorter residence time.

The GF nanoparticles are also analyzed by dynamic light scattering. First pure water was contacted with original GF, then the GF-saturated water was filter out using a 200 nm filter. DLS analysis of this solution was done to ensure absence of particles.

Now GF nanoparticles were suspended in above solution and analyzed by DLS. The number average diameter of 154 nm is observed in nanosuspension form, as shown in Figure 5.17.

5.6   Conclusion

To address two major challenges of RESS process (low solute solubility and particle growth by coagulation), a new process RESS-SC is developed. By using menthol as a solid cosolvent, RESS-SC process is successfully demonstrated for nanoparticle formation of griseofulvin. The solubility is enhanced by as high as 28 fold and the particle size is reduced by 10 fold, when compared to conventional RESS process. The concept is supported by SEM, XRD, DLS, and DSC analyses. In addition, the solubility enhancement data and its correlation are presented.

REFERENCES

1. Kompella, U.B.; Koushik, K., Preparation of Drug Delivery Systems Using Supercritical Fluid Technology. Critical reviews in Therapeutic Drug Carrier Systems, 2001, 18(2), 173-199.

2. Sane, A.; Taylor, S.; Sun, Y.-P.; Thies, M.C., RESS for the preparation of flourinated porphyrin nanoparticles. Chemical Communications (Cambridge, England), 2003, 21, 2720-1.

3. Meziani, M.J.; Pathak, P.; Hurezeanu, R.; Thies, M.C., Supercritical-fluid processing technique for nanoscale polymer particles. Angewandte Chemie, International Edition, 2004, 43(6), 704-707.

4. Weber, M.; Russel, L.M.; Debenedetti, P.G., Mathematical modeling of nucleation and growth of particles formed by the rapid expansion of a supercritical solution under subsonic conditions. J. of Supercritical Fluids, 2002, 23, 65-80.

5. Helfgen, B.; Turk, M.; Schaber, K., Hydrodynamic and aerosol modelling of the rapid expansion of supercritical solutions (RESS-process). J. of Supercritical Fluids, 2003, 26, 225-242

6. Chattopadhyay, P., Gupta, Ram B., Production of griseofulvin nanoparticles using supercritical CO2 antisolvent with enhanced mass transfer. International Journal of Pharmaceutics, 2001. 228: p. 19-31.

7. Tavana, A., Chang, J., Randolph, A.D. , Rodriguez, N., Scanning of cosolvents for supercritical fluids solubilization of organics. AIChE Journal, 1989. 35(4): p. 645-648.

8. Saito, M.U., Takashi; Nozawa, Yasuo; Sadzuka, Yasuyuki; Miyagishima, Atsuo; Sonobe, Takashi, Preparation and dissolution characteristics of griseofulvin solid dispersions with saccharides. International Journal of Pharmaceutics, 2002. 249: p. 71-79.

9. Kallinteri, P.A., Sophia G., Solubility of drugs in the presence of gelatin:effect of drug lipophilicity and degree of ionization. International Journal of Pharmaceutics, 2001. 221: p. 219-226

10. Hu, G.C., Hongyan; Cai, Jianguo; Deng, Xiu., Micronization of griseofulvin by ress in supercritical CO2 with cosolvent acetone. Chinese Journal of Chemical Engineering, 2003. 11(4): p. 403-407.

11. Gioannis, B.D., Gonzalez, A. V., Subra, P., Anti-solvent and co-solvent effect of CO_2 on the solubility of griseofulvin in acetone and ethanol solutions. Journal of Supercritical Fluids, 2004. 29: p. 49-57.

12. Reverchon, E., Porta, G. Della, Taddeo, R., Pallado, P., Stassi, A., Solubility and micronization of Griseofulvin in Supercritical CHF_3. Ind. Eng. Chem. Res., 1995. 34: p. 4087-4091.

13. Reverchon, E., Porta, G. Della, Production of antibiotic micro- and nano-particles by supercritical antisolvent precipitation. Powder Technology, 1999. 106: p. 23-29.

14. Chen, H., Lai, J., Deng X., Dai G.,, Fine Griseofulvin particles formation by rapid expansion of supercritical solutions. Huagong Xuebao (Chin. Ed.), 2001. 52(1): p. 56-60.

15. Sovova, H., Jez, Jaromir, Solubility of menthol in Supercritical Carbon Dioxide. J. Chem. Eng. Data, 1994. 39: p. 840-841.

16. Mendez-Santiago, J., Teja, Amyn S., The solubility of solids in supercritical fluids. Fluid Phase Equilibria, 1999. 158-160: p. 501-510.

17. Mendez-Santiago, J., Teja, Amyn S., Solubility of solids in Supercritical Fluids: Consistency of Data and a New Model for Cosolvent Systems. Ind. Eng. Chem. Res., 2000. 39: p. 4767-4771.

18. Saykhedkar, S.S.A.S., Rekha S., Supercritical Carbon Dioxide Extraction of Griseofulvin from the Solid Matrix Obtained after Solid-State Fermentation. Biotechnol. Prog., 2004. 20: p. 818-824.

19. Prausnitz, J.M.L., Rudiger N. and Azevedo, Edmundo Gomes de, Molecular Thermodynamics of Fluid-Phase Equilibria. Prentice Hall, 1999. 3rd edition.

20. Zlger, D.H., Eckert, Chrales A., Correlation and Prediction of Solid-Supercritical Fluid Phase Equilibria. Ind. Eng. Chem. Res., 1983. 22: p. 582-588.

21. Charoenchaitrakool, M.D., F.; Foster, N.R.; Chan, H.K., Micronization by Rapid Expansionof Supercritical Solutions to Enhance the Dissolution Rates of Poorly Water-Soluble Pharmaceuticals. Ind. Eng. Chem. Res., 2000. 39: p. 4794-4802.

22. McHugh, M.A.; Yogan, T.J., A study of three-phase solid-liquid-gas equilibria for three CO_2-solid hydrocarbon systems, two ethane-hydrocarbon systems, and two ethylene-hydrogen systems. J. Chem. Eng. Data, 1984, 29, 112

23. McHugh, M.A.; .Krukonis, V. J., Supercritical Fluid Extraction Principles and Practice. Butterworth, Boston, 1986, p228.

24. Sun, Ya-Ping; Meziani, M.J.; Pathak, P.; Qu, L., Polymeric nanoparticles from rapid expansion of supercritical fluid solution. Chemistry-A European Journal, 2005, 11(5), 1366-1373.

25. Turk, M.; Hils, P.; Helfgen, B.; Schaber, K.; Martin, H.-J.; Wahl, M.A., Micronization of pharmaceutical substances by the Rapid Expansion of Supercritical Solutions (RESS): a promising method to improve bioavailability of poorly soluble pharmaceutical agents. J. of Supercritical Fluids, 2002, 22, 75-84.

26. Span, R.; Wagner, W., A new equation of state for carbon dioxide covering the fluid region from the triple point temperature to 1100 K at pressure up to 800 MPa. J. Phy. Chem. Ref. Data, 1996, 25(6), 1509-1596.

Table 5.1 Solubility of pure menthol in supercritical CO$_2$

P (bar)	T (^oC)	CO$_2$ Density[26] (g/ml)	Menthol Solubility (mol fraction x 10^3)
72.9	35	0.26	2
77.6	35	0.35	3
79.2	35	0.44	6
95.4	35	0.70	11
128.9	35	0.79	29
129.9	35	0.79	29
163.5	35	0.83	31
163.9	35	0.83	33
94.8	40	0.59	18
129.0	40	0.74	40
235.6	40	0.87	51
94.8	50	0.34	3
128.9	50	0.64	12

Table 5.2 Solubility of pure griseofulvin in supercritical CO_2

P (bar)	T (^{o}C)	CO_2 Density[26] (g/ml)	Griseofulvin Solubility (mol fraction x 10^6)
130.2	35	0.79	6
130.9	35	0.79	7
95.4	40	0.60	1
114.9	40	0.71	2
128.7	40	0.74	7
195.7	40	0.84	14
235.2	40	0.87	18
95.1	50	0.34	0.1
129.1	50	0.64	4
161.8	50	0.73	7
195.6	50	0.78	13
232.2	50	0.82	18

Table 5.3 Solubility of griseofulvin in supercritical CO_2 with menthol cosolvent

P (bar)	T (^{o}C)	CO_2 Density[26] (g/ml)	Menthol amount (mol fraction x 10^3) y_3	Griseofulvin Solubility (mol fraction x 10^6) y_2	Enhance-ment Factor*
96	40	0.59	21	27	28
117	40	0.71	25	71	-
130	40	0.74	37	133	20
198	40	0.84	42	217	15
239	40	0.87	60	266	15
96	50	0.34	5.0	2	15
130	50	0.64	24	43	12.0
164	50	0.73	34	110	15

*ratio of GF solubilities in CO_2 with menthol to that without menthol
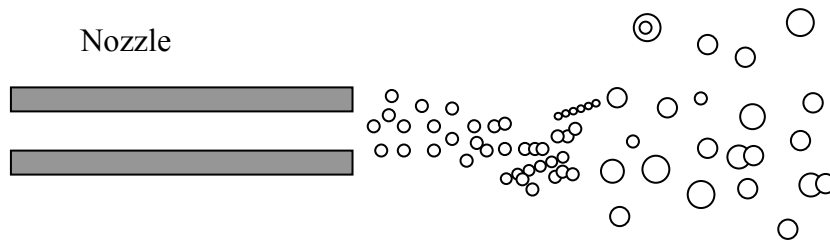
Figure 5.1 Schematic of RESS process

Figure 5.2 Schematic of RESS-SC process.

[Here ✧ are menthol particles and ○ are GF particles]
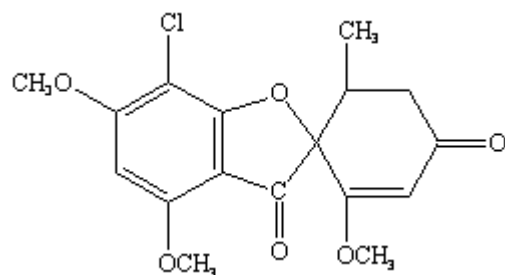
Figure 5.3 Molecular structure of griseofulvin (drug solute, mp. 220 °C)
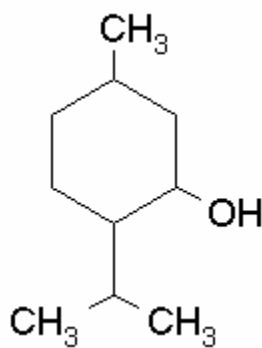
Figure 5.4 Molecular structure of menthol (solid cosolvent, mp. 32-34 °C)
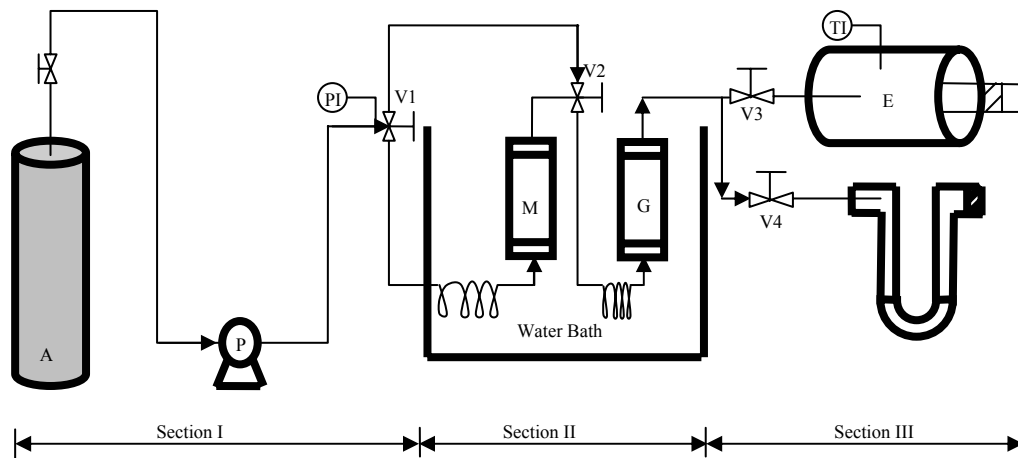
Figure 5.5 Schematic of RESS-SC apparatus
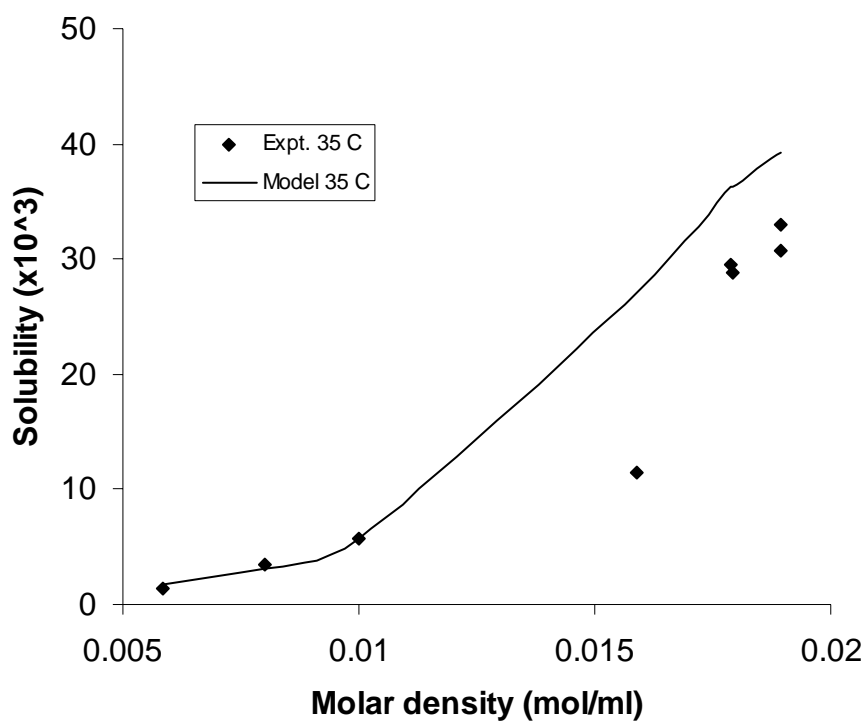
Figure 5.6 Comparision of experimental and model solubility of pure menthol in
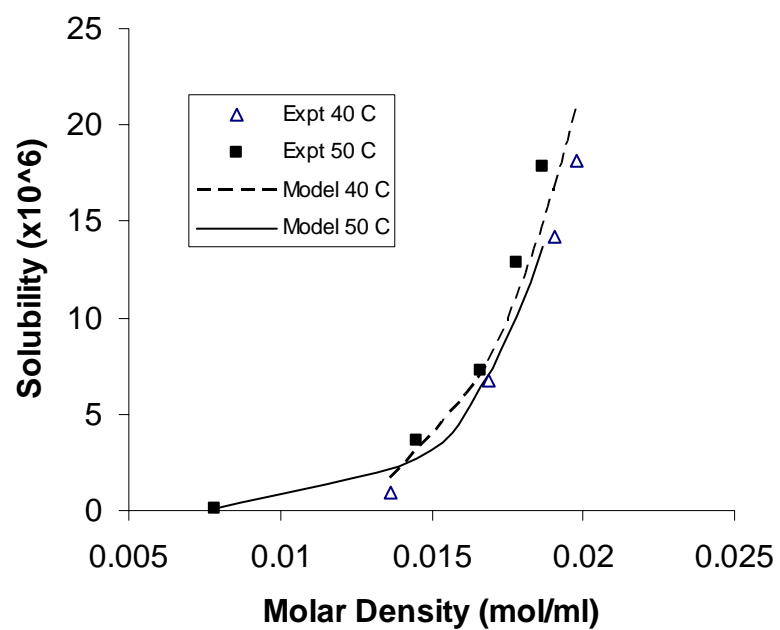
supercritical CO_2 .

**Figure 5.7 Model and experimental solubility of pure griseofulvin in supercritical**

CO_2.
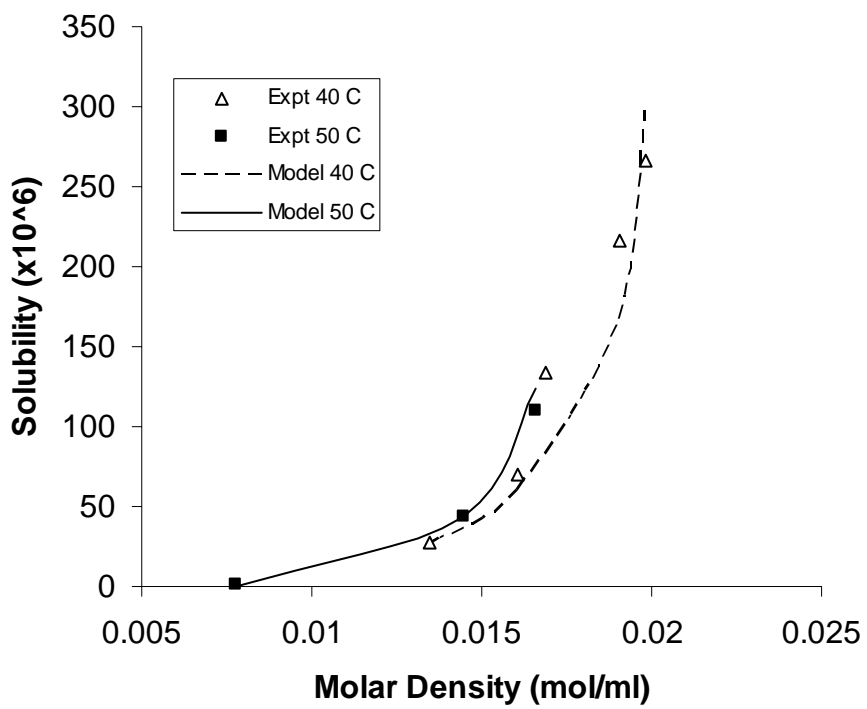
**Figure 5.8 Model and experimental solubility of griseofulvin in supercritical CO$_2$ with menthol cosolvent.**
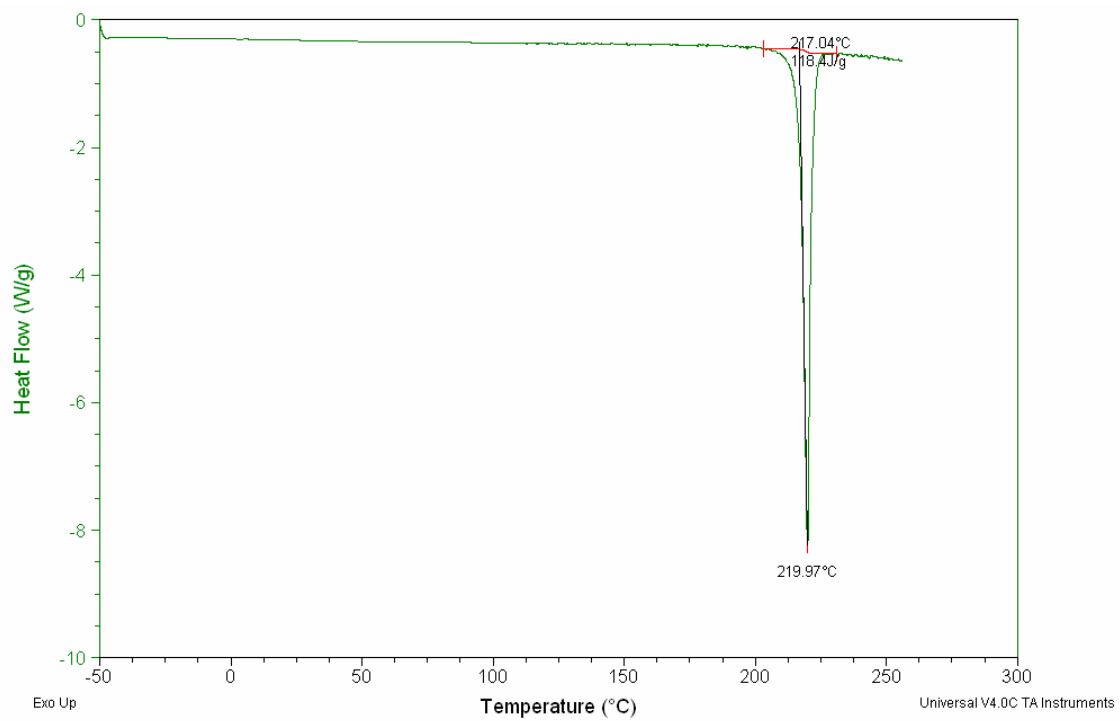
**Figure 5.9 DSC thermograph of original griseofulvin crystals**
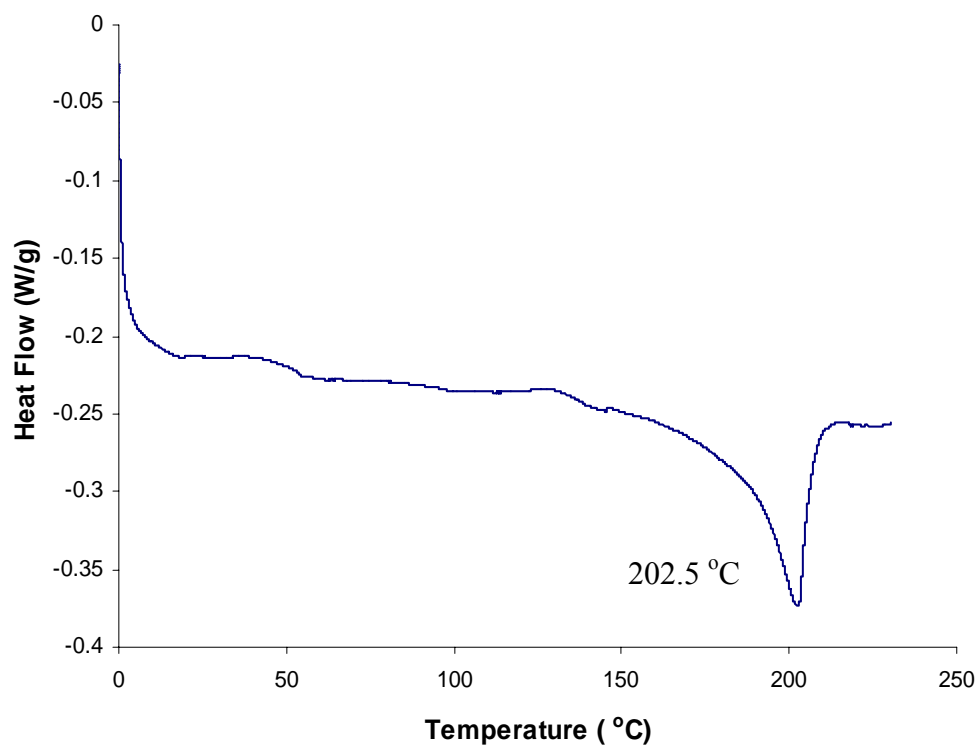
**Figure 5.10 DSC thermograph of griseofulvin particles obtained from RESS-SC process**
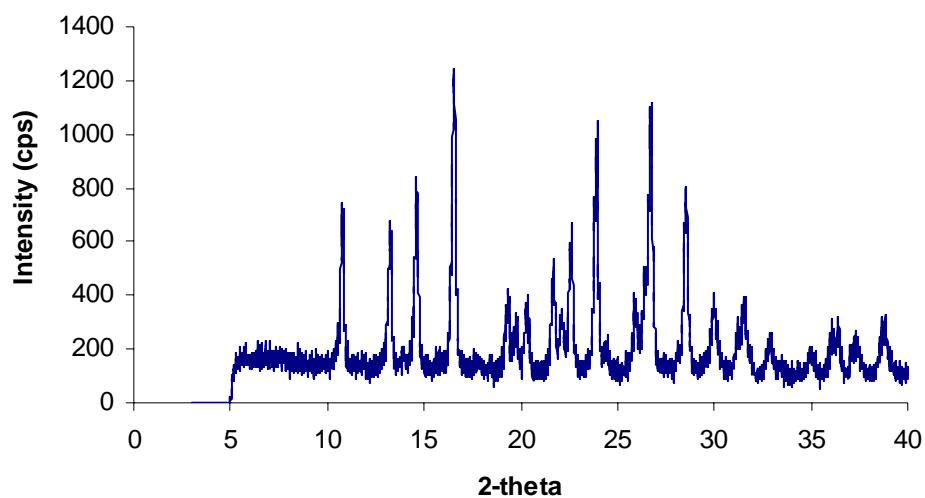
**Figure 5.11 XRD of unprocessed griseofulvin particles**
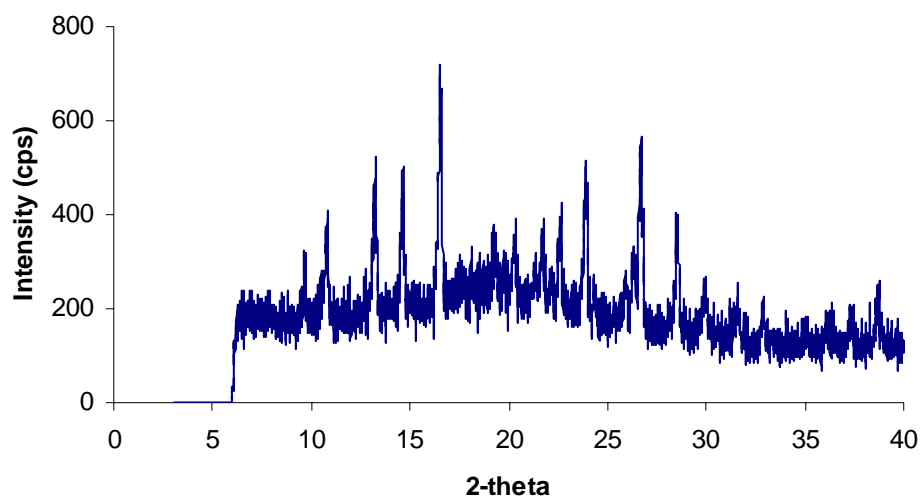
**Figure 5.12 XRD of griseofulvin particles obtained from RESS-SC process**
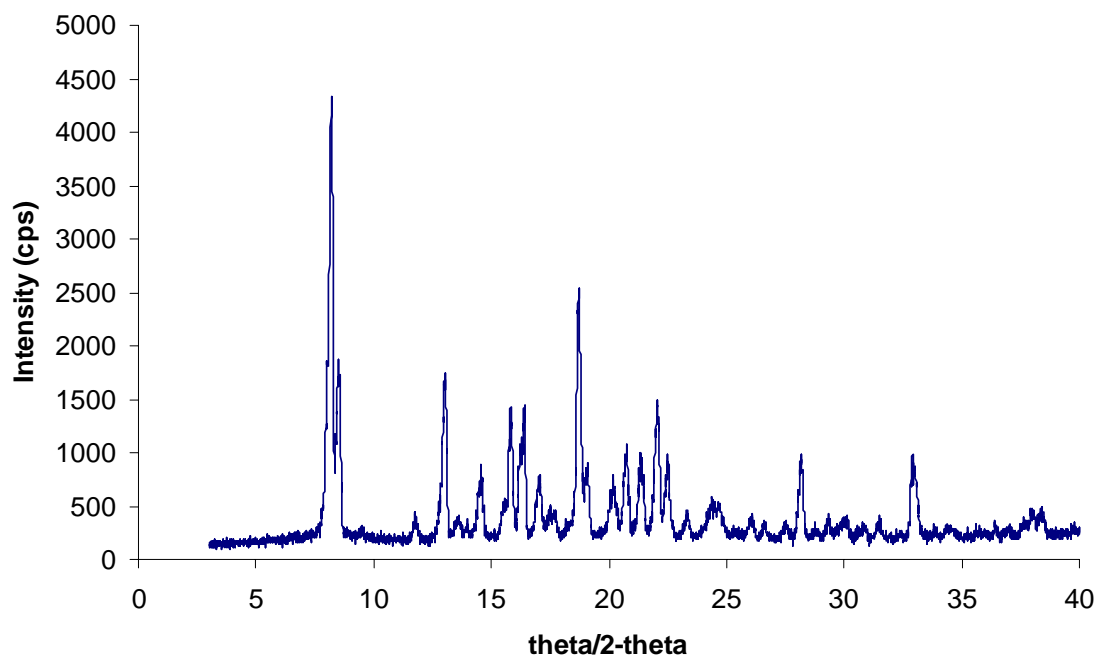
Figure 5.13 XRD of pure menthol particles

111
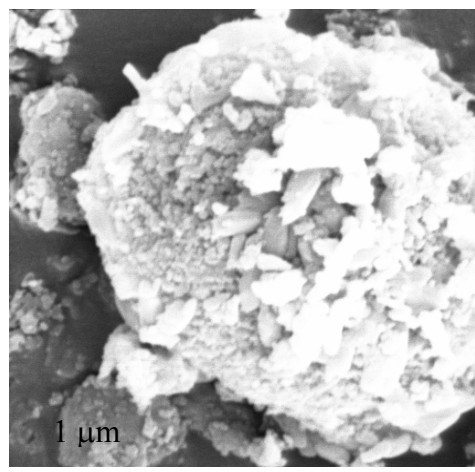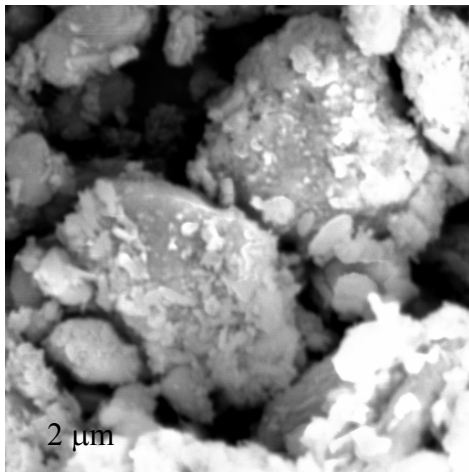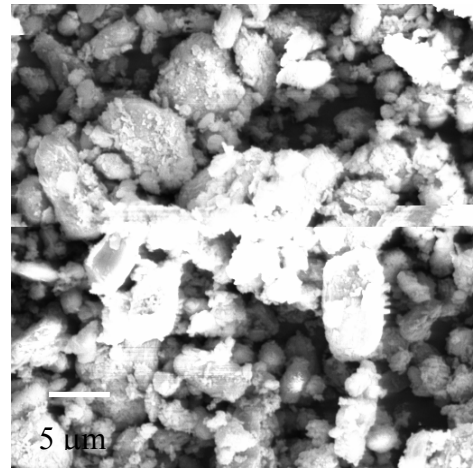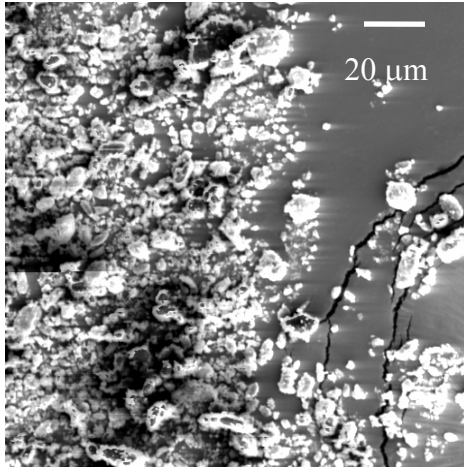
Figure 5.14 SEM of unprocessed griseofulvin particles
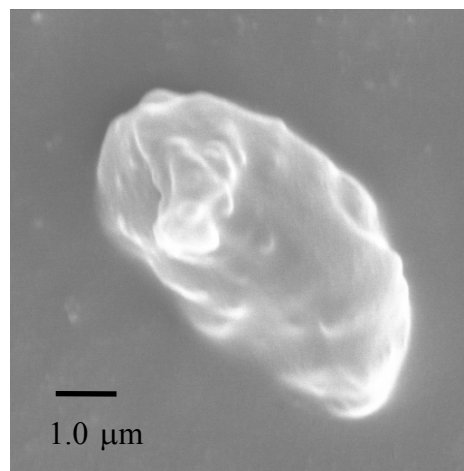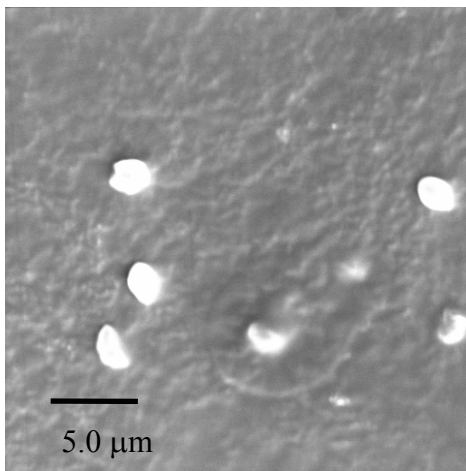
Figure 5.15 SEM of griseofulvin particles obtained from RESS process

(196 bar, 40 °C)
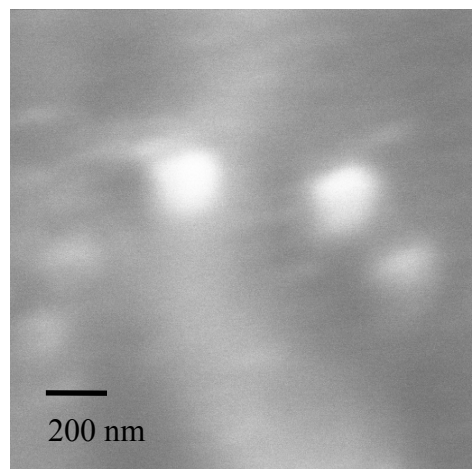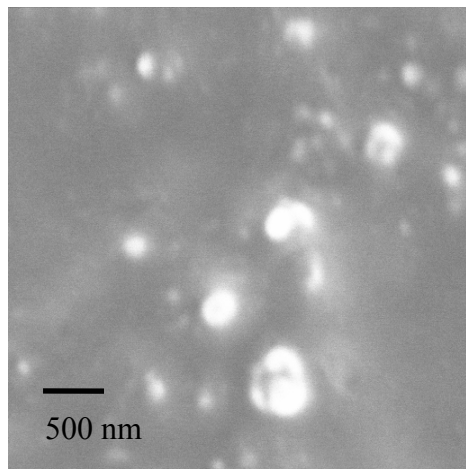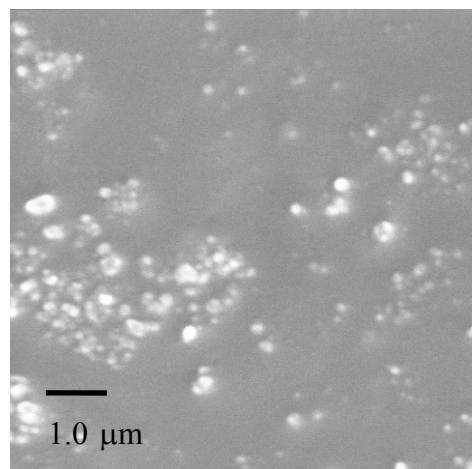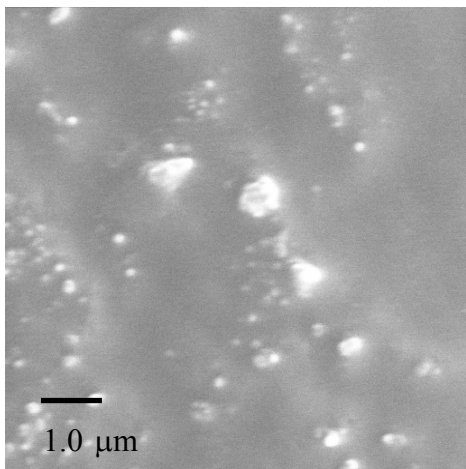
Figure 5.16 SEM of GF particles obtained from RESS-SC process (196 bar, 40 °C)
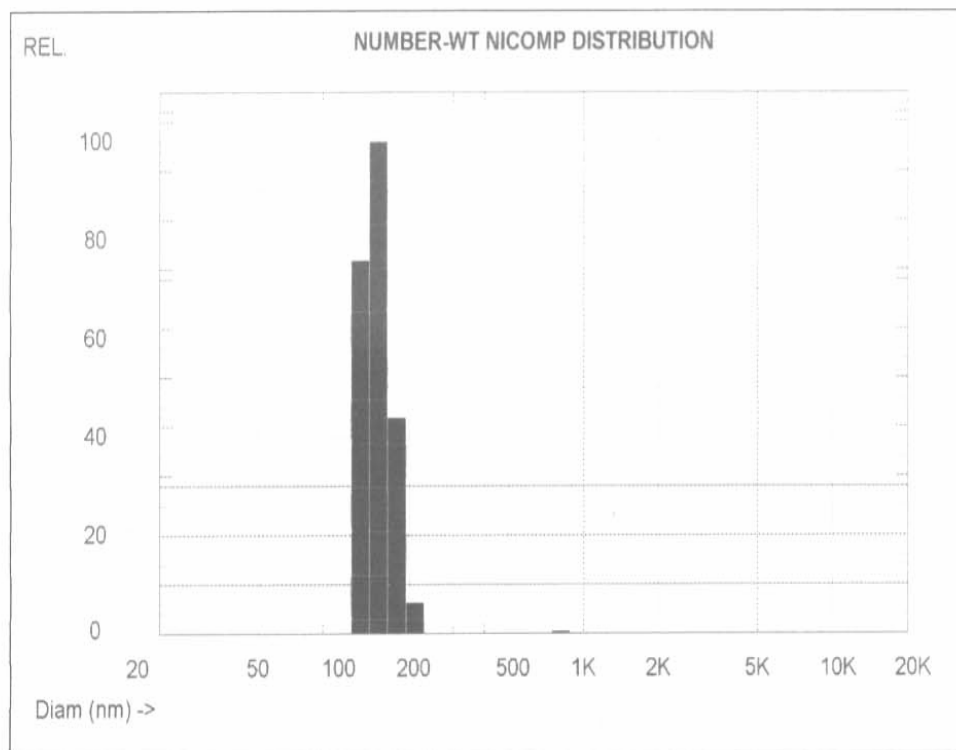
Figure 5.17 Dynamic light scattering analysis of GF nanoparticles suspended in water.

CHAPTER 6

RAPID EXPANSION OF SUPERCRITICAL SOLUTION WITH SOLID COSOLVENT

(RESS-SC) PROCESS: FORMATION OF 2-AMINOBENZOIC ACID

NANOPARTICLE

6.1 Abstract

A high solubility in supercritical fluid is desired for performing rapid expansion of supercritical solutions (RESS) to produce particles. Unfortunately, extremely low solubility of polar compounds in supercritical CO_2 makes RESS unviable for commercial applications. Liquid cosolvents can improve the solubility, but are unsuitable due to the dissolution of particles in expansion chamber. This work uses a solid cosolvent, menthol, for 2-aminobenzoic acid (ABA) solubilization in CO_2. ABA solubility is increased from 57 to 6600 μmol/mol at 236 bar and 50 $^{\circ}$C by using menthol-saturated CO_2. The other drawback of the conventional RESS process is the size of the particles obtained which is mostly in the micron range, due to growth by agglomeration in expansion chamber. In rapid expansion of supercritical solution with solid cosolvent (RESS-SC) process, solid cosolvent hinders the particle growth resulting in small nanoparticles. For example, RESS-SC process produced ~80 nm size ABA particles, which is significantly smaller than ~610 nm size particles obtained from RESS process. Menthol is easily removed

from ABA nanoparticles by sublimation (lyophilization). DSC, XRD and SEM analyses are used to characterize the particles.

6.2   Introduction

With the present focus of environmentally benign processes for particle manufacturing, CO_2-based processing is an attractive option. CO_2 is non-toxic, non-flammable, inexpensive fluid having mild critical conditions. Low critical temperature (31.1 ^{o}C) of CO_2 makes it more viable for thermally labile compounds. In addition, high diffusivity, adjustable density and low viscosity make supercritical CO_2 a suitable fluid for particle formation [1, 2]. Based on the solute solubility in the fluid, particles can be produced by two different processes: a) supercritical antisolvent process (SAS) and b) rapid expansion of supercritical solutions (RESS) process. In SAS process, one needs another organic solvent to dissolve the desired solute before expanding in supercritical fluid (SCF), whereas in RESS process the solute is dissolved in SCF and then expanded. There has been a significant development on SAS [3, 4, 5] and RESS processes [6, 7, 8, 9] for pharmaceutical particle formation. Due to its simplicity and low equipment cost, RESS process is preferable. Calculations for RESS show that the particle size at the tip of the nozzle is less than 20 nm [10], but experiments show the final particles are ~1 μm in size. This 50 fold increase of particle diameter is attributed to coagulation and agglomeration in the expansion zone.

A majority of the pharmaceuticals are organic polar compounds. CO_2, due to its low polarity, is not a good solvent for these compounds. The poor solubility leads to a limited use of supercritical CO_2 (scCO_2) as a solvent for commercial production. For

example, organic compounds such as griseofulvin, 2-aminobenzoic acid (ABA), and anthracene have solubility in the order of 10 μmole/mole CO_2 [11, 12, 13, 14]. To overcome the low solubility, researchers have used various liquid cosolvents to enhance the solubility. For example, Liu and coworkers [15] increased o- and p-aminobenzoic acid solubilities using ethanol cosolvent. The polarity of the cosolvent influences the solubility [11, 12]. Jin and coworkers [16] observed that benzoic acid has better solubility in $scCO_2$ with polar cosolvent ethanol rather than with mixed cosolvent of ethanol and ethyl acetate with intermediate polarity.

Rapid expansion of supercritical solution with solid cosolvent (RESS-SC) [13] process overcomes the drawbacks present in RESS process. The solid cosolvent not only enhances the solubility of polar compounds in supercritical CO_2, but also avoids particle growth by hindering agglomeration. In this work, both the challenges (low solubility and growth by coagulation) are addressed by utilizing a cosolvent that is solid at the nozzle exit conditions. The solid cosolvent is later removed from the solute particles by lyophilization (sublimation). This new process is termed RESS-SC. In RESS, all the nuclei or small particles of solute are surrounded by the same kind of particles as shown in Figure 6.1. But in RESS-SC process, nuclei or small particles of the solute are surrounded by excess solid co-solvent particles. This reduces the probability of solute-particle growth by coagulation. The RESS-SC concept is depicted in Figure 6.2. Though lyophilization step is shown in Figure 6.2, that is the final step after collecting all the particles and is not included in the high pressure RESS-SC apparatus.

Here, RESS-SC process concept is tested for the production of ABA (Figure 6.3) particles. From the chemical structure it is quite clear that ABA is highly polar

compound having both H-bond donor and acceptor groups which is why this compound is soluble in alcohols and ethers. ABA has a high melting point of 144-148 ^{o}C and a flash point of 150 ^{o}C. ABA is used for non-selective fluorescent labeling of glycans, an intermediate for dyes, pigments and saccharin productions. Previously, acetone and methanol have been used for solubilization of ABA in scCO$_2$ and were able to enhance the solubility by approximately 6 fold with maximum solubility of 960 μmol/mol at 35 °C and 300 bar [11].

6.2.1 Choice of Cosolvent

In RESS-SC process, the choice of cosolvent is very important. A good solid cosolvent should meet the following requirements:

   a) Non-reactive with the solute or scCO$_2$

   b) Appreciable solubility in scCO$_2$

   c) Solid at nozzle exit conditions (typically, -5 to 25 ^{o}C as observed experimentally)

   d) Sufficiently high vapor pressure for easy removal by sublimation

   e) Inexpensive

   f) Non-flammable and non-toxic

Menthol easily meets the above requirements (Figure 6.4), as it has a good solubility in supercritical CO$_2$ [13, 17] and is easy to remove from ABA by applying vacuum. The melting point of menthol is 34-36 ^{o}C, hence it is in the solid phase at the nozzle exit. Menthol is extracted from mint or can be synthesizes, and has a good commercial availability due to numerous uses in foods and pharmaceuticals.

In this work solubilities of menthol and ABA in CO_2 are measured using gravimetric and spectrometric methods, respectively. The solubility of ABA is about 57 μmol/mol-CO_2, which can be enhanced to as high as 6600 μmol/mol by adding menthol cosolvent. Solubility and its enhancement are modeled using a model developed by Mendez-Santiago and Teja [18, 19] and later modified by Thakur and Gupta [13]. Size and morphology of the particles obtained in RESS-SC process are characterized by SEM, DSC and XRD methods. The effect of pre-expansion CO_2 pressure is studied.

6.3   Experimental Section

6.3.1   Materials

CO_2 (99.99% pure) from Air Gas, menthol (99% pure) with melting point of 34-36 ^{o}C and ethanol from Fisher Scientific, 2-aminobenzoic acid (98+% pure) from Aldrich were used as received.

6.3.2   Apparatus

The schematic of RESS-SC process is shown in Figure 6.5. The apparatus is mainly divided into three parts − a pre-extraction chamber (section I), an extraction chamber (section II) and an expansion chamber (section III). In section I, P is a high pressure syringe pump for pressurizing CO_2 at desired pressure using CO_2 from cylinder A. Two vessels, M and S were used as extraction column for menthol and ABA respectively in section II. Glass wool was used on both the ends of vessels M and S to avoid any undissolved material carry over with the CO_2 flow. Both vessels containing solute and co-solvent were kept in a water bath to keep constant extraction temperature (±

0.1 ^{o}C) by temperature controller. The pressure of extraction section was measured using an online Heise ST-2H pressure transducer connected just before valve V1. Section III is either an expansion chamber of 3 liters capacity for RESS-SC experiment or a U-tube for solubility experiments and is kept at atmospheric pressure and ambient conditions. Valve V1 connects section I with section II whereas valve V3 connects section II and section III. Valve V1 and V2 are 3-way valves for CO_2 bypass connection to vessel S to perform conventional RESS experiments for comparison. Glass wool was used at the end of the expansion chamber outlet or at the end of the second leg of the U-tube to entrap the particles. Temperature in the expansion chamber was recorded to be less than 5 ^{o}C using a thermocouple.

6.3.3   Solubility Measurement

A syringe pump was filled with CO_2 from tank A and set at a desired pressure. Vessels, M and S, having 7 ml capacity each, were filled with menthol and ABA, respectively. These vessels act as extraction/solubilization columns. After filling, the extraction columns were connected as per Figure 6.5. The extraction column containing menthol was connected first in line to the ABA extraction column. Both columns were kept in a water bath at a desired temperature in such a way that the inlet was at the bottom while the outlet was at the top for proper distribution of SCF. CO_2 was fed to the first extraction column and was allowed to stabilize for 30-45 minutes by closing valve V2 at a desired pressure. After stabilizing the first column, menthol-enriched CO_2 was supplied to the second extraction column containing ABA using valve V2. Again, the entire system was equilibrated for 30-45 minutes before expanding ABA solution in the

U-tube. The U-tube was kept in an ice bath with glass wool at the other end to trap the formed particles. For pure ABA solubility experiments, only one column was used and system was equilibrated for 60-75 minutes. For measuring ABA solubility, powder obtained in the U-tube was dissolved in ethyl alcohol and was analyzed by UV spectrophotometer (Spectronic Genesys2) set at 335 nm (at this wavelength menthol is transparent, but ABA absorbs light).

6.3.4   Particle Formation by RESS-SC

For RESS-SC, the expansion chamber having 3 liters capacity was used for expansion of the menthol/ABA/CO_2 solution from a desired pressure to atmospheric pressure. A PEEK nozzle of L/D ratio of 300 was used for expansion with a fixed diameter of 100 μm. Particles were collected in the expansion chamber. Before analyzing the particles for size, crystallinity or morphology, the particles were subjected to 3-4 mbar (absolute) vacuum for 12-14 hrs to remove all the menthol by sublimation. No change in weight of particles was observed by applying vacuum for additional 3 hrs. Also, the lyophilized powder did not give any mint smell. These were the sufficient test for checking menthol presence in lyophilized ABA particles. ABA particles obtained after menthol removal were analyzed by SEM, differential scanning calorimeter (DSC) and powder X-ray diffraction (XRD) methods. RESS experiments were also conducted for ABA prior to RESS-SC experiments for comparison.

6.3.5   SEM Analysis

The particle size and morphology analysis was carried out using SEM (Zeiss, model DSM940). For analysis, the particles were attached to the carbon tape on the top

of SEM aluminum stubs and were coated with gold using a sputter coater (Electron Microscopy Sciences, model 550X) for 2 runs of 2 minutes each. In order to have a proper representation of the particles collected in the expansion chamber SEM micrographs of different regions were obtained. In menthol/ABA system wherein menthol was the co-solvent, processed powder was first kept in a high vacuum of 3-4 mbar (absolute) to remove all the menthol from the particle mixture. All the SEM analyses were done after 60-70 hrs of experiments at an accelerating voltage of 10 kv.

6.3.6 DSC Analysis

Thermal analysis was carried out using DSC (TA instruments, model DSC Q100) for processed and unprocessed ABA particles. Analysis was performed for 3 mg ABA sample at a temperature heating rate of 5 ^{o}C/min and a temperature range of 40 ^{o}C to 148 ^{o}C.

6.3.7 X-Ray Diffraction

ABA particle crystallinity was analyzed using Rigaku X-ray diffractometer which was equipped with Cu Kα_1 radiation source and a Miniflex gonoiometer. The powder was filled to same depth inside the sample holder and scanning rate was same for all XRD analysis.

6.4 Results and Discussions

6.4.1 Solubility Enhancement

Table 6.1 summarizes the solubility results for pure ABA in scCO$_2$. Pure menthol solubility is given elsewhere [13]. The solubility of pure ABA increases with pressure as

shown in Figure 6.6. The solubility data is obtained at temperatures of 40 and 50 $^{\circ}$C in the pressure range of 96 to 236 bar. The crossover behavior is also observed at 160-170 bar pressure for ABA (Figure 6). Figure 6.7 shows the ABA solubility variation with molar density.

The effect of the cosolvent menthol on the ABA solubility is shown in Table 6.2. ABA solubility was enhanced by 118 fold giving solubility as high as 6600 μmol/mol which can be attributed to a high polarity of supercritical CO_2-menthol mixture. Polar solvents including acetone and methanol have been used earlier for ABA solubility enhancement [11, 12]. Figure 6.8 shows a variation of ABA solubility (mole fraction) with CO_2 molar density at two different temperatures using menthol as cosolvent.

6.4.2 Modeling

For subcritical and supercritical systems, a semi-empirical solubility correlation method has been proposed [20] but there is great difficulty in finding saturation pressure and interaction parameters for high molecular weight solutes. To overcome this problem Mendez-Santiago and Teja [18, 19] proposed a new model where solubility is expressed as a function of temperature and CO_2 molar density (ρ_1):

$$T \ln(y_2 P) = A^{'} + B^{'} \rho_1 + C^{'} T \qquad (1)$$

The three parameters A', B', C' are calculated by fitting the experimental data. These three parameters for ABA are -3220.21, 89358.88 and 0.0, respectively. Here, the units of temperature, pressure and density are K, bar and mols/ml, respectively. The correlated solubilities at different temperature and pressure are compared with the experimental values in Figure 6.7.

124

ABA solubility with cosolvent is modeled using a modified model as explained earlier [13]. Two new parameters are included to account for cosolvent concentration.

$$T \ln(P y_2) = A' + B' \rho_1 + (D' \rho_1 + E') y_3 \qquad (2)$$

where y_2 is ABA mole fraction and y_3 is menthol mole fraction. D' and E' are two parameters due to the cosolvent effect whereas A' and B' are pure ABA solubility parameters. These two additional parameters are obtained by fitting the data points. For ABA-menthol-CO_2 system, D' and E' are -6474895 and 144910, respectively. Figure 6.8 shows a comparison between solubilities calculated from model and experiment at 40 and 50 $^{\circ}$C.

6.4.3 Particle Size and Characterization

After achieving considerable solubility enhancement with the cosolvent, the next aim was to form ABA nanoparticles. Unprocessed ABA particles have an average size of 70 μm and are irregular in shape (Figure 6.9). But after RESS processing particles in the size range of 610 nm (number average) were obtained (Figure 6.10). Figure 6.11 shows the average particle size of 100 nm as obtained in the RESS-SC process. Also the particles are spherical from RESS-SC process. Both RESS and RESS-SC were operated at same conditions of 196 bar and 50 $^{\circ}$C with 100 μm diameter nozzle having L/D ratio of 300. It is quite evident from Figures 6.12 and 6.13 that there is not only a change in the particle morphology after processing with solid cosolvent but also a sharp decrease in particle size.

The particles obtained by RESS process are agglomerated as evident from SEM micrographs (Figure 6.10). This agglomeration of particles occurred in expansion zone

as the particles have ample time to collide with each other and coagulate to form bigger particles. Turk and co-workers [21] also reported that the particles grow in expansion chamber and the conditions inside expansion chamber are the key factor for controlling particle size. It is clear from Figure 6.10-b that the particles are fused with each other though the expansion chamber temperature was between 5-10 $^{\circ}$C. RESS-SC processed particles have less tendency to coagulate with each other as every particle is surrounded by solid cosolvent which was later removed by lyophilization (Figure 6.11-a and -b). These results satisfy the scheme proposed earlier for RESS-SC process (Figure 6.2).

Various parameters, nozzle length, spraying distance to pre-expansion pressure, have been changed earlier in RESS to observe their effect on particle size [8]. In this work pre-expansion CO_2 pressure was varied (163, 196 and 236 bar) at constant extraction temperature of 50 $^{\circ}$C. A nozzle of diameter 100 μm was used with L/D ratio of 300 in all these experiments. Figures 6.12 and 6.13 show the particles obtained at 163 and 236 bar pressures. The number average particle diameter at 163 bar is 110 nm whereas at 236 bar average size decreases to 80 nm. So, by changing pressure from 163 to 236 bar particle size is reduced from 110 to 80 nm. Since these changes are not more significant then the 20% standard deviation it is difficult to conclude about the change of particle size in 160-236 bar pressure range. Charoenchaitrakool and co-workers [8] also observed similar trend for ibuprofen particles in RESS process with CO_2 along with some other researchers [6, 22].

The obtained particles were characterized by DSC and XRD analyses. The melting point of unprocessed ABA is 147.2 $^{\circ}$C whereas RESS-SC processed ABA has a melting point of 146 $^{\circ}$C. Figure 6.14 shows the heat flow with temperature plot of

unprocessed and RESS-SC processed ABA particles. The decrease of heat flow for processed ABA is attributed to the lowering of the crystallinity after RESS-SC processing.

This decrease in crystallinity is further investigated by X-ray diffraction method. Figure 6.15 shows the XRD results for processed and unprocessed ABA particles. Though the peaks are at the same angles, the intensity of the peaks are lower for RESS-SC processed particles (Figure 6.15 a and b). Lower intensity is attributed to the lowering of crystallinity of the particles. XRD of pure menthol particles are shown elsewhere [13].

6.5   Conclusion

The limited solubility of solutes in CO_2 and final micron size particle are the two major challenges of RESS process. New RESS-SC process is not only able to enhance the solubility by using solid cosolvent but also reduces the particles size to nanometer range. This concept has been demonstrated in this paper by using 2-aminobenzoic acid. By using menthol as solid cosolvent, ABA solubility is enhanced by 118 fold to 0.6 mole% and average particle size was reduced from 610 nm to 80 nm.   The characterization of particles by XRD and DSC shows a decrease in the crystallinity after RESS-SC processing. The experimental solubilities are fit to a model and parameters are estimated.

6.6   Acknowledgement

REFERENCES

1. Debenedetti, Pablo G., Supercritical Fluids as Particle Formation Media. Supercritical fluids, 1994, 719-729.

2. Tom, Jean W. and Debenedetti, Pablo G., Particle Fomration with Supercritical Fluids-A Review. J. Aerosol Sci., 1991, 22(5), 555-584.

3. Reverchon, E.; Della Porta, G. and Pallado, P., Supercritical Antisolvent precipitation of salbutamol microparticles. Powder Technology, 2001, 114, 17-22.

4. Gupta, R.B.; Chattopadhyay, P. Method of forming nanoparticles and microparticles of controllable size using supercritical fluids with enhanced mass transfer, US Patent 6,620,351; September 16, 2003.

5. Luna-Barcenas, G.; Kanakia, S.K.; Sanchez, I.C. and Johnston, K.P., Semicrystalline microfibrils and hollow fibres by precipitation with a compressed-fluid antisolvent. Polymer, 1995, 36(16), 3173-3182.

6. Reverchon, E.; Della Porta, G.; Taddeo, R.; Pallado, P.; Stassi, A., Solubility and Micronization of Grieseofulvin in supercritical CHF_3. Ind. Eng. Chem. Res., 1995, 34, 4087-4091.

7. Matsuyama, K.; Mishima, K.; Hayashi, K.I.; Ishikawa, H.; Matsuyama, H.; Harada, T., Formation of microcapsules of medicines by the Rapid expansion of a supercritical solution with a Nonsolvent. J. of Applied Polymer Sci., 2003, 89, 742-752.

8. Charoenchaitrakool, M.; Dehghani, F.; Foster, N. R.; Chan, H.K., Micronization by Rapid Expansion of Supercritical Solutions to Enhance the Dissolution Rates

of Poorly Water-Soluble Pharmaceuticals. Ind. Eng. Chem. Res. 2000, 39, 4794, 4802.

9. Tom, J. W.; Debenedetti, P.G.; Jerome, R., Precipitation of Poly(L-lactic acid) and Composite Poly(L-lactic acid)-Pyrene Particles by Rapid Expansion of Supercritical Solutions. The Journal of Supercritical Fluids, 1994, 7, 9-29.

10. Helfgen, B.; Turk, M.; Schaber, K., Hydrodynamic and aerosol modeling of the rapid expansion of supercritical solutions (RESS-process).   Journal of Supercritical Fluids, 2003, 26, 225-242.

11. Dobbs, J.M.; Wong, J.M.; Lahiere, R.J.; Johnston, K.P., Modification of Supercritical Fluid Phase Behavior using Polar Cosolvents. Ind. Eng. Chem. Res., 1987, 26(1), 56-65.

12. Dobbs, J.M. and Johnston, K.P., Selectivities in Pure and Mixed Supercritical Fluid Solvents. Ind. Eng. Chem. Res., 1987, 26(7), 1476-1482.

13. Thakur, Ranjit and Gupta, Ram B., Rapid Expansion of Supercritical Solution with Solid Cosolvent (RESS-SC) process for Nanoparticle formation. Submitted to Ind. Eng. Chem. Res., 2005.

14. Bartle, K.D.; Clifford, A.A.; Jafar, S.A.; Shilstone, G.F., Solubilities of Solids and Liquids of Low Volatility in Supercritical Carbon Dioxide. Phys. Chem. Ref. Data, 1991, 20(4), 713-756.

15. Liu, Z.; Yang, G.; Ge, L.; Han, B., Solubility of 0- and p-Aminobenzoic Acid in Ethanol + Carbon Dioxide at 308.15 K to 318.15 K and 15 bar to 85 bar. J. Chem. Eng. Data, 2000, 45, 1179-1181.

16. Jin. J.; Zhong, C.; Zhang, Z.; Li, Y., Solubilities of benzoic acid in supercritical CO_2 with mixed cosolvent. Fluid Phase Equilibria, 2004, 226, 9-13.

17. Sovova, H. and Jez, J., Solubility of Menthol in Supercritical Carbon Dioxide. J. Chem. Eng. Data, 1994, 39, 840-841.

18. Mendez-Santiago, J., Teja, Amyn S., The solubility of solids in supercritical fluids. Fluid Phase Equilibria, 1999. 158-160: p. 501-510.

19. Mendez-Santiago, J., Teja, Amyn S., Solubility of solids in Supercritical Fluids: Consistency of Data and a New Model for Cosolvent Systems. Ind. Eng. Chem. Res., 2000. 39: p. 4767-4771.

20. Zlger, D.H., Eckert, Chrales A., Correlation and Prediction of Solid-Supercritical Fluid Phase Equilibria. Ind. Eng. Chem. Res., 1983. 22: p. 582-588.

21. Turk, M.; Hils, P.; Helfgen, B.; Schaber, K.; Martin, H.-J.; Wahl, M.A., Micronization of pharmaceutical substances by the Rapid Expansion of Supercritical Solutions (RESS): a promising method to improve bioavailability of poorly soluble pharmaceutical agents. J. Supercritical Fluids, 2002, 22, 75-84.

22. Domingo, C.; Berends, E.; van Rosmalen, G.M., Precipitation of Ultrafine Organic Crystals from the Rapid Expansion of Supercritical Solutions over a capillary and a Frit Nozzle. J. Supercritical Fluids, 1997, 10, 39-55.

Table 6.1 Solubility of 2-aminobenzoic acid in pure CO_2

Pressure (bar)	CO_2 Density (mol/ml)	Temperature (^oC)	Solubility (mol fraction $x10^6$)	Standard Deviation ($x10^6$)
96	0.01365	40	13	n/a
129	0.01694	40	25	1.3
163	0.01822	40	32	2
196	0.01906	40	38	3
96	0.00790	50	5	3
130	0.01459	50	24	n/a
163	0.01665	50	31	5
197	0.01779	50	42	6
237	0.01983	50	56	8

Table 6.2 Solubility of 2-aminobenzoic acid in CO_2 with menthol cosolvent

Pressure (bar)	Temperature (^oC)	CO_2 Density (mol/ml)	Solubility (mol fraction x 10^6)	Standard Deviation (x 10^6)	Enhancement Factor[*]
129	40	0.01694	440	90	18
163	40	0.01822	1051	45	33
196	40	0.01907	3131	179	82
96	50	0.00800	19	7	4
163	50	0.01665	1363	28	44
197	50	0.01781	3416	74	82
237	50	0.01876	6641	234	119

*ABA solubility in CO_2 with menthol/ ABA solubility in pure CO_2
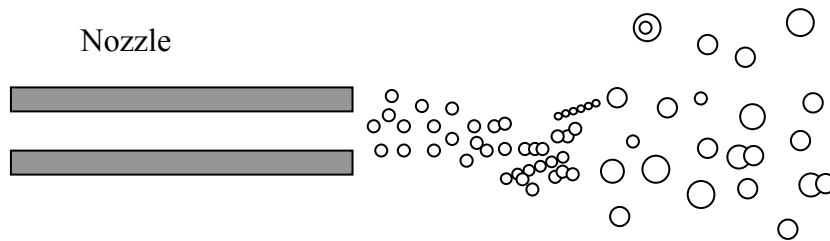
Figure 6.1 Schematic of RESS process
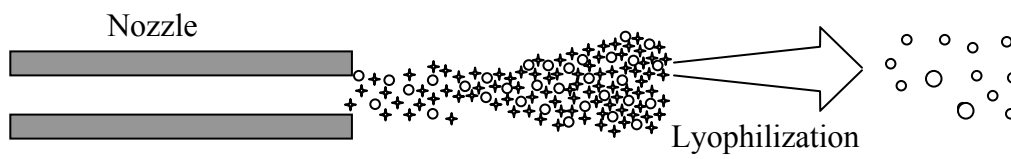
Figure 6.2 Schematic of RESS-SC process.

[Here ✧ are menthol particles and ○ are ABA particles]

134
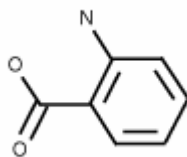
Figure 6.3 Chemical structure of 2-aminobenzoic acid (ABA)
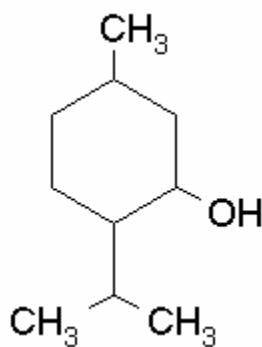
**Figure 6.4 Molecular structure of menthol (cosolvent)**
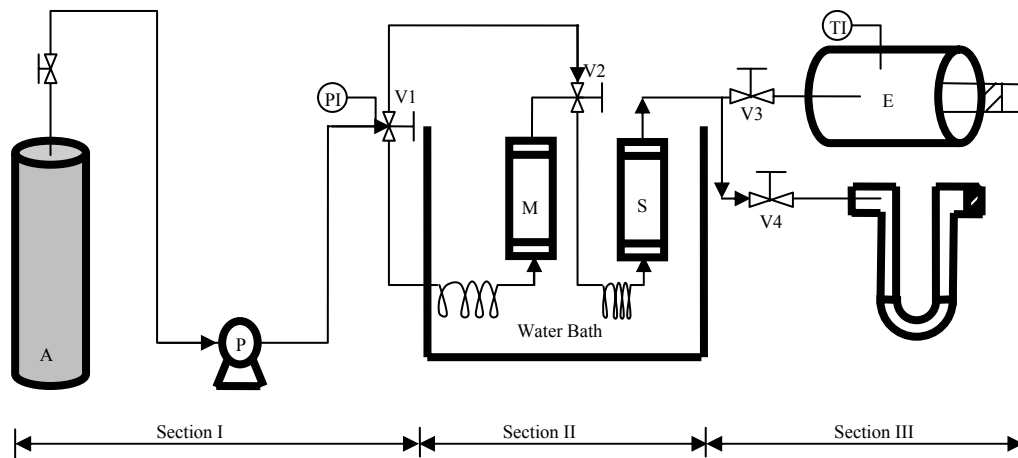
Figure 6.5 Schematic of RESS-SC apparatus
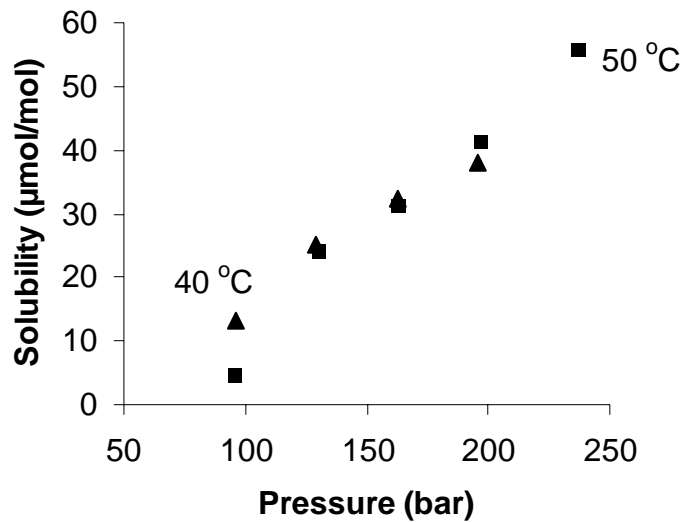
**Figure 6.6 Solubility of pure 2-aminobenzoic acid in supercritical CO$_2$ versus**

pressure
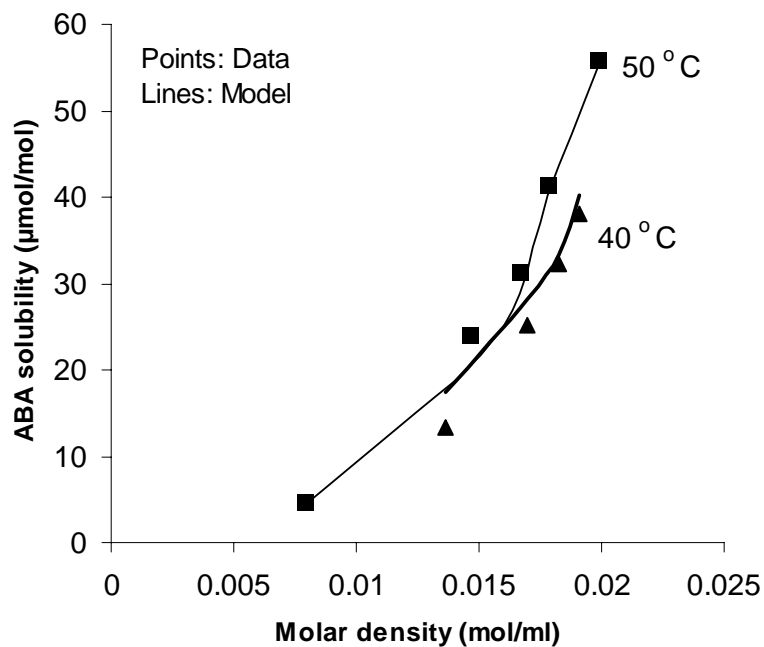
**Figure 6.7 2-aminobenzoic acid solubility variation with CO$_2$ molar density.**
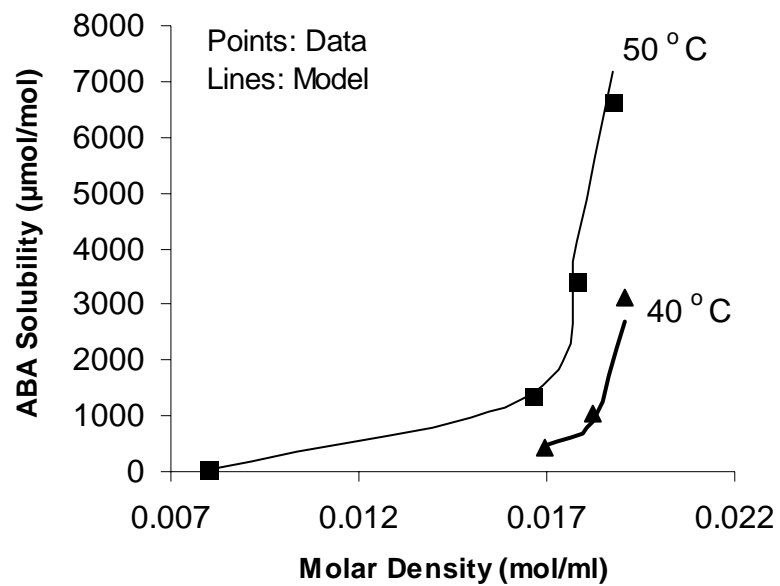
**Figure 6.8 Solubility of 2-aminobenzoic acid in sc CO$_2$ using menthol cosolvent**
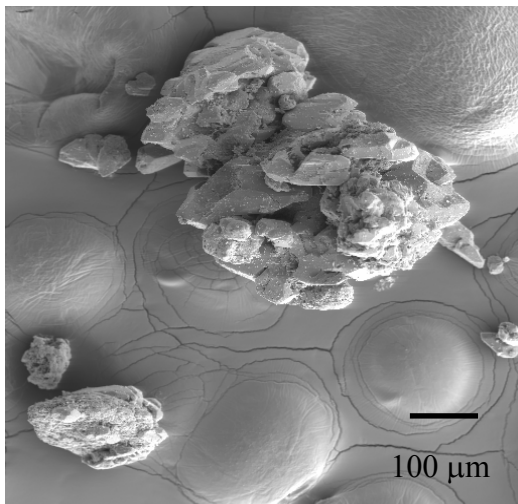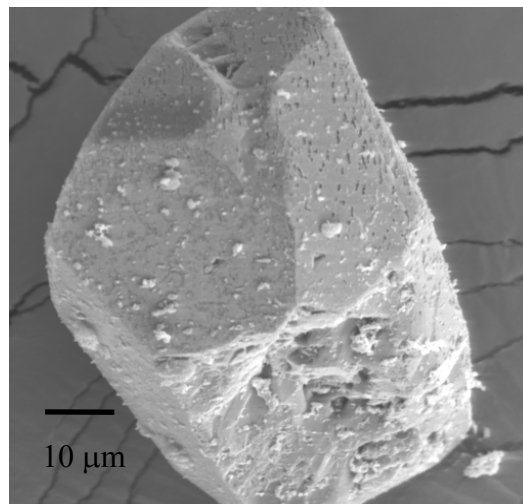
(a)   (b)

**Figure 6.9 Unprocessed 2-aminobenzoic acid particles**
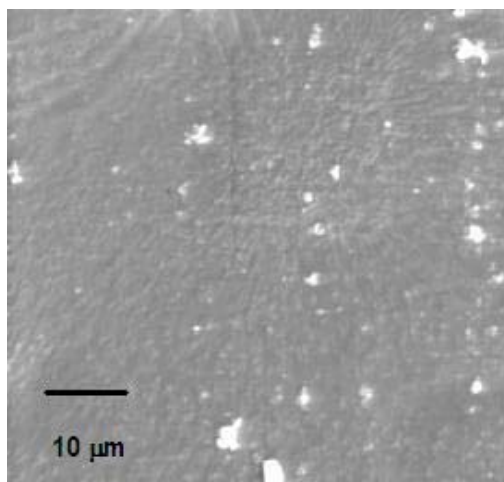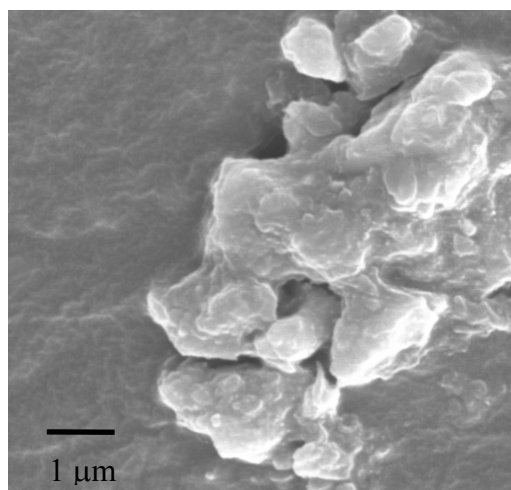
(a)   (b)

Figure 6.10 2-Aminobenzoic particles obtained from RESS at 196 bar and 50 ^{o}C
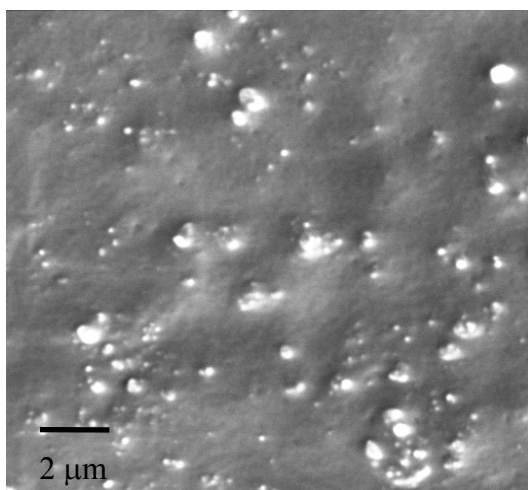
with 100 μm nozzle
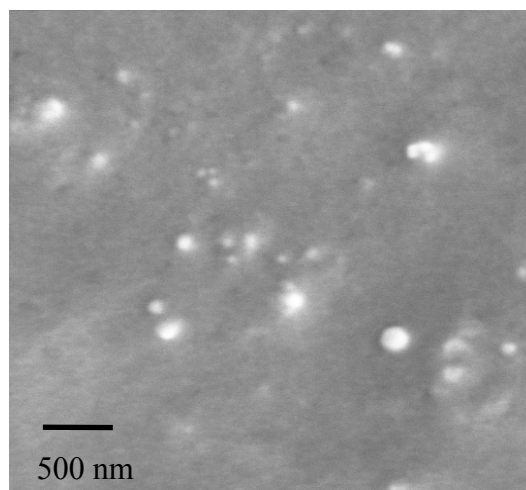
(a)   (b)

Figure 6.11 2-Aminobenzoic particles obtained from RESS-SC at 196 bar and 50 ^{o}C with 100 μm nozzle
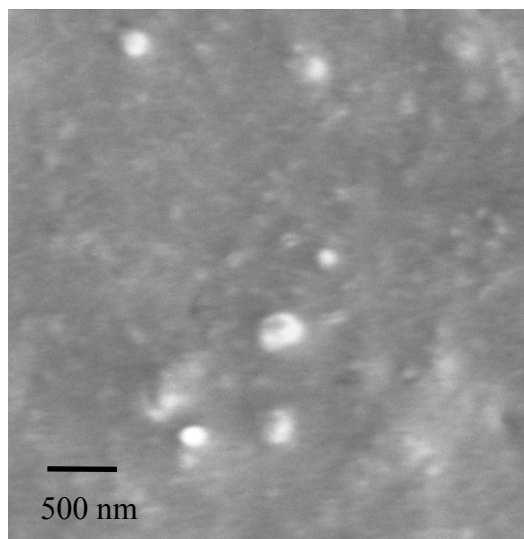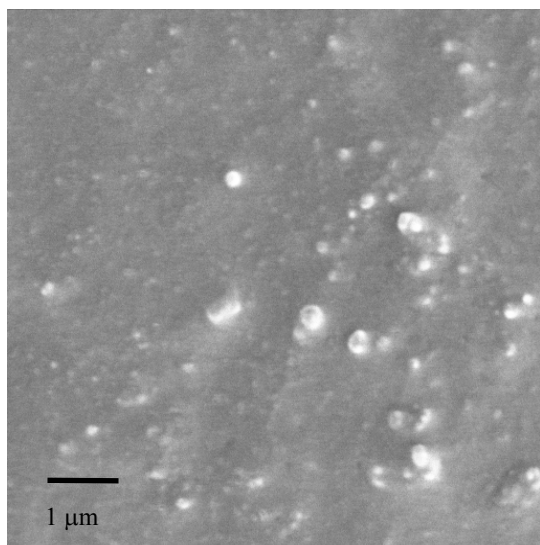

**Figure 6.12 2-Aminobenzoic particles obtained from RESS-SC at 163 bar and 50 ^{o}C.**
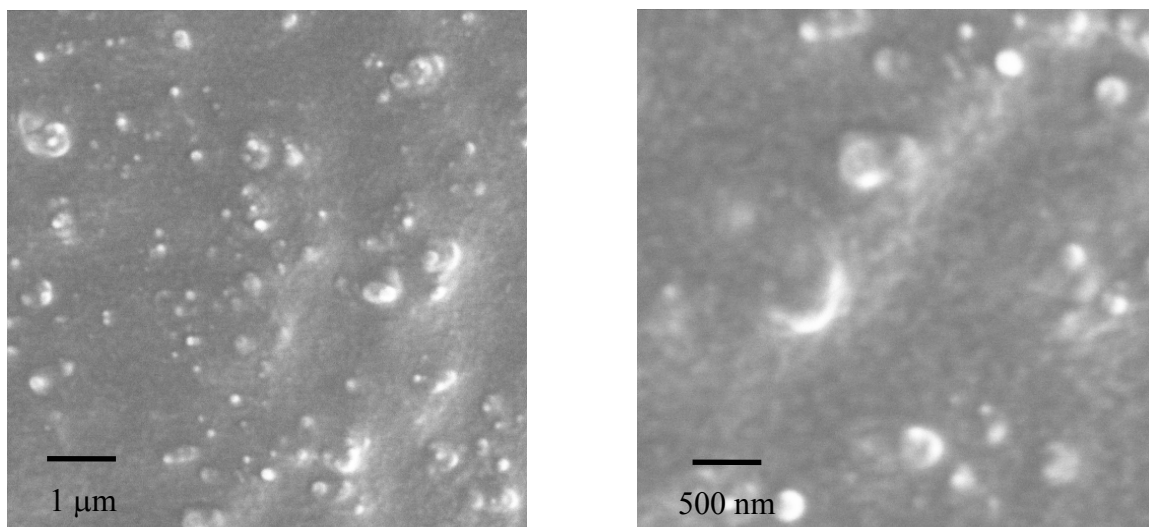
Figure 6.13 2-Aminobenzoic particles obtained from RESS-SC at 236 bar and 50 ^{o}C.
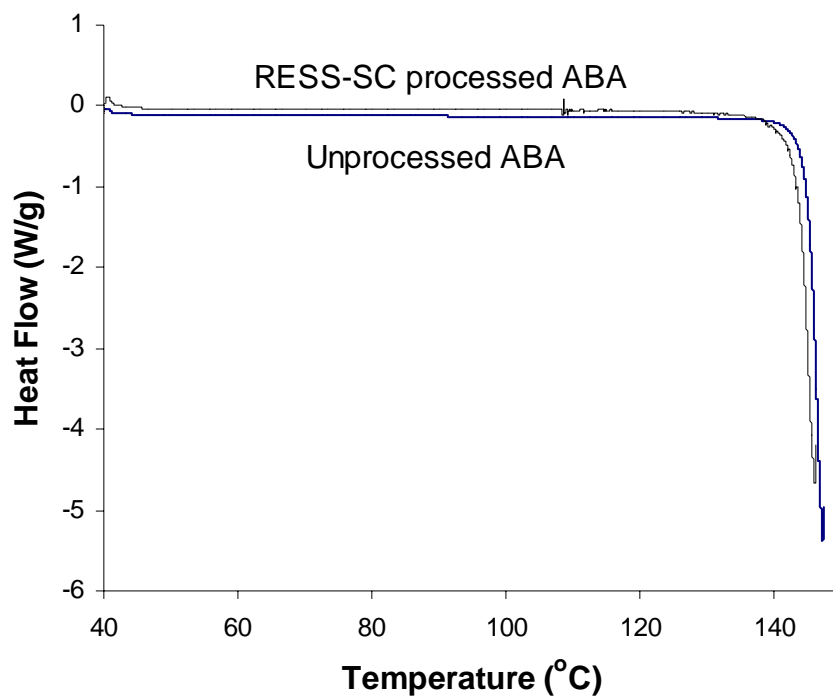

Figure 6.14 DSC analysis of unprocessed and RESS-SC processed 2-aminobenzoic

acid particles

(a)

142
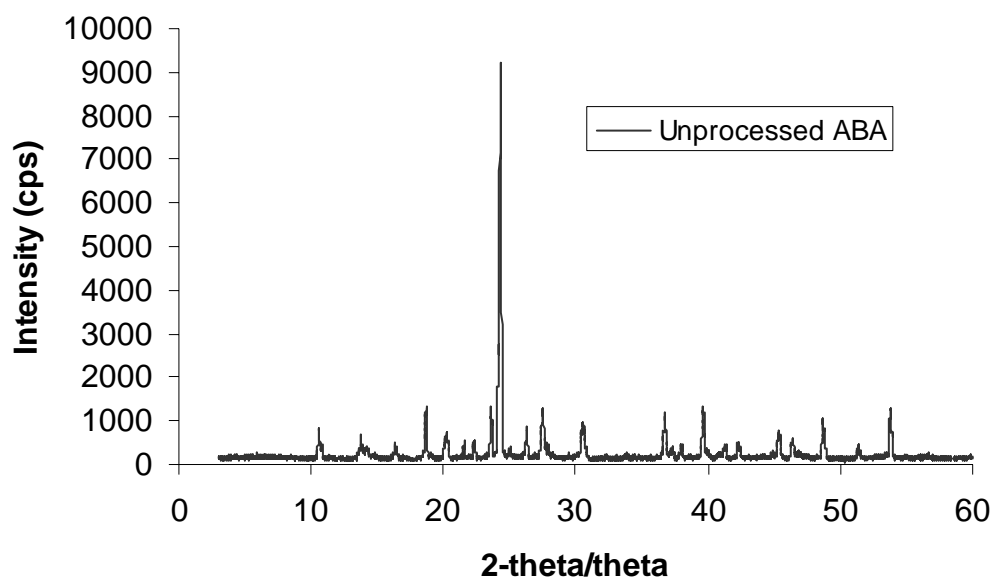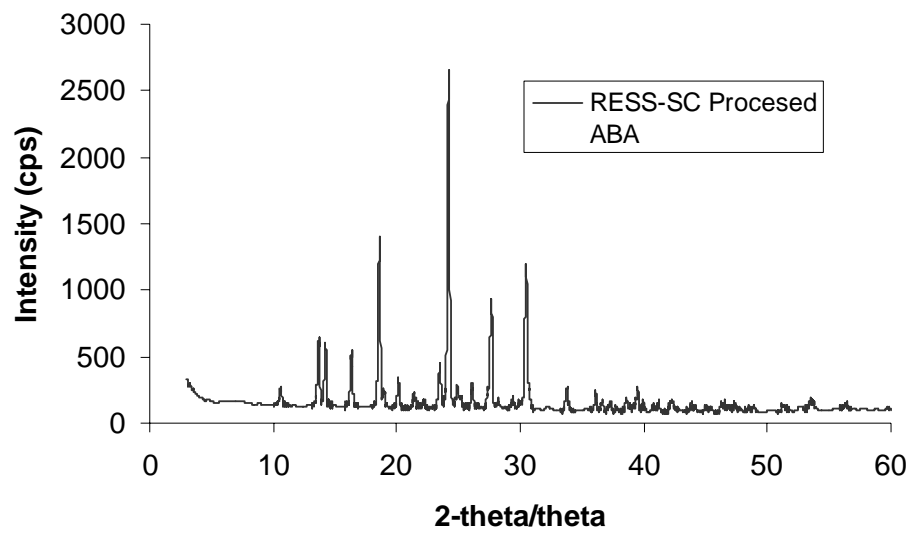
(b)

Figure 6.15 X-ray diffraction analyses of (a) unprocessed and (b) RESS-SC

processed 2-aminobenzoic acid (ABA)

CHAPTER 7

FORMATION OF PHENYTOIN NANOPARTICLES USING RAPID EXPANSION OF

SUPERCRITICAL SOLUTION WITH SOLID COSOLVENT (RESS-SC) PROCESS

7.1   Abstract

Pure drug nanoparticles are of significant importance in drug delivery. Rapid expansion of supercritical solution (RESS) process can produce pure and high quality particles. However, due to extremely low solubility of polar drugs in supercritical CO_2 (sc CO_2), RESS has limited commercial applicability. To overcome this major limitation, a modified process RESS-SC is proposed which uses a solid cosolvent. Here the new process is tested for phenytoin using menthol solid cosolvent. Phenytoin solubility in pure sc CO_2 is only 3 µmol/mol but when menthol solid cosolvent is used the solubility is enhanced to 1302 µmol/mol, at 196 bar and 45 ^{o}C. This four hundred fold increase in the solubility can be attributed to the increase in the polarity of sc CO_2 due to polar menthol.

Particle agglomeration in expansion zone is another major issue with conventional RESS process. In proposed RESS-SC process solid cosolvent hinders the particle growth resulting in the formation of small nanoparticles. For example, the average particle size of phenytoin in conventional RESS process is 200 nm whereas, with RESS-SC process, the average particle size is 120 nm at 96 bar and 45 ^{o}C. Similarly at 196 bar and 45 ^{o}C,

105 nm average particles were obatined by RESS and 75 nm average particles were obtained in RESS-SC process. The particles obtained were characterized by FTIR, XRD DLS, and DSC analyses. Phenytoin nanoparticle production rate in RESS-SC is about 400 fold more in comparision to that in RESS process.

7.2   Introduction

The dissolution of poorly water soluble drugs is a major concern for pharmaceutical industry, considering the fact that many new drugs toxicity limit is near dosage requirement. The particle size reduction is one of the methods which can achieve desired bioavailability of poorly soluble drugs. Also, several researchers have reported dissolution rate dependence on the particle size [1, 2]. Mechanical methods have been used for particle size reduction but broad size distribution and difficulty in commuting are some of the problems associated with these methods. Also, heat sensitive materials can degrade by milling. To overcome these disadvantages, new methods have been devised including supercritical fluid (SCF) based particle size reduction method [3]. SCF based processes can be divided into two major processes: rapid expansion of supercritical solution (RESS) for CO_2-soluble drugs and supercritical antisolvent (SAS) process for CO_2-insoluble drugs.

In RESS process, the desired solute is solubilized in SCF and then resulting solution is expanded through a nozzle to cause a sudden decrease in the solubility and hence, particle formation [4, 5]. Homogenous nucleation in RESS is caused by supersaturation and several mathematical models have been presented to explain this process theoretically [6, 7, 8]. In SAS process, the desired solute is dissolved in an

organic solvent and then injected inside SCF media causing small particle formation by volumetric expansion and removal of solvent [9, 10, 11, 12]. RESS is simpler and less expensive when compared to SAS process. But the solubility of most polar drugs is almost negligible in supercritical CO_2 (sc CO_2) which makes RESS process unviable for practical application. Due to this reason, other less benign SCFs been used to produce polar particles using RESS method [13]. Also, organic compounds tend to agglomerate due to their adhesive nature, resulting in agglomeration which generally produces bigger particles. Both challenges are addressed in this work by improving the drug solubility in sc CO_2 and also producing sub 100 nm particles by avoiding particle growth. Here the new concept is tested for the phenytoin.

Phenytoin (5, 5-diphenyl-2, 4-imidazolidinedione, Figure 7.1a) is widely used as an anticonvulsant and antiepileptic drug. As phenytoin is a blocker for inactivated sodium channels, it is also used as antiarrhythmic drug for treatment of heart rhythm disturbances [14]. The side effects of phenytoin include nausea, insomnia and other central nervous system disorders [15, 16]. Phenytoin is a highly crystalline compound having high melting point of 295-298 ^{o}C due to strong intermolecular hydrogen bonding. Phenytoin solubility in water is as low as 80 μmol/L [17]. For better bioavailability, low melting prodrugs have been proposed which later on convert to phenytoin [17]. Also, some excipients have been added to phenytoin to obtain better dissolution [18]. β-cyclodextrin-phenytoin complexation has been used for enhancing phenytoin bioavailability [19]. Most common route of phenytoin exposure is oral, though parenteral mode is used intravenously in status epilepticus.

Due to the high polarity it is difficult to solubilize phenytoin in sc CO_2. At 196 bar and 45 °C, phenytoin solubility in sc CO_2 is only 3 µmol/mol. With this low solubility RESS is not economically viable for industrial production. Earlier, micron sized phenytoin particles were formed by supercritical assisted atomization process after dissolving in methyl alcohol [20]. To overcome the limitation of low solubility, this work proposes addition of solid cosolvent to enhance the phenytoin solubility in sc CO_2. Though the mathematical model predicts particles of size less than ~ 20 nm at the tip of the nozzle, RESS particles obtained are in the range of 200-1000 nm [8]. In conventional RESS process, each particle is surrounded by same kind of particles in the expansion zone which results in larger particles due to coagulation (Figure 7.2). So far various solvents and techniques have been used for phenytoin crystals modifications [21]. A new method, rapid expansion of supercritical solution with solid cosolvent (RESS-SC), has been proposed which overcomes this particle growth in expansion zone resulting in smaller nanoparticles. In RESS-SC phenytoin particles are surrounded by a solid cosolvent, avoiding surface to surface interaction to other phenytoin particles, hence hindering the particle growth. RESS-SC concept is shown in Figure 7.3. The cosolvent removal is simply done by applying high vacuum in lyophilizer and it is the final step after particle recovery from expansion chamber.

7.2.1 Choice of Cosolvent

The choice of cosolvent is very important as it needs to enhance the CO_2 polarity for solubilizing polar drugs. Polar cosolvents like acetone, ethanol have been tried so far which are liquid at operating and exit conditions and can cause particle dissolution [11,

147

12, 15, 16]. In this work solid cosolvent is proposed which should have following properties:

a) Sufficiently high vapor pressure for easy removal by applying high vacuum

b) Solid at nozzle exit conditions (typically -5 $^{\circ}$C to 25 $^{\circ}$C, observed experimentally)

c) Appreciable solubility in sc CO_2

d) Non-reactive with desired solute or sc CO_2

e) Non-flammable and non-toxic

f) Inexpensive

Menthol is one such compound which meets all these requirements (Figure 7.1b). Its melting point is 34-36 $^{\circ}$C with high vapor pressure. Also menthol has comparatively high solubility in sc CO_2 [17, 13]. Menthol is already widely used in food and pharmaceutical industry.

In this work menthol solubility is measured at 45 $^{\circ}$C by gravimetric analysis whereas phenytoin solubility is measured by UV analysis at 264 nm. Size and morphology of obtained particles were characterized by scanning electron microscopy (SEM), x-ray diffraction (XRD), differential scanning calorimetery (DSC), dynamic light scattering (DLS) and fourier-transform infrared spectroscopy (FTIR).

7.3 Experimental Section

7.3.1 Materials

CO$_2$ (99.99% pure) from Air Gas, menthol (99% pure) with melting point of 34-36 $^{\circ}$C from Fisher Scientific, phenytoin (5, 5-diphenyl-2, 4-imidazolidinedione) (98+%

pure) from Aldrich were used as received. ACS grade (200 proof) ethanol was purchased from Pharmco products.

7.3.2 Apparatus

The schematic of RESS-SC process is shown in Figure 7.4. The apparatus is mainly divided into three parts: a pre-extraction chamber (section I), an extraction chamber (section II) and an expansion chamber (section III). In section I, P is a high pressure syringe pump for pressurizing CO_2 at desired pressure using CO_2 from cylinder A. Two vessels, M and S were used as extraction column for menthol and phenytoin respectively in section II. Glass wool was used on both the ends of vessels M and S to avoid any undissolved material carry over with the CO_2 flow. Both vessels containing solute and co-solvent were kept in a water bath to keep constant extraction temperature ($\pm$ 0.1 ^{o}C) by temperature controller. The pressure of extraction section was measured using an online Heise ST-2H pressure transducer connected just before valve V1. Section III is either an expansion chamber for RESS-SC experiment or a U-tube for solubility experiments and is kept at atmospheric pressure and ambient conditions. Valve V1 connects section I with section II whereas valve V3 connects section II and section III. Valves V1 and V2 are 3-way valves for CO_2 bypass connection to vessel S to perform conventional RESS experiments for comparison. Glass wool was used at the end of the expansion chamber outlet or at the end of the second leg of the U-tube to entrap the particles. Temperature in the expansion chamber was recorded to be less than 5 ^{o}C using a thermocouple.

7.3.3 Solubility Measurement

A syringe pump was filled with CO_2 from tank A and set at a desired pressure. Vessels, M and S, having 7 ml capacity each, were filled with menthol and phenytoin powders. These vessels act as extraction/solubilization columns. After filling, the extraction columns were connected as per Figure 7.4. Both columns were kept in a water bath at a desired temperature in such a way that the inlet was at the bottom while the outlet was at the top for proper distribution of SCF. CO_2 was fed to the first extraction column and was allowed to stabilize for 30-45 minutes by closing valve V2 at a desired pressure. After stabilizing the first column, menthol-enriched CO_2 was supplied to the second extraction column containing phenytoin using valve V2. Again, the entire system was equilibrated for 60-75 minutes before expanding phenytoin solution in the U-tube. The U-tube was kept in an ice bath with glass wool at the other end to trap the formed particles. For pure phenytoin solubility experiments, only one column was used filled with phenytoin and system was equilibrated for 110-120 minutes. For measuring phenytoin solubility, powder obtained in the U-tube was dissolved in ethyl alcohol and was analyzed by UV spectrophotometer (Spectronic Genesys 2) set at 264 nm.

For pure menthol solubility at 45 ^{o}C extraction column was filled with menthol powder and sc CO_2 was expanded in U-tube after 120 minutes of stabilization (to reach equilibrium). Gravimetric analysis method was used for menthol solubility.

7.3.4 Particle Formation by RESS-SC

For RESS-SC, the expansion chamber was used for the expansion of menthol/phenytoin/CO_2 solution from a desired pressure to atmospheric pressure. A tube

nozzle (PEEK nozzle from Upchurch) with a fixed diameter of 64 μm was used for expansion. Particles were collected in the expansion chamber. Before analyzing the particles for size, crystallinity or morphology, the particles were subjected to 300 mTorr (absolute) vacuum for 24 hrs to remove all the menthol by sublimation. No change in weight of particles was observed by applying vacuum for additional 3 hrs. Also, the lyophilized powder did not give any mint smell. These were the sufficient tests for ensuring menthol absence from lyophilized phenytoin particles. After menthol removal, the particles were analyzed by SEM, dynamic light scattering (DLS), differential scanning calorimeter (DSC) and powder X-ray diffraction (XRD) methods along with FTIR. RESS experiments were also conducted for phenytoin prior to RESS-SC experiments for comparison.

7.3.5   SEM Analysis

The particle size and morphology analysis was carried out using SEM (Zeiss, model DSM940). For analysis, the particles were attached to the carbon tape on the top of SEM aluminum stubs and were coated with gold using a sputter coater (Electron Microscopy Sciences, model 550X) for 2 runs of 1 minute each. In order to have a proper representation of the particles collected in the expansion chamber SEM micrographs of different regions were obtained. In menthol/phenytoin system, wherein menthol was the co-solvent, processed powder was first kept in a high vacuum of 300 mTorr (absolute) to remove all the menthol from the particle mixture. All the SEM analyses were done after 60-70 hrs of experiments at an accelerating voltage of 10 kv.

7.3.6 DSC Analysis

Thermal analysis was carried out using DSC (TA instruments, model DSC Q100) for processed and unprocessed phenytoin particles. Analysis was performed for 1.5 mg phenytoin sample at a temperature heating rate of 5 $^{\circ}$C/min and a temperature range of 30 to 300 $^{\circ}$C.

7.3.7 X-Ray Diffraction

Phenytoin particle crystallinity was analyzed using Rigaku X-ray diffractometer which was equipped with Cu Kα_1 radiation source and a Miniflex gonoiometer. The powder was filled to same depth inside the sample holder by leveling with spatula and scanning rate (2 deg/min) was same for all XRD analysis.

7.3.8 FTIR Analysis

Chemical analysis of unprocessed and RESS-SC processed phenytoin particles were performed by FTIR spectroscopy using Nicolet instrument. The spectra were collected in transmission mode at room temperature in 4000-400 cm^{-1} range at a resolution of 2 cm^{-1}.

7.3.9 DLS Analysis

Nanosuspension in water was made for phenytoin particles from RESS-SC process. The water was pre-saturated with phenytoin to avoid dissolution of the nanoparticles. The suspension was analyzed in DLS (PSS NICOMP model 380) for measuring hydrodynamic radius of phenytoin particles. Measurements were made using laser light of 638 nm wavelength with a 90° scattering angle at room temperature.

7.4   Results and Discussion

7.4.1   Solubility Enhancement

Table 7.1 summarizes the pure menthol solubility at 45 $^{\circ}$C in sc CO_2. Menthol solubility is as high as 0.147 mol/mol at 196 bar and 45 $^{\circ}$C. Contrary to menthol, phenytoin has extremely low solubility in sc CO_2. Table 7.2 summarizes phenytoin solubility in sc CO_2. Due to high crystallinity and molecular polarity, phenytoin has a limited solubility in sc CO_2, only 3 μmol/mol at 196 bar and 45 $^{\circ}$C.

Menthol saturated sc CO_2 can solubilize higher amount of phenytoin, at the given pressure and temperature. Phenytoin solubility with menthol cosolvent in sc CO_2 is summarized in Table 7.3. It is quite evident from Tables 7.2 and 7.3 that phenytoin solubility is enhanced as high as 400 fold using menthol cosolvent. Menthol containing CO_2 has a higher polarity which helps in solubilizing phenytoin. Similar results were obtained earlier with griseofulvin and 2-aminobenzoic acid solubility [13, 28]. Maximum solubility of 1302 μmol/mol was measured at 196 bar and 45 $^{\circ}$C. Figure 7.5 shows the variation of phenytoin solubility with and without menthol with increasing density. Phenytoin solubility increases with increase in density.

7.4.2   Phenytoin Nanoparticles

After addressing the solubility issue, the next goal was to form phenytoin nanoparticles by rapid expansion. The original unprocessed particles were rectangular shaped with average length of 4 μm long and width of 3 μm (Figure 7.6). Figure 7.7 shows particles from RESS at 96 bar and 45°C. The average size of phenytoin particles was 200 nm. There is not only a change in the particles morphology from rectangular to

spherical but also the particle size after processing with sc CO_2. Experiments were also performed at a higher pressure of 196 bar to analyze pressure effect on particle size. The average particle size reduced to 105 nm at the higher pressure (Figure 7.8). Due to lower solubility, exiting sc CO_2 has low concentration of phenytoin which helps in getting nanoparticles, as opposed to microparticles for other more CO_2-soluble drugs.

After processing with menthol enriched sc CO_2, phenytoin concentration increases but still the particles obtained are in nanometer range. Figure 7.9 shows SEM micrograph for RESS-SC processed phenytoin particles at 96 bar with average size of 120 nm. Here again the particles are in spherical shape. As phenytoin is surrounded by menthol solid cosolvent, even higher phenytoin concentration in RESS-SC process produces nanometer particles. This verifies the scheme proposed for RESS-SC (Figure 7.3). Like RESS process, the particle size reduces to 75 nm at higher pressure of 196 bar in RESS-SC process (Figure 7.10). This decrease in particle size is due to higher supersaturation value at higher pressure, while keeping same exit condition. However, the particle size reduction is not that significant considering 20% standard deviation in size measurement. Several researchers observed a similar behavior of pressure effect on particle size for their RESS experiments [28, 8].

All RESS-SC processed SEM micrographs are for menthol free phenytoin particles. Menthol cosolvent is removed by applying high vacuum in lyophilizer. Digital pictures of vial containing menthol and phenytoin after lyophilization are taken with a CCD camera (Sony model DFW-V500) having close focus lens (maximum magnification 10x). Figure 7.11-a shows the overall picture of vial containing menthol fibers at rim and drug particle at bottom of the vial. Parafilm was used at the top of the vial to trap

154

menthol particles which can be seen in Figure 7.11-b. Figure 7.11 –c and –d show close up pictures of rim and base of the vial. The purpose of Figure 7.11 is to show physical difference between drug particles and menthol particles. Earlier, precipitation by compressed antisolvent (PCA) and gas antisolvent (GAS) process had been used, but micron sized rod like particles were obtained in both methods using two different solvents (Figure 7.12) [30].

RESS-SC processing does not affect the chemical structure of drug particles which is supported by FTIR analysis. Figure 7.13 shows the FTIR spectra of RESS-SC processed and unprocessed phenytoin particles. –NH stretch can be seen at 3280 cm^{-1} frequency whereas –C=O stretch is evident at 1780 cm^{-1}. Both spectra overlap each other, though for RESS-SC processed particles slight bump at 3500 cm^{-1} can be seen which may be because of the ambient moisture attracted to the large surface area present on the phenytoin nanoparticle surface.

DSC was performed for thermal analysis of RESS-SC processed and unprocessed phenytoin particles. The melting point of unprocessed phenytoin is 296.78 ^{o}C whereas after processing it is 296.62 ^{o}C. There is no significant change in melting point which suggests that particle crystallinity form does not change after RESS-SC. Figure 7.14 shows heat flow with temperature plot of unprocessed and RESS-SC processed phenytoin particles.

To further investigate particles crystallinity XRD analysis was performed. Figure 7.15 shows the XRD intensity variation with 2-theta for unprocessed and processed phenytoin particles. Though all the peaks are overlapping, RESS-SC processed phenytoin particles have lower intensity values (Figure 7.15-b). Though care has been

taken to analyze same sample mass for XRD, due to lower bulk density of processed particles there might be some difference in the mass used. This difference in sample mass can be the cause of lower intensity of processed particles. XRD of pure menthol particles is shown elsewhere [13].

According to SEM analysis, the average size of phenytoin particles was 75 nm from RESS-SC at 196 bar and 45 $^{\circ}$C. These particles were also subjected to DLS analysis to obtain hydrodynamic size, which gave a number average diameter of 57.4 nm for phenytoin nanosupension. Figure 7.16 shows the DLS number average distribution for the nanosuspension. Such a small hydrodynamic size makes these phenytoin particles, an ideal candidate for injectable drug delivery.

7.5   Conclusion

The two major issues of the RESS process – low solubility in sc CO_2 and formation of nanoparticles are addressed in this paper for phenytoin drug using menthol solid cosolvent. Menthol cosolvent not only enhances the phenytoin solubility in sc CO_2 but also form particles as small as 75 nm. At 196 bar and 45 oC, solubility of phenytoin is only 3 μmol/mol, which is enhanced to 1302 μmol/mol by using menthol cosolvent. Due to the enhancement, phenytoin nanoparticle production rate in RESS-SC is about 400 fold more in comparision to that in RESS process.

7.6 Acknowledgement

REFERENCES

1. Unno, K.; Suto, I.; Fukui, R.; Kagaya, S.; Nakata, H., Concentration of anticonvulsant drugs in blood 6. Dissolution of commercial phenytoin products. Byoin Yakugaku, 1984, 10(5), 323-30. Journal written in japanese.

2. Yakou, S.; Umehara, K.; Sonobe, T.; Nagai, T.; Sugihara, M.; Fukuyama, Y., Particle size dependecy of dissolution rate and human bioavailability of phenytoin in powders and phenytoin-polyethylene glycol soild dispersions. Chemical and Pharmaceutical Bulletin, 1984, 32(10), 4130-6.

3. Tom, Jean W. and Debenedetti, Pablo G., Particle Formation with Supercritical Fluids-A Review. J. Aerosol Sci., 1991, 22(5), 555-584

4. Tom, Jean W.; Debenedetti, Pablo G.; Jerome, R., Precipitation of Poly(L-lactic acid) and Composite Poly(L-lactic acid)-Pyrene Particles by Rapid Expansion of Supercritical Solutions. J. Supercritical Fluids, 1994, 7, 9-29.

5. Turk, M.; Hils, P.; Helfgen, B.; Schaber, K.; Martin, H.-J.; Wahl, M.A., Micronization of pharmaceutical substances by the Rapid Expansion of Supercritical Solutions (RESS): a promising method to improve bioavailability of poorly soluble pharmaceutical agents. J. Supercritical Fluids, 2002, 22, 75-84.

6. Kwauk, X.; Debenedetti, Pablo G., Mathematical modeling of aerosol formation by rapid expansion of supercritical solutions in a converging nozzle. J. Aerosol Sci., 1993, 24 (4), 445-469.

7. Shaub, Gina R.; Brennecke, Joan F.; McCready, Mark J., Radial Model for Particle Formation from the Rapid Expansion of Supercritical Solutions. J. Supercritical Fluids, 1995, 8, 318-328.

158

8. Helfgen, B.; Turk, M.; Schaber, K., Hydrodynamic and aerosol modelling of the rapid expansion of supercritical solutions (RESS-process). J. of Supercritical Fluids, 2003, 26, 225-242.

9. Luna-Barcenas, G.; Kanakia, S.; Sanchez, I. C.; Johnston, K.P., Semicrystalline microfibrils and hollow fibres by precipitation with a compressed-fluid antisolvent. Polymer, 1995, 36(16), 3173-3182.

10. Werling, Jane O.; Debenedetti, Pablo G., Numerical modeling of mass transfer in the supercritical antisolvent process: miscible conditions. J. of Supercritical Fluids, 2000, 18, 11-24.

11. Elvassore, N.; Baggio, M.; Pallado, P.; Bertucco, A., Production of different morphologies of biocompatible polymeric materials by supercritical CO_2 antisolvent technique. Biotechnology and Bioengineering, 2001, 73(6), 449-457.

12. Reverchon, E.; Della Porta, G.; Pallado, P., Supercritical antisolvent precipitation of salbutamol microparticles. Powder Technology, 2001, 114, 17-22.

13. Reverchon, E.; Della Porta, G.; Taddeo, R.; Pallado, P.; Stassi, A., Solubility and Micronization of Griseofulvin in supercritical CHF_3. Ind. Eng. Chem. Res., 1995, 34, 4087-4091.

14. Dylag, T.; Zygmunt, M.; Maciag, D.; Handzlik, J.; Bednarski, M.; Filipek, B.; Kiec-Kononowicz, K., Synthesis and evaluation of in vivo activity of diphenylhydantoin basic derivatives. European Journal of Medicinal Chemistry, 2004, 39, 1013-1027.

15. Page, C.; Curtis, M.; Sutter, M.; Walker, M.; Hoffman, B. In: Integrated Pharmacology, Mosby, Edinburgh-Toronto, 2002, pp. 361-376.

16. Reynolds, J. E. F. Martindale Extra Pharmacopeia. The Pharmaceutical Press, London, 1982, p. 1235.

17. Stella, V.J.; Martodihardjo, S.; Rao, V.M., Aqueous Solubility and Dissolution Rate Does Not Adequtly Predict in Vivo Performance: A Probe Utlizing Some N-Acyloxymethyl Phenytoin Prodrugs. J. Pharmaceutical Sciences, August 1999, 88 (8), 775-779.

18. Hashim, F.; El-Din, E. Z., Efect of some excipients on the dissolution of phenytoin and acetazolamide from capsule formations. Acta Pharmaceutica Fennica, 1989, 98(3), 197-204.

19. Tsuruoka, M.; Hashimoto, T.; Seo, H.; Ichimasa, S.; ueno, O.; Fujinaga, T.; Otagiri, M.; Uekama, K., Enhanced bioavailability of phenytoin by β-cyclodextrin complexation. Yakugake Zasshi, 1981, 101(4), 360-7.

20. Reverchon, E., Process for the production of micro and /or nanoparticlesI. Patent No. WO03004142.

21. Nokhodchi, A.; Bolourtchian, N.; Dinarvand, R., Crystal modifictaion of phenytoin using different solvents and crystallization conditions. Intl. J. Of Pharm., 2003, 250, 85-97.

22. Dobbs, J.M.; Wong, J.M.; Lahiere, R.J.; Johnston, K.P., Modification of Supercritical Fluid Phase Behavior using Polar Cosolvents. Ind. Eng. Chem. Res., 1987, 26(1), 56-65.

23. Dobbs, J.M. and Johnston, K.P., Selectivities in Pure and Mixed Supercritical Fluid Solvents. Ind. Eng. Chem. Res., 1987, 26(7), 1476-1482.

24. Liu, Z.; Yang, G.; Ge, L.; Han, B., Solubility of o- and p-Aminobenzoic Acid in Ethanol + Carbon Dioxide at 308.15 K to 318.15 K and 15 bar to 85 bar. J. Chem. Eng. Data, 2000, 45, 1179-1181.

25. Jin. J.; Zhong, C.; Zhang, Z.; Li, Y., Solubilities of benzoic acid in supercritical CO_2 with mixed cosolvent. Fluid Phase Equilibria, 2004, 226, 9-13.

26. Sovova, H. and Jez, J., Solubility of Menthol in Supercritical Carbon Dioxide. J. Chem. Eng. Data, 1994, 39, 840-841.

27. Thakur, Ranjit and Gupta, Ram B., Rapid Expansion of Supercritical Solution with Solid Cosolvent (RESS-SC) process: Formation of Griseofulvin Nanoparticles. Accepted in Ind. Eng. Chem. Res., 2005.

28. Thakur, Ranjit and Gupta, Ram B., Rapid Expansion of Supercritical Solution with Solid Cosolvent (RESS-SC) process of 2-Aminobenzoic Acid Nanoparticle formation. Submitted to J. of Supercritical Fluids, 2005.

29. Charoenchaitrakool, M.; Dehghani, F.; Foster, N. R.; Chan, H.K., Micronization by Rapid Expansion of Supercritical Solutions to Enhance the Dissolution Rates of Poorly Water-Soluble Pharmaceuticals. Ind. Eng. Chem. Res. 2000, 39, 4794, 4802.

30. Muhrer, G.; Meier, U.; Albano, S.; Fusaro, F.; Mazzotti, M., Use of compressed gas precipitation to enhance the dissolution behavior of a poorly water-soluble drug: Generation of drug microparticles and drug-polymer solid dispersions. Submitted to Intl. J. of Pharm., 2005.

31. Span, R.; Wagner, W., A new equation of state for carbon dioxide covering the fluid region from the triple point temperature to 1100 K at pressure up to 800 MPa. J. Phy. Chem. Ref. Data, 1996, 25(6), 1509-1596.

Table 7.1 Solubility of pure menthol in sc CO_2

Pressure (bar)	Temperature (^{o}C)	CO_2 Density[31] (mol/ml)	Solubility (mmol/ml)	Standard Deviation (mmol/mol)
96	45	0.01004	43	5
129	45	0.01582	84	9
163	45	0.01746	121	7
196	45	0.01844	147	10

Table 7.2 Solubility of phenytoin in pure sc CO_2

Pressure (bar)	Temperature (^{o}C)	CO_2 Density (mol/ml)	Solubility (μmol/mol)
96	45	0.01004	0.8
129	45	0.01582	1.6
196	45	0.01844	3

Table 7.3 Solubility of phenytoin in CO_2 with menthol solid cosolvent

Pressure (bar)	Temperature (^{o}C)	CO_2 Density (mol/ml)	Solubility (μmol/mol)	Standard Deviation (μmol/mol)	Enahncement Factor *
96	45	0.01004	561	45	701
129	45	0.01582	829	90	518
196	45	0.01844	1302	125	434

*Phenytoin solubility in CO_2 with menthol/ phenytoin solubility in pure CO_2
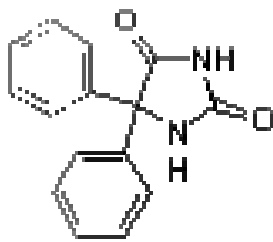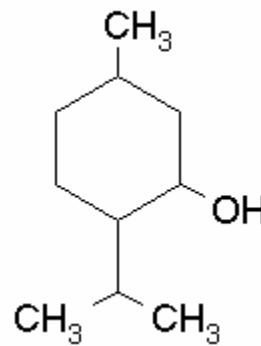
(a)   (b)

Figure 7.1 Chemical structure of (a) phenytoin (5, 5-diphenyl-2, 4-imidazolidinedione) (b) menthol
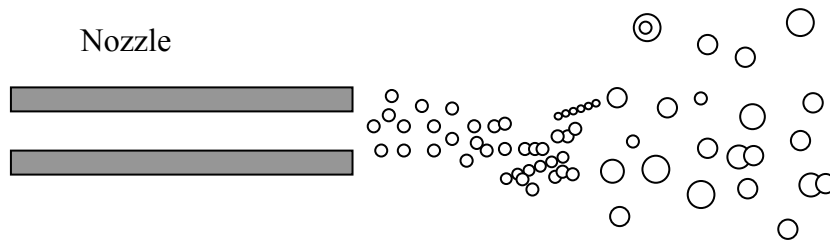
Figure 7.2 Schematic of RESS process
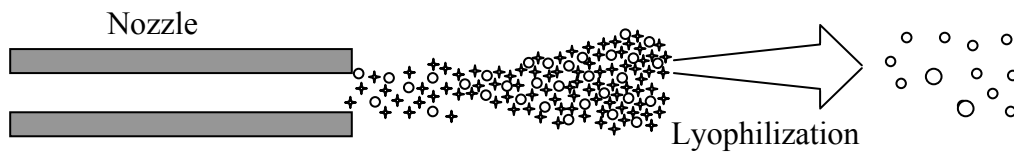
Figure 7.3 Schematic of RESS-SC process

[Here ✦ are menthol particles and ○ are phenytoin particles]

165
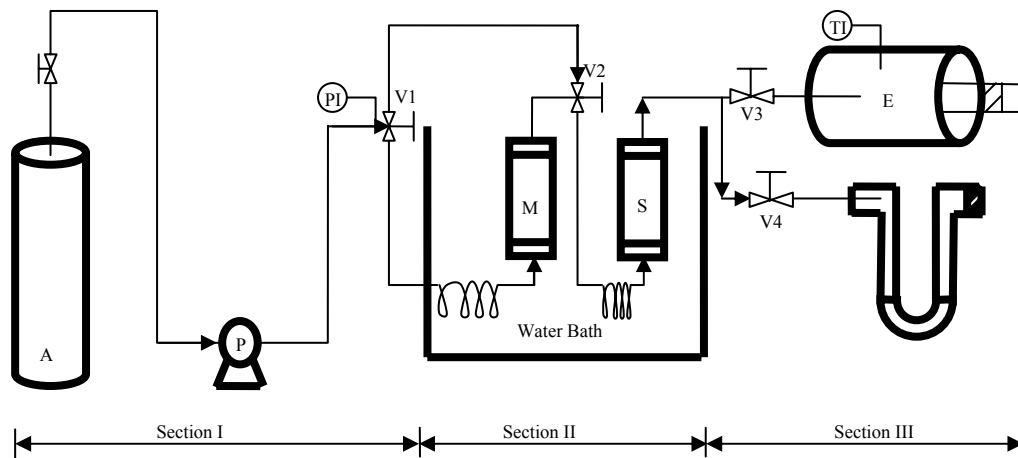
Figure 7.4 Schematic of RESS-SC experimental apparatus
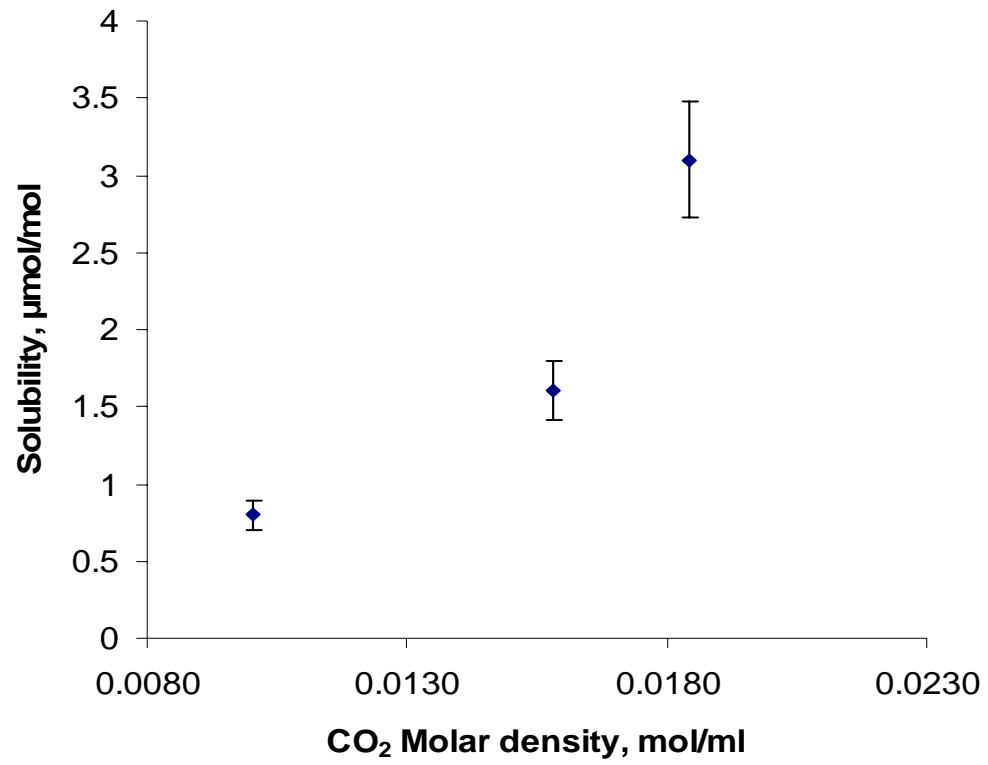
(a)
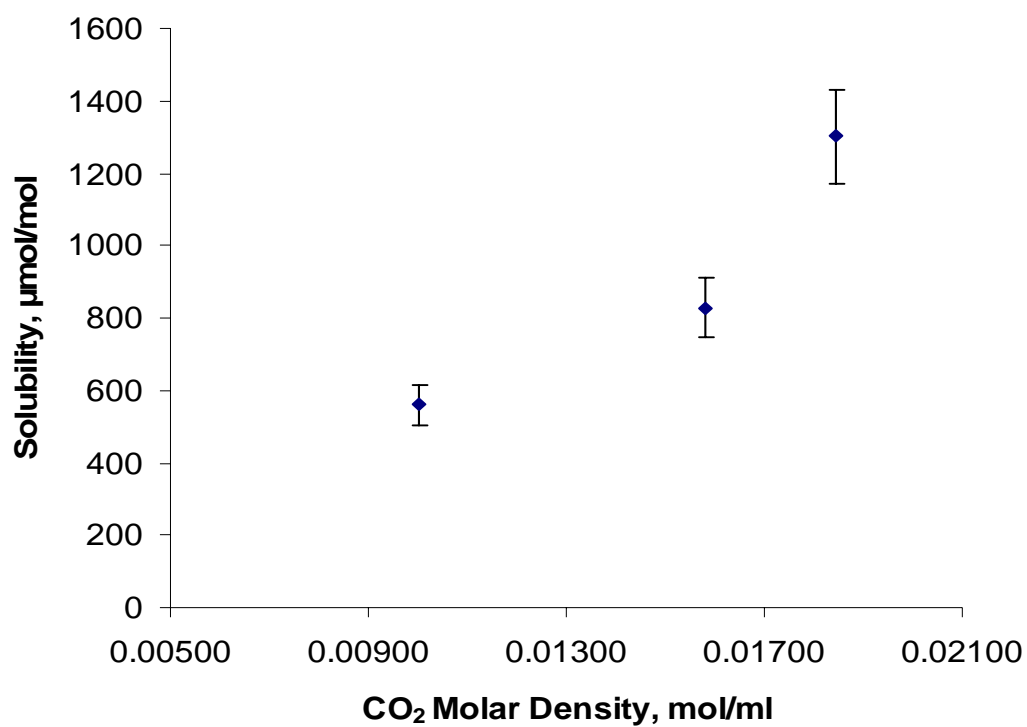
(b)

**Figure 7.5 Phenytoin solubility in sc CO_2 (a) without menthol, and (b) with menthol**
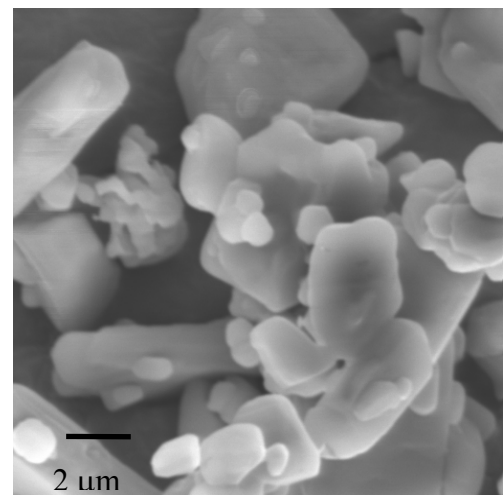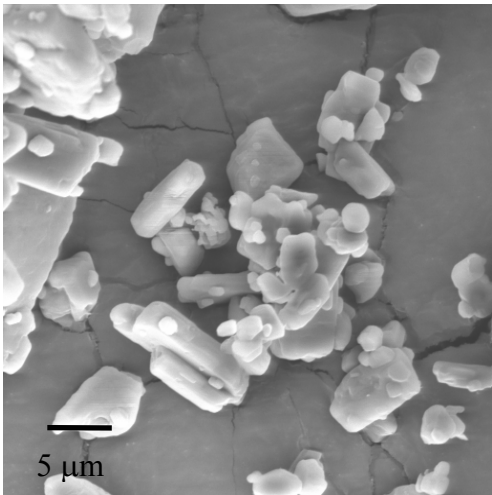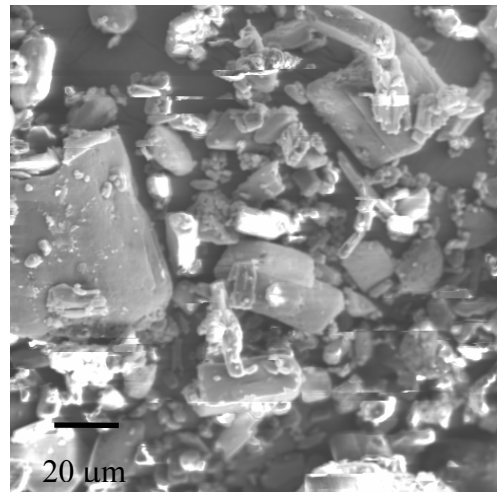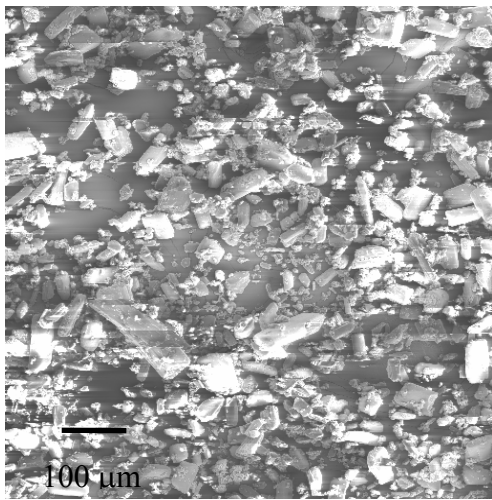
Figure 7.6 Original phenytoin particles
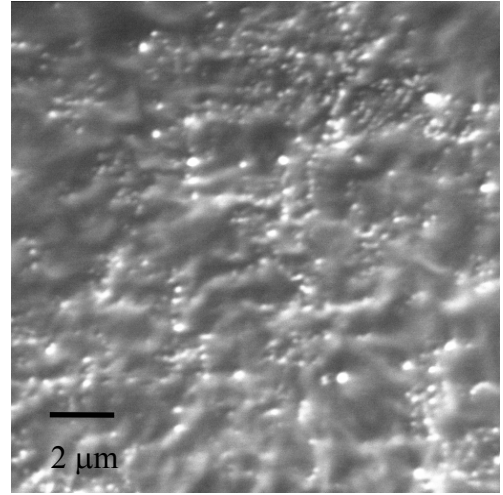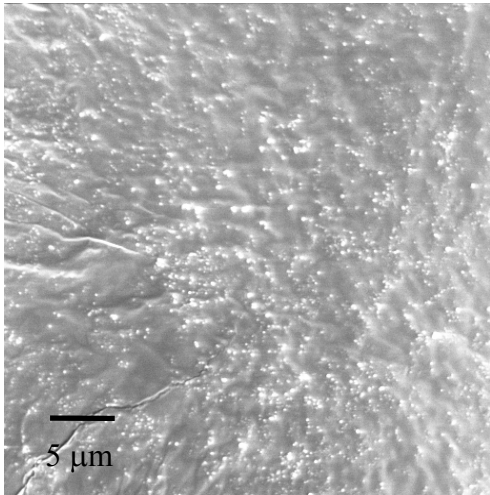
**Figure 7.7 Phenytoin particles obtained from RESS at 96 bar and 45 ^{o}C.**
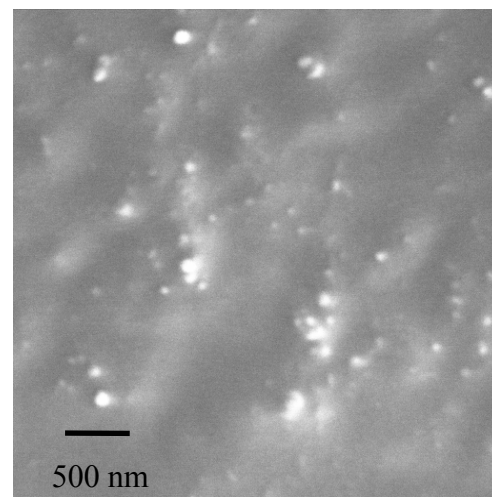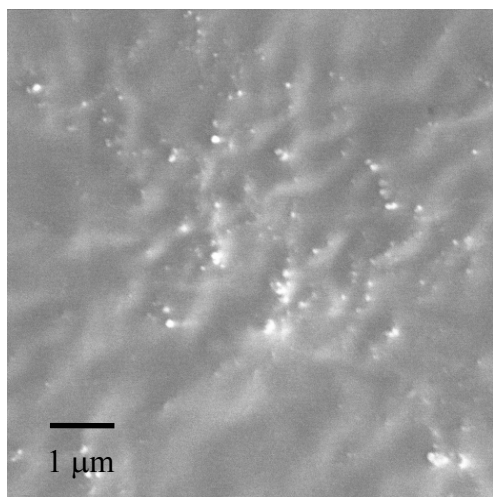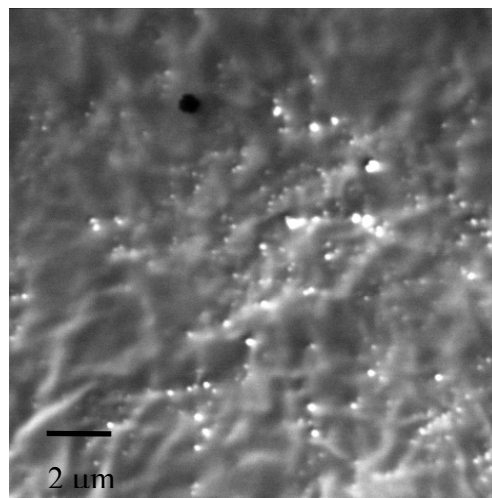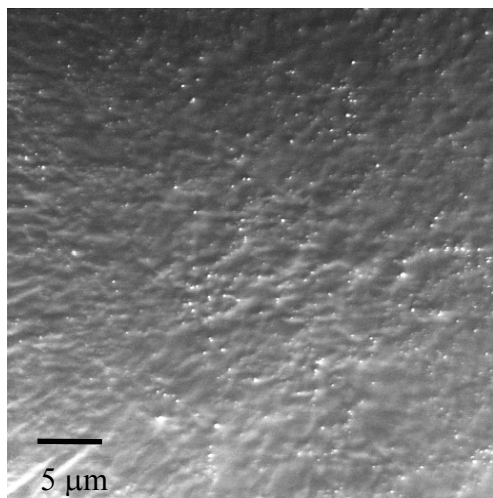
Figure 7.8 Phenytoin particles obtained from RESS at 196 bar and 45 ^{o}C
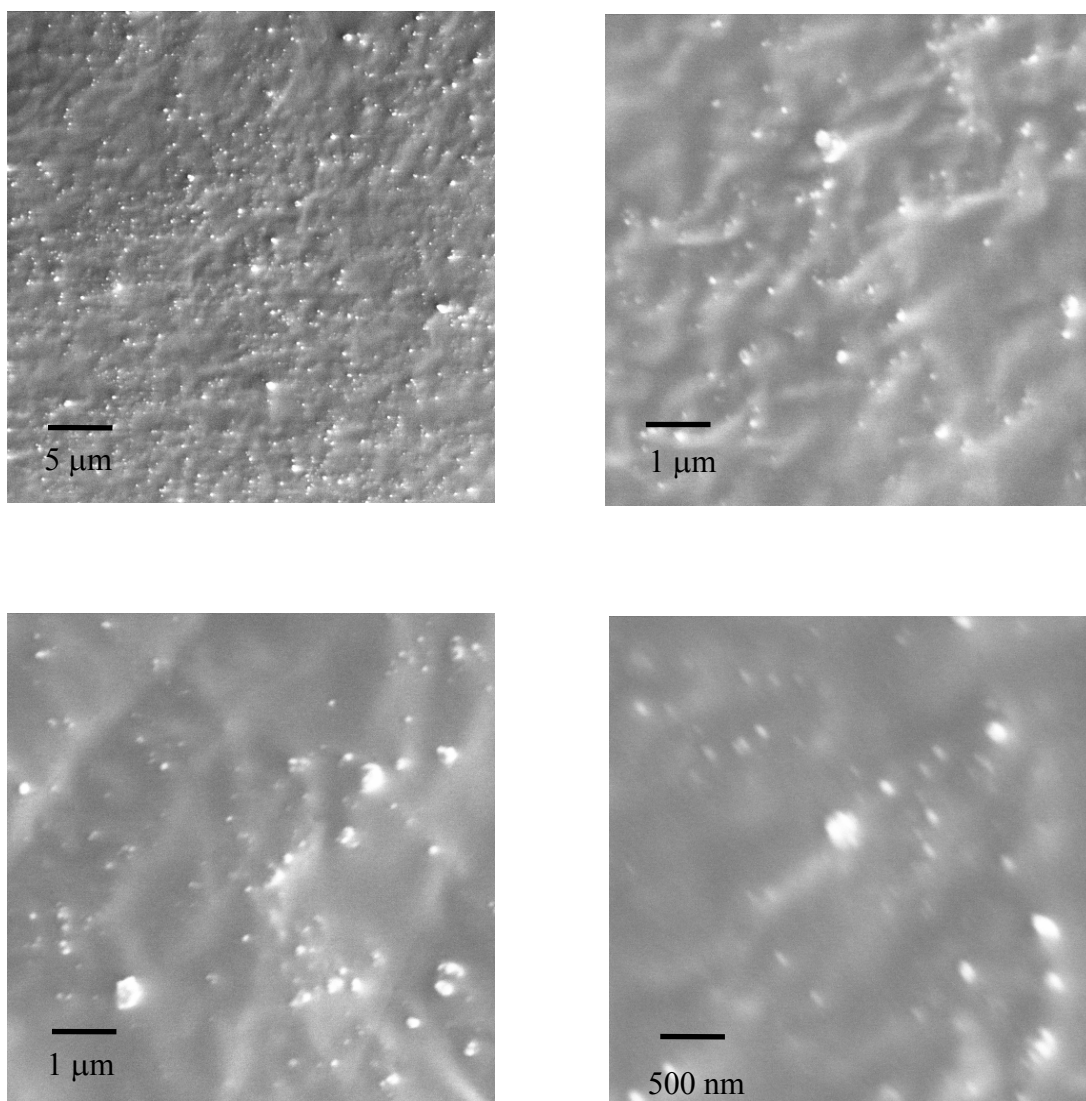
**Figure 7.9 Phenytoin particles obtained from RESS-SC at 96 bar and 45 ^{o}C.**
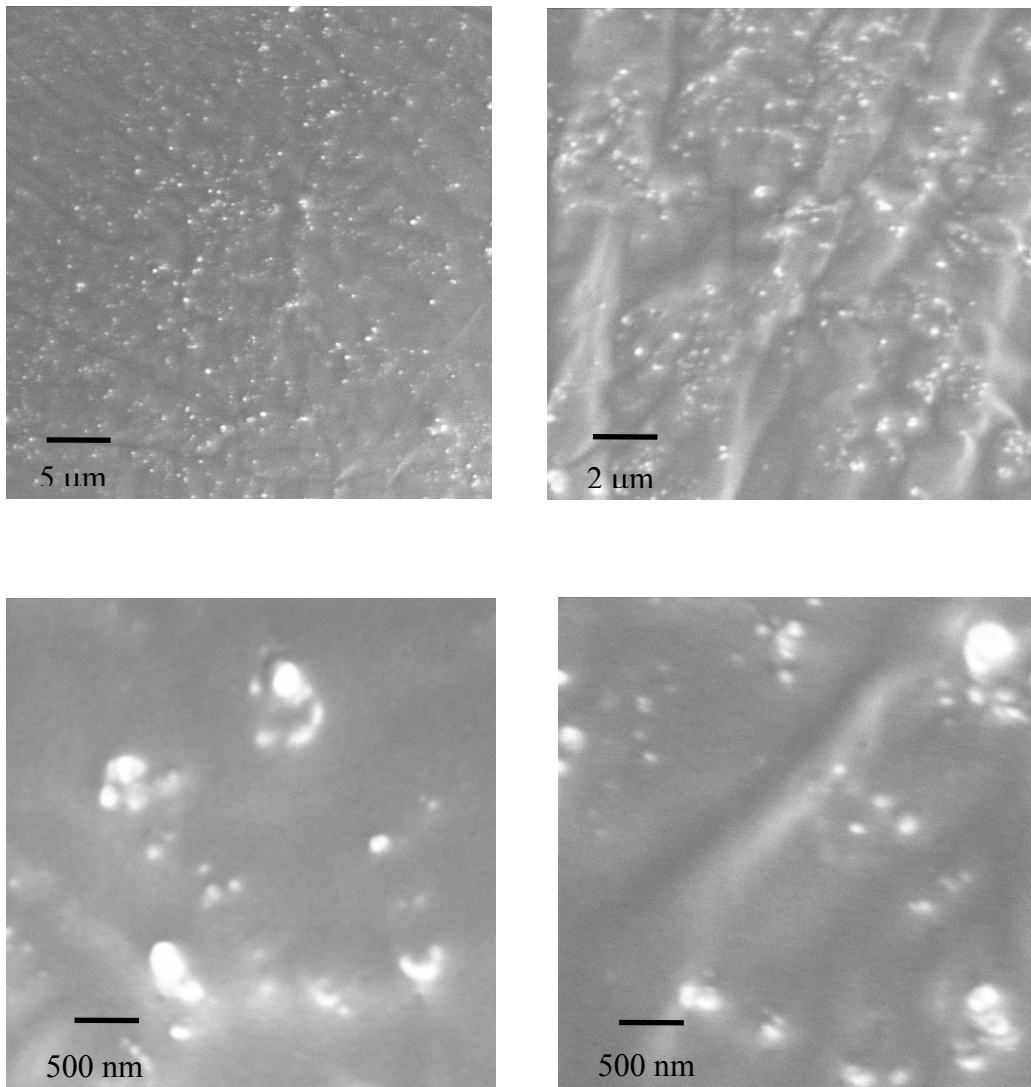
Figure 7.10 Phenytoin particles obtained from RESS-SC at 196 bar and 45 $^{\circ}$C.
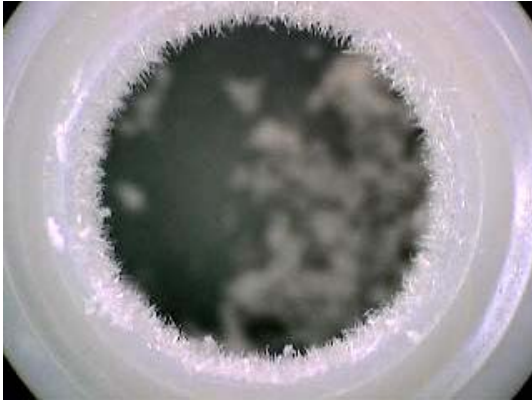
(a)

(b)

(c)

(d)

Figure 7.11 Optical pictures of vial containing menthol fibers on rim (a, c) and bottle cap (b), and phenytoin particles at bottom of vial (d) after partial lyophilization.
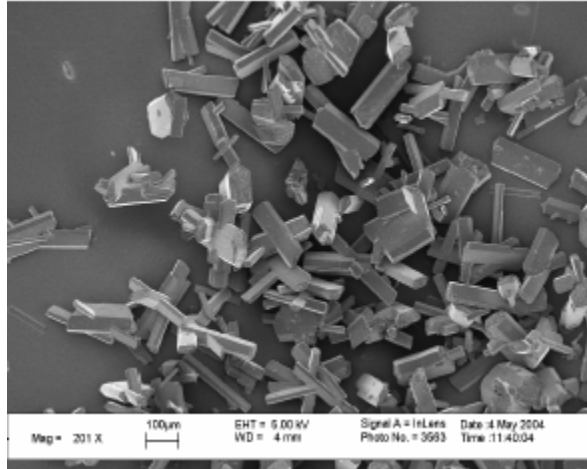
(a)
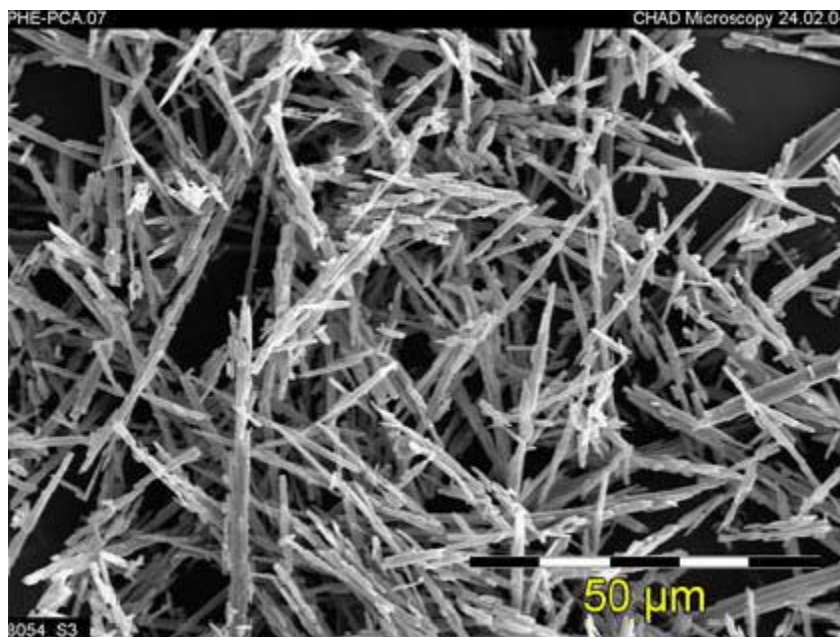
(b)

Figure 7.12 (a) GAS recrystallization and (b) PCA precipitation of phenytoin particles from acetone (Muhrer et al., 2005 Submitted to Intl. J. of Pharm.) [30].
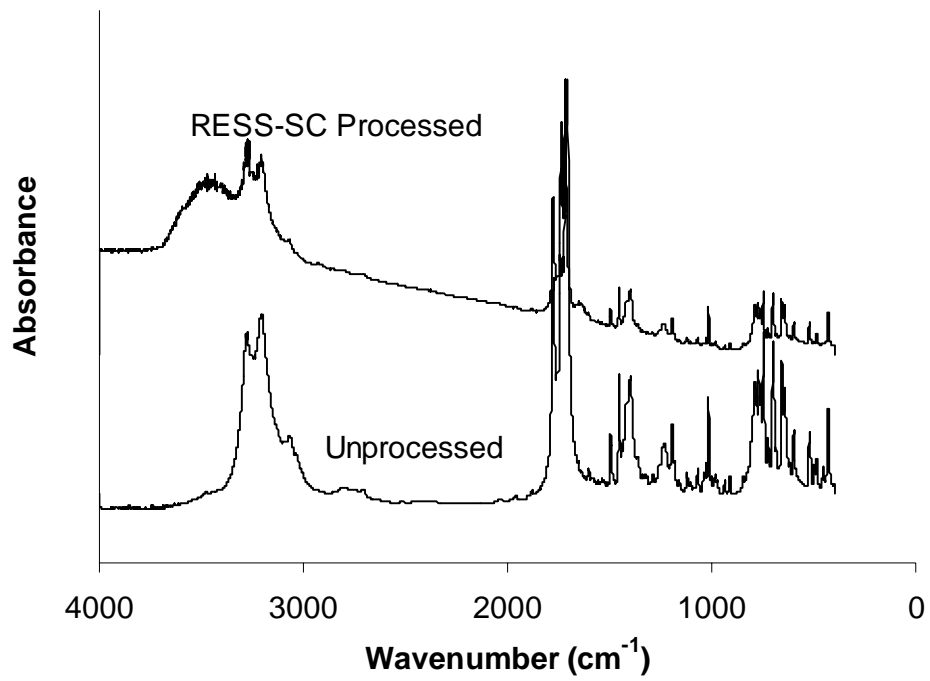
Figure 7.13 FTIR analysis of unprocessed and RESS-SC processed phenytoin

particles

Unprocessed

296.78 $^{\circ}$C

RESS-SC Processed

296.62 $^{\circ}$C
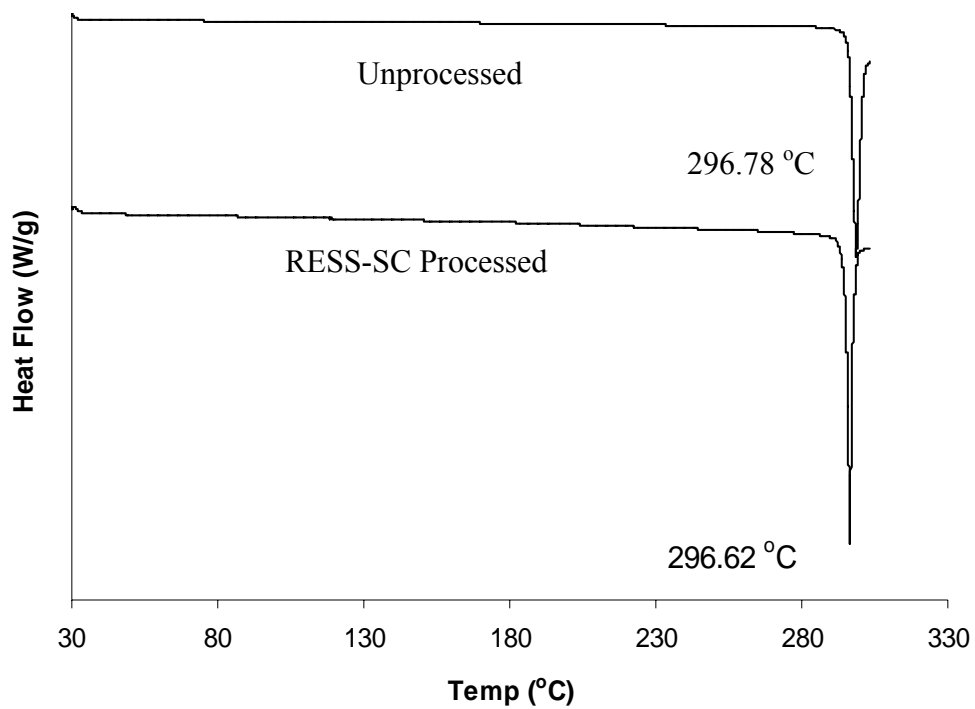
Figure 7.14 DSC thermograph of unprocessed and RESS-SC processed phenytoin
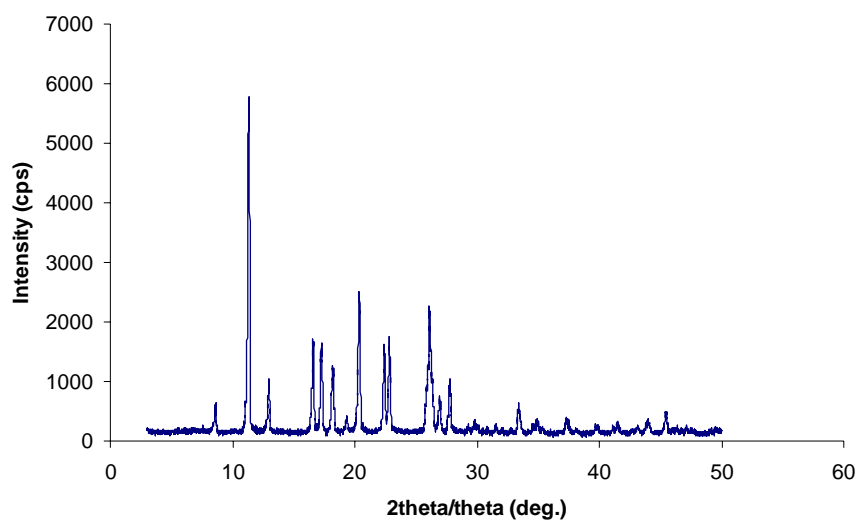
particles

(a)
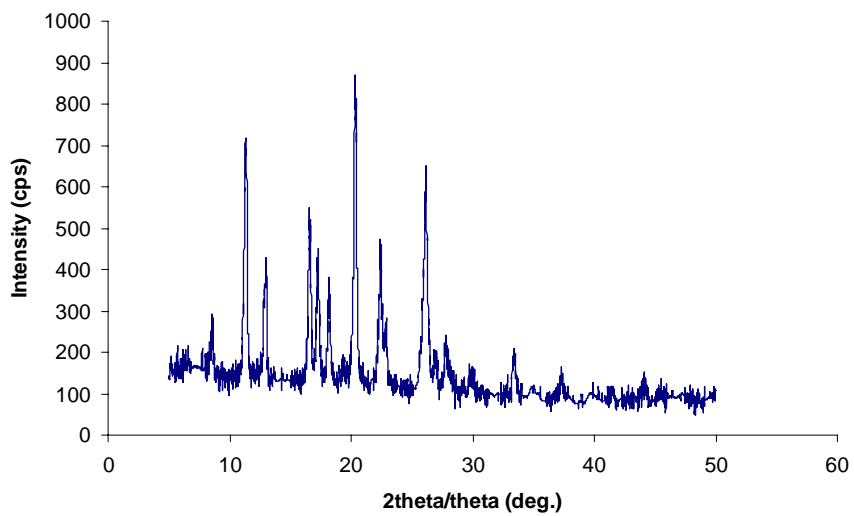
(b)

Figure 7.15 XRD analysis of (a) unprocessed and (b) RESS-SC processed phenytoin
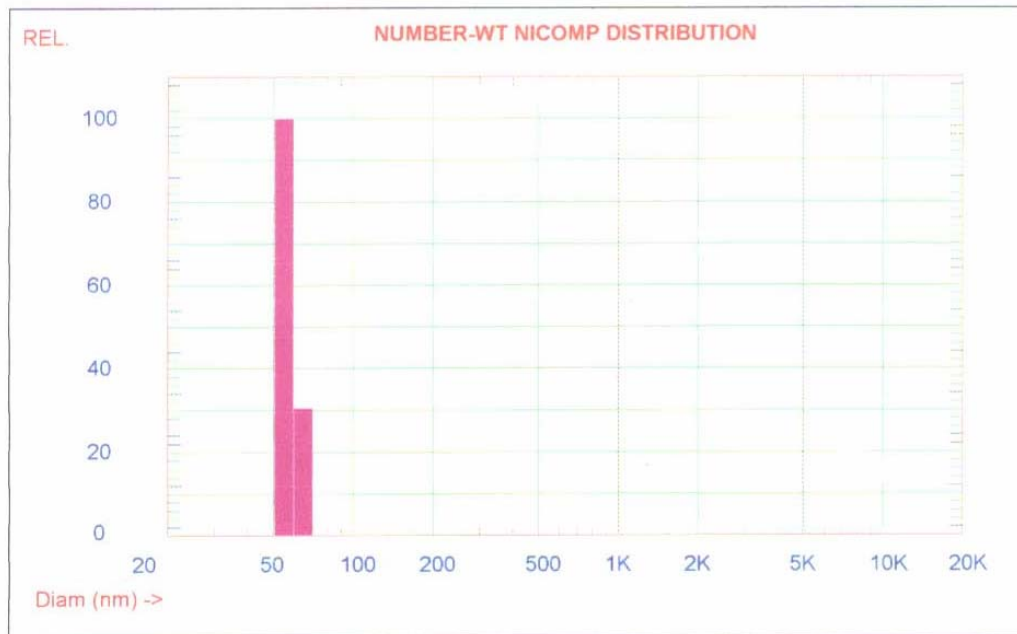
particles

Figure 7.16 DLS analysis of phenytoin nano-suspension.

CHAPTER 8

ACETAZOLAMIDE NANOPARTICLES BY RESS-SC PROCESS

8.1   Abstract

The low solubility of polar compounds and particle aggregation in expansion zone are two major limitations of conventional rapid expansion of supercritical solution (RESS) process using CO_2 as a supercritical fluid (SCF). To overcome these limitations this work proposes RESS with solid cosolvent (RESS-SC) process. To demonstrate RESS-SC concept acetazolamide, an antiepileptic drug, is used as a solute drug and menthol as a solid cosolvent. Menthol having low vapor pressure is easy to remove from the system by sublimation at high vacuum. Acetazolamide has almost zero solubility in supercritical CO_2 but with menthol cosolvent 24.2 μmol/mol solubility was achieved at 236 bar and 45 °C. The solid cosolvent menthol acts as a spacer in expansion zone between drug particles and avoids agglomeration. The number average particle size obtained for acetazolamide in RESS-SC process was 95 nm at 196 bar and 45 °C.

8.2   Introduction

The dissolution of poorly water soluble drugs is a major concern for the pharmaceutical industry. Most of the high value drugs have not only low solubility but also their toxicity limit is close to dosage limit. However, literature shows that drug dissolution increases by decreasing particle size [1]. This means that bioavailability of

drug can be increased by reducing the particle size. Supercritical fluid (SCF) based particle formation method is one of the methods which can form small particles with high quality. Due to significant polarity of these high end compounds, it is difficult to dissolve these compounds in supercritical CO_2 which is environmentally benign and safe SCF to work with. Acetazolamide is one such compound which is polar in nature. It is a carbonic anhydrase inhibitor used as anti-epileptic and for reduction of intraocular pressure in case of glaucoma. The molecular weight of acetazolamide is 222.25 and melting point is 258-259 $^{\circ}C$. Large oral doses of acetazolamide are required to reduce intraocular pressure which leads to diuresis and metabolic acidosis like side effects. Water soluble polymers have been used for increasing the bioavailability of acetazolamide [2]. Size reduction is one of the methods to enhance drug dissolution and expanding the toxicity-dosage window.

There are two major SCF based particle formation method – supercritical antisolvent (SAS) and rapid expansion of supercritical solution (RESS) [3]. In RESS process, the desired solute is solubilized in SCF and then resulting solution is expanded through a nozzle to cause a sudden decrease in the solubility and hence, particle formation [4, 5]. Homogenous nucleation in RESS is caused by supersaturation and several mathematical models have been presented to explain this process theoretically [6, 7, 8]. In SAS process, the desired solute is dissolved in an organic solvent and then injected inside SCF media causing small particle formation by volumetric expansion and removal of solvent [9, 10, 11, 12]. RESS is simpler and less expensive when compared to SAS process. For RESS process knowledge of compound solubility is highly desirable. Most common SCF for these processes are CO_2.

Due to polar nature, acetazolamide has limited solubility in supercritical CO_2. Acetazolamide solubility in supercritical CO_2 is below detection limit. Duarte et. al. (2005) used ethanol as a cosolvent to enhance acetazolamide solubility in supercritical CO_2 [13]. The maximum solubility achieved was 1.392×10^{-5} with 10% ethanol cosolvent. However, ethanol cosolvent is not viable to use for RESS process as ethanol is liquid at exit condition and may re-dissolve the obtained powders. To overcome this challenge, this work proposed use of solid cosolvent. By use of solid cosolvent not only solubility can be enhanced but also particle size can be controlled. Thakur et. al. [14, 15, 16] showed the advantage of using menthol as a solid cosolvent in RESS process for griseofulvin, aminobenzoic acid and phenytoin particles. This work also uses menthol as a cosolvent for acetazolamide. The maximum acetazolamide solubility achieved was 2.4×10^{-5} mol/mol in menthol saturated supercritical CO_2 at 236 bar and 45 $^{\circ}$C. The experimental set up and procedure is reported elsewhere [16].

8.3   Results and Discussion

Figure 8.1 is the chemical structure for acetazolamide compound. It is a highly polar compound which is evident from the chemical structure. As CO_2 is not polar in nature, it can not dissolve polar compounds in significant amount. This leads to use of another polar compound as a cosolvent for higher solubilization. Acetazolamide solubility in supercritical CO_2 is in the range of 10^{-8} mol/mol which is below detection limit. By using menthol saturated supercritical CO_2 as cosolvent solubility enhanced to 24.2 μmol/mol at 236 bar and 45 $^{\circ}$C. Table 8.1 summarizes the solubility results of acetazolamide in supercritical CO_2 with menthol cosolvent. In all the experiments CO_2 is

fully saturated with menthol. Drug solubility increases with increase in pressure. This increase is due to higher solvent density at higher pressure (Figure 8.2).

The other major limitation in conventional RESS process is agglomeration of particles in expansion zone. Mathematical model shows that particles at tip of the nozzle are only about 10 nm in size [8] but final particles are in the micron range. This particle agglomeration happens in expansion zone where particle collide with each other after nucleation and stick to each other as every particles are surrounded by similar particles. In RESS-SC solid cosolvent has higher solubility than desirable solute which surrounds these drug particles in expansion zone and avoids surface to surface collision and so agglomeration. Figure 8.3 shows the SEM micrograph of acetazolamide particles obtained from supplier (unprocessed). The average particle size of this unprocessed particles are 40-50 µm in size with irregular morphology. After RESS-SC processing not only particle size reduces to 95 nm (average number weighted) but also morphology change was observed. RESS-SC processed particles are spherical with uniform distribution as can be seen in Figure 8.4. Similar results were obtained earlier for griseofulvin, 2-aminobenzoic acid and phenytoin particles [14, 15, 16].

REFERENCES

1. Perrut, M.; Jung, J.; Leboeuf, F., Enhancement of dissolution rate of poorly-soluble active ingredients by supercritical fluid processes Part I: Micronization of neat particles. Intl. J. of Pharmaceutics, 288, 3-10, 2005.

2. Kaur, I.P.; Singh, M.; Kanwar, M., Formulation and evaluation of ophthalmic preparation of acetazolamide. Intl. J. of Pharmaceutics, 199, 119-127, 2000.

3. Tom, Jean W. and Debenedetti, Pablo G., Particle Formation with Supercritical Fluids-A Review. J. Aerosol Sci., 1991, 22(5), 555-584

4. Tom, Jean W.; Debenedetti, Pablo G.; Jerome, R., Precipitation of Poly(L-lactic acid) and Composite Poly(L-lactic acid)-Pyrene Particles by Rapid Expansion of Supercritical Solutions. J. Supercritical Fluids, 1994, 7, 9-29.

5. Turk, M.; Hils, P.; Helfgen, B.; Schaber, K.; Martin, H.-J.; Wahl, M.A., Micronization of pharmaceutical substances by the Rapid Expansion of Supercritical Solutions (RESS): a promising method to improve bioavailability of poorly soluble pharmaceutical agents. J. Supercritical Fluids, 2002, 22, 75-84.

6. Kwauk, X.; Debenedetti, Pablo G., Mathematical modeling of aerosol formation by rapid expansion of supercritical solutions in a converging nozzle. J. Aerosol Sci., 1993, 24 (4), 445-469.

7. Shaub, Gina R.; Brennecke, Joan F.; McCready, Mark J., Radial Model for Particle Formation from the Rapid Expansion of Supercritical Solutions. J. Supercritical Fluids, 1995, 8, 318-328.

8. Helfgen, B.; Turk, M.; Schaber, K., Hydrodynamic and aerosol modelling of the rapid expansion of supercritical solutions (RESS-process). J. of Supercritical Fluids, 2003, 26, 225-242.

9. Luna-Barcenas, G.; Kanakia, S.; Sanchez, I. C.; Johnston, K.P., Semicrystalline microfibrils and hollow fibres by precipitation with a compressed-fluid antisolvent. Polymer, 1995, 36(16), 3173-3182.

10. Werling, Jane O.; Debenedetti, Pablo G., Numerical modeling of mass transfer in the supercritical antisolvent process: miscible conditions. J. of Supercritical Fluids, 2000, 18, 11-24.

11. Elvassore, N.; Baggio, M.; Pallado, P.; Bertucco, A., Production of different morphologies of biocompatible polymeric materials by supercritical CO_2 antisolvent technique. Biotechnology and Bioengineering, 2001, 73(6), 449-457.

12. Reverchon, E.; Della Porta, G.; Pallado, P., Supercritical antisolvent precipitation of salbutamol microparticles. Powder Technology, 2001, 114, 17-22.

13. Duarte, A, R. C.; Santiago, S.; de Sousa, H. C.; Duarte, C.M.M., Solubility of Acetazolamide in supercritical carbon dioxide in the presence of ethanol as a cosolvent. J. Chem. Eng. Data, 50, 216-220, 2005.

14. Thakur, Ranjit and Gupta, Ram B., Rapid Expansion of Supercritical Solution with Solid Cosolvent (RESS-SC) process: Formation of Griseofulvin Nanoparticles. Ind. Eng. Chem. Res., 44(19), 7380-7387, 2005.

15. Thakur, Ranjit and Gupta, Ram B., Rapid Expansion of Supercritical Solution with Solid Cosolvent (RESS-SC) process of 2-Aminobenzoic Acid Nanoparticle formation. Submitted to J. of Supercritical Fluids, 2005.

16. Thakur, Ranjit and Gupta, Ram B., Formation of phenytoin nanoparticles using rapid expansion of supercritical solution with solid cosolvent (RESS-SC) process. Submitted to Intl. J. of Pharmaceutics, 2005.

Table 8.1 Acetazolamide solubility in supercritical CO_2 with menthol cosolvent

| Pressure (bar)	Temperature (°C)	CO_2 Density (mol/ml)	Solubility, y ($\times 10^6$)
95	45	0.00988	1.3
129	45	0.01579	4.4
162	45	0.01743	17
196	45	0.01842	21.5
236	45	0.01929	24.2
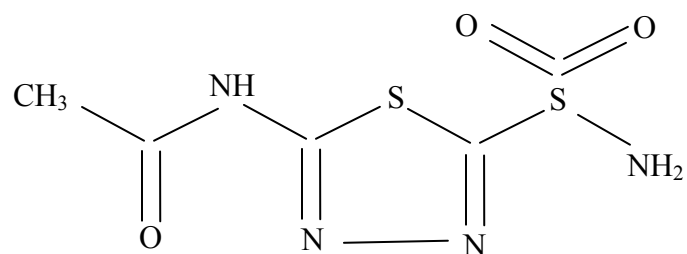
Figure 8.1 Chemical structure of acetazolamide [(N-5-(aminosulfonyl)-1, 3, 4-thiadiazole-2-yl) acetamide].
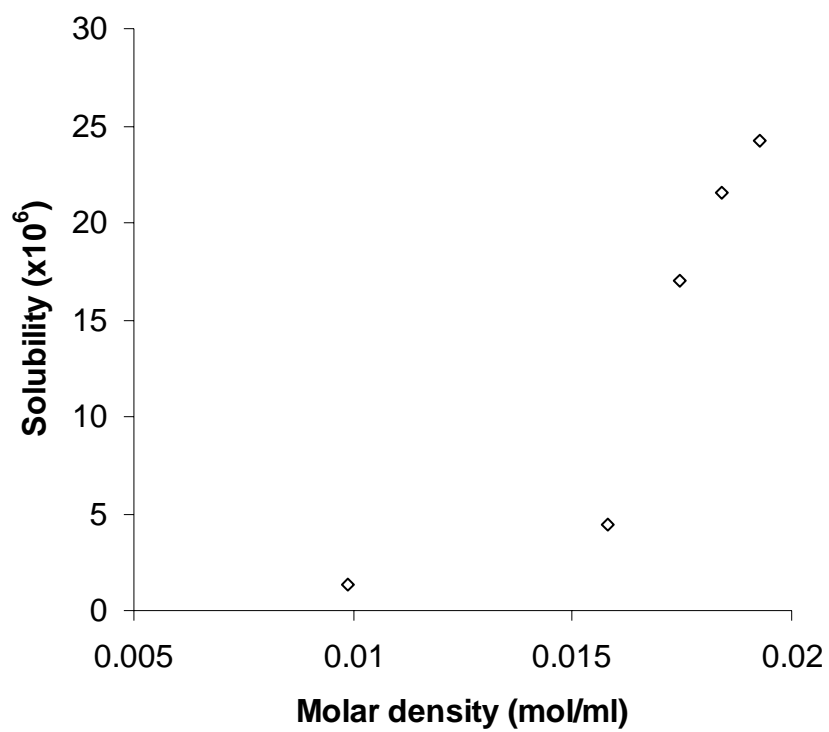
Figure 8.2 Acetazolamide solubility in supercritical CO$_2$ with menthol cosolvent.
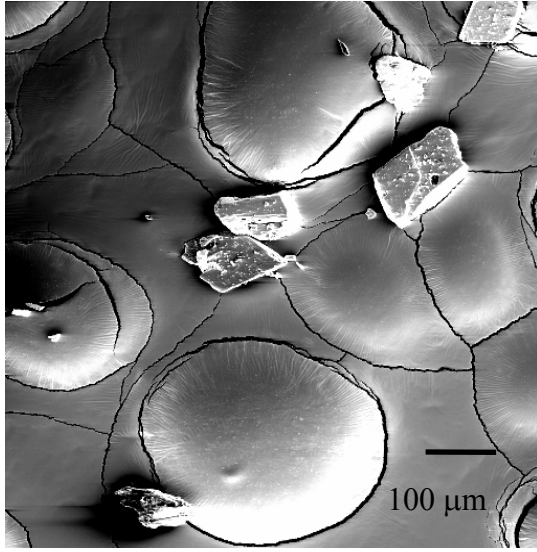
(a)
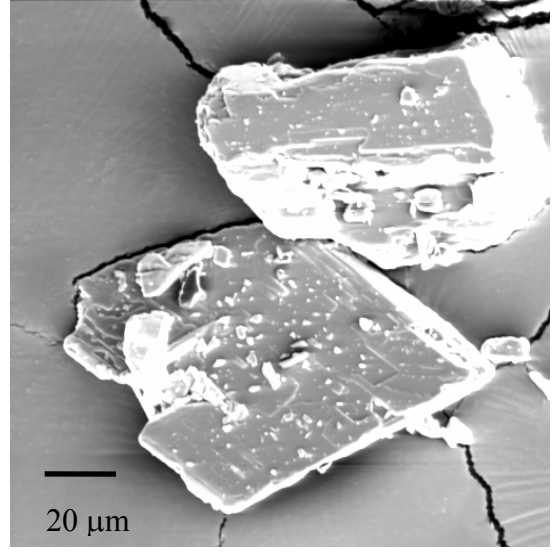
(b)
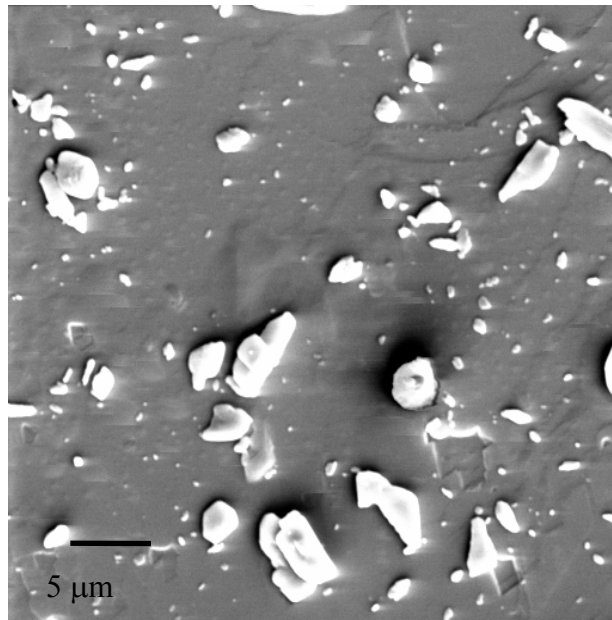
(c)

**Figure 8.3 SEM micrographs of unprocessed acetazolamide particles (a, b) and on surface of particle (c).**
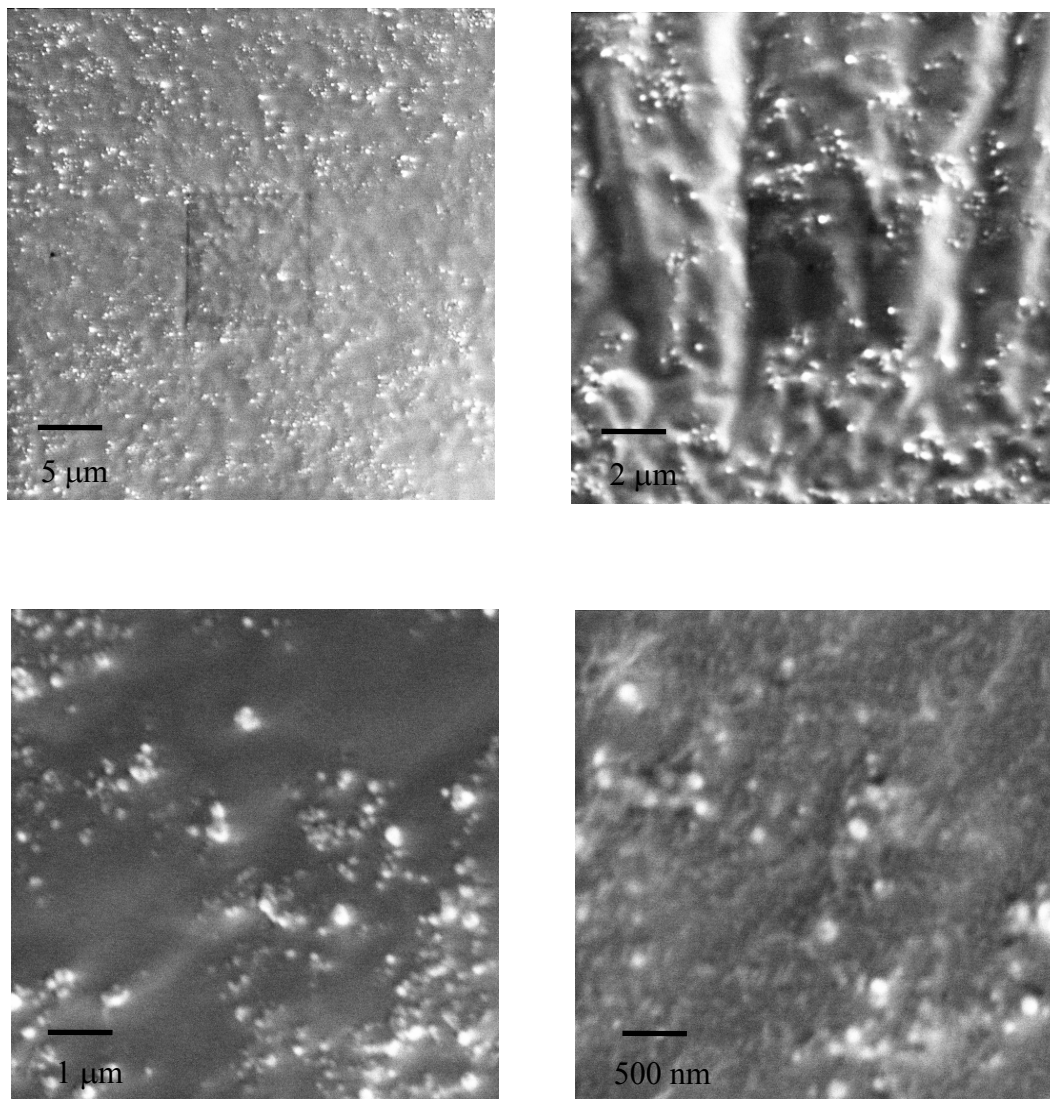
Figure 8.4 SEM micrographs of RESS-SC processed acetazolamide particles at 196 bar and 45 ^{o}C.

CHAPTER 9

FUTURE WORK

9.1   Modeling of RESS and RESS-SC Process

Modeling of any process helps in finding data at conditions which are difficult to perform experimentally and also provide the information about controlling parameters. A lot of research has been carried out in last decade or so for RESS modeling but most of them are for supersonic zone. There are very few research on particle formation in expansion zone and incorporated in their modeling work. As per most of the model work particle size at tip of the nozzle is only 5 nm but final product is usually 800 nm size. This explains that agglomeration of particles is very important parameter in RESS process. By incorporating well defined agglomeration and breakage terms from aerosol dynamic equation with fluid dynamics and thermodynamic equations, we can obtain real picture of RESS process. The choice of equation of state for thermodynamic calculation is also very important. It is important to use that equation which can be used for any fluid or system at any conditions.

RESS-SC process is ternary system due to presence of solid cosolvent. Also, cosolvent acts as a spacer in between drug solute to avoid agglomeration. Due to these new factors modeling of RESS-SC is a little complicated. Not only fluid dynamics but also particle dynamics change in this process.

Writing the codes of RESS and RESS-SC model work is also important for wider applications. FORTRAN being one of the robust engineering programming techniques can be one language in which these codes can be written.

9.2   DME as Supercritical Fluid Solvent

Although CO_2 is used widely as supercritical solvent for organic particles, its lack of dipole moment decreases solubility of most of the polar compounds. Dimethylether (DME) can be one of the compounds which can be used in supercritical form for dissolving polar compounds. DME is highly polar compound having critical point of 128 $^{\circ}$C and 54 bar pressure. DME can be utilized as novel supercritical solvent for highly polar compounds.

PUBLICATIONS

This dissertation is a collection of the following patent, peer reviewed journal papers and conference presentation:

Provisional Patent:

- Ram B. Gupta and Ranjit Thakur (2004). 'Rapid Expansion of Supercritical Solution with Solid Cosolvent (RESS-SC) Process for Nanoparticle Formation" US Provisional Patent Application # 60/634, 354.

Journal Papers and Conference Proceedings:

- "Supercritical CO_2 based formation of silica and silica-coated nanoparticles using water-in-oil microemulsions", Ranjit Thakur and Ram B. Gupta, Proceedings of 227th ACS National Meeting, Anaheim, CA, USA (IEC-055, AN 2004:225094), 2004.

- "Formation of Chitin nano-fibers by supercritical antisolvent", Jose Francisco Louvier, Gabriel Luna Barcenas, Ranjit Thakur and Ram B. Gupta, Journal of Biomedical Nanotechnology, vol. 1,1, 1-6, 2005.

- "Production of Hydrocortisone Micro- and Nano-particles using Supercritical Antisolvent with Enhanced Mass Transfer", Ranjit Thakur and Ram B. Gupta, Chemical Engineering Communication, In press - 2005.

- "Supercritical CO_2 based Silica Coating of Gold Nanoparticles Using Water-in-oil Microemulsions", Ranjit Thakur and Ram B. Gupta, Industrial and Engineering Chemistry Research, 44(9), 3086-3090, 2005

- "Rapid Expansion of Supercritical Solution with Solid Cosolvent (RESS-SC) Process for Particle Formation: Griseofulvin Nanoparticles", Ranjit Thakur and

Ram B. Gupta, Industrial and Engineering Chemistry Research, 44(19), 7380-7387, 2005.

- "Rapid expansion of supercritical solution with solid cosolvent (RESS-SC) process for 2-Aminobenzoic acid nanoparticle formation", Ranjit Thakur and Ram B. Gupta, In review-Journal of Supercritical Fluids.

- "Formation of phenytoin nanoparticles using rapid expansion of supercritical solution with solid cosolvent (RESS-SC) process", Ranjit Thakur and Ram B. Gupta. In press-2005, International Journal of Pharmaceutics.

Conference Presentations

- "Supercritical CO_2 based formation of silica nanoparticles using water-in-oil microemulsions", **Ranjit Thakur**, P. Chattopadhyay, Ram B Gupta, AIChE annual meeting, Indianapolis, Nov-2002.

- "Supercritical CO_2 based formation of silica and silica-coated nanoparticles using water-in-oil microemulsions", **Ranjit Thakur** and Ram B Gupta, 227th ACS National Meeting, Anaheim, 2004.

- "Formation of Chitin nanoparticles and nano-fibers using supercritical CO_2", Ranjit Thakur, J. F. Louvier, G. L. Barcenas and Ram B Gupta, AIChE annual meeting, Nov-2004 at Austin, TX, USA.

- "Reactive polymerization in the supercritical antisolvent precipitation process", Philip Bell, Ranjit Thakur, Ram B Gupta and C. B. Roberts, AIChE annual meeting, Nov-2004 at Austin, TX, USA.

- "Supercritical CO_2 based formation of silica coated nanoparticles using water-in-oil microemulsions", **Ranjit Thakur**, Ram B Gupta, AIChE annual meeting, Nov-2004 at Austin, USA.

- "Silica coating on nanoparticles", **Ranjit Thakur** and Ram B Gupta, International Symposium of Supercritical Fluids (ISSF), May-2005, Orlando, FL, USA.

- "Formation of nano-structured chitin by supercritical antisolvent precipitation", Ranjit Thakur, J. F. Louvier, G. L. Barcenas, Ram B Gupta. ISSF May-2005, Orlando, FL, USA.

- "Rapid expansion of supercritical solutions with solid cosolvent (RESS-SC) process for nanoparticle formation", **Ranjit Thakur** and Ram B Gupta. ISSF May-2005, Orlando, FL, USA.

- "Rapid expansion of supercritical solution with solid cosolvent (RESS-SC) process for particle formation: Pharmaceutical Nanoparticles", **Ranjit Thakur** and Ram B Gupta. AIChE Annual Meeting, Nov-2005, Cincinnati, USA.